MAGNETO-OPTICAL STUDY OF ELECTRON-HOLE DROPS IN GERMANIUM

by

Hiroyasu Nakata

1980

CONTENTS

ABSTRACT

Physical properties of highly photo-excited germanium are investigated by time resolved far-infrared magneto-absorption at low temperatures (2.0-23 k). Cyclotron resonance of free holes, inter-discrete level absorption of excitons and magneto-plasma resonance of electron-hole drops are observed at the wavelengths of 84-513 μm in magnetic fields up to 7 T.

Magneto-oscillations associated with electron-hole drops, similar to de Haas-van Alphen oscillations, are observed at 2.0 K for pure germanium at the wavelengths of 146-233 μm and also for antimony- and indium-doped germanium at 171-433 μm. Idea of oscillation of carrier pair density explains the wavelength dependence of oscillation amplitude, difference in oscillation amplitude between far-infrared absorption and photo-luminescence, and delay time dependence of the oscillation amplitude.

Variation of the carrier pair density with magnetic field is evaluated by a calculation based on Keldysh and Silin's theory. Using the result of the calculation and from the magnetic fields of dips in the magneto-oscillation, the Fermi energy of electrons in the electron-hole drop is estimated to be 2.2 meV and the carrier pair density to be 2.1×10^{17} cm^{-3} in low magnetic fields. The calculation also gives a good oscillation profile consistent with the experimental result.

The carrier pair density keeps constant in doped samples with impurity concentration up to 8.5×10^{14} cm^{-3} for antimony and up to 8.0×10^{15} cm^{-3} for indium.

The critical temperature of the electron-hole drop is obtained to be near 6.5 K from three kinds of temperature dependence measurements; magnetoplasma absorption of the electron-hole drop, inter-discrete level of the exciton and decay profile of the electron-hole drop as well as the exciton. The work function of the electron-hole drop is roughly estimated to be 14.7 K by analysing the exciton decay process at 3.0-4.2 K.

Several peaks of magneto-plasma resonance of electron-hole drops are observed at the wavelength longer than 200 μm. Origin of the peaks are assigned with the help of time resolved measurement. As a result, about ten percent mass renormalization is required to explain the magnetic fields of the peaks. The observed frequency dependence of the half-width of magneto-plasma resonance indicates that the damping of plasma-oscillation is due mainly to the electron-hole scattering.

Several impurity effects are recognized : peak shift of the magneto-plasma resonance, decrease of the total lifetime of the drop, increase of the linewidth of magneto-plasma resonance, and decrease of the amplitude of magneto-oscillation. Some of these features can be qualitatively explained by the increased drop radius.

Acknowledgements

I am very grateful to Prof. E. Otsuka for providing the opportunity to do research in a fascinating area of solid state physics, and for providing continual and active support, advice and encouragement throughout the course of this work.

I am so much indebted to Dr. T. Ohyama, who helped me to construct the optically pumped laser, split off superconducting magnet and many other experimental apparatus. I would also like to thank him for his fruitful discussions.

It is a pleasure to thank Dr. K. Fujii for his help and many discussions in the early stage of this work. I also thank Dr. O. Matsuda, Mrs. T. Matsuda and Dr. S. Ishida for sharing uncounted hours in the lab and in discussions of results and theories.

I am also indebted to Mr. Y. Okada for his help and to Dr. M. Yamanaka and Dr. A. Tanaka for their discussions in the construction of the optically pumped laser.

Special thanks are due to Mr. K. Enjouji for his generous offer of the double core glass rod.

The laborious help of Miss T. Moriguchi and Miss M. Tanaka, who kindly typed the manuscript for me, is deeply appreciated.

I. Introduction

Very few free carriers exist in such semiconductors as pure germanium and silicon at liquid helium temperatures. If we illuminate the semiconductor by radiation with energy higher than the band-gap energy, finite number of electrons and holes can be generated. In a direct gap semiconductor electrons and holes recombine promptly, while in the case of an indirect gap semiconductor electrons and holes do not recombine immediately since phonons are necessary for the recombination process. As a result, electrons and holes in an indirect gap semiconductor have a long lifetime of the order of a few microseconds. This long lifetime brings about the carriers in quasi-thermal equilibrium. Physical properties of these carriers have been studies by many kinds of measurements.[1] When the intensity of excitation producing the free carrier pairs is increased, several species of complexity are suggested. The most typical and fundamental one is an exciton, which is composed of an electron and a hole. Existence of an exciton in germanium has been well confirmed by interband magneto-absorption, luminescence and far-infrared absorption.[2,3] The second complexity would possibly be an excitonic molecule, as Lampert predicted, which consists of two excitons.[4] Haynes reported the first observation of an excitonic molecule in highly excited silicon.[5] Though his experimental result has been reinterpreted in terms of electron-hole drops, he was the first to investigate a highly excited silicon systematically.

Asnin and Rogachev observed discontinuity in photoconductivity

of germanium with excitation.[6] They presumed that too many excitons induce a kind of the Mott transition into the metallic phase. Keldysh remarked that droplets of metallic liquid were generated in their experiment.[7] We call them electron-hole drops (or droplets) (EHD). Existence of EHD has been revealed by various kinds of experiments;[8,9] for example, photoluminescence,[10] light scattering,[11] plasma resonance,[12] carrier injection through p-n junction[13,14] or microwave photoresponse as well as conductivity.[15,16]

Photoluminescence of EHD in germanium was first observed by Pokrovskii and Svistunova.[10] They demonstrated that there was sharp onset of a new luminescence line as temperature was lowered at the constant excitation level. Vavilov et al. first reported plasma resonance of EHD in far-infrared absorption and determined the carrier pair density of 2×10^{17} cm^{-3}.[12] Two groups, Asnin et al. and Benoît á la Guillaume et al., showed that large pulses of charge were liberated when the droplets were dissociated by strong electric fields of a reverse biased p-n junction.[13,14] Pokrovskii and Svistunova decided from light scattering that the radius of a droplet is a few microns.[11] Hensel et al. observed the cyclotron resonance of an electron surrounding EHD and the binding energy of the metallic liquid of 16 K was obtained by a kinetic method of analysis.[16]

There are several channels through which electron-hole drops decay. Three ways of recombination take place; the first is nonradiative recombination, the second radiative recombination and the last Auger recombination. Another decay process is

exciton evaporation from the electron-hole drop surface. The inverse process of evaporation is exciton backflow into the drop. The excitons recombine radiatively and nonradiatively or dissociate into electrons and holes.

In the microwave measurements, electrons can be observed which are evaporating from electron-hole drops or have not condensed yet into electron-hole drops. Hensel et al. performed cyclotron resonance experiments and obtained total lifetime τ_0 = 40 μs from the decay of electron-hole drops at low temperatures (< 2 K) and work function ϕ = 16 K from the temperature dependence of the cut-off time.[17] They also estimated an initial drop radius of 8.4 μm.

Photoluminescence also gives us information about the decay kinetics of electron-hole drops. Benoît à la Guillaume et al. measured an exponential drop decay at low temperatures (< 2 K) with a total lifetime of $\tau_0 \sim 40$ μs.[18] Besides luminescence from electron-hole drops, luminescence from excitons can be observed. By investigating the two luminescence signals, it is possible to obtain profounder insight about decay kinetics of both drops and excitons. Westervelt et al. made such a measurement and analyzed their data by parameter fitting with a computer.[19] They obtained several parameters including $\phi \sim 17$ K.

The other effective method to study decay kinetics of drops is time resolved far-infrared absorption, which was first observed by Fujii and Otsuka.[20] They derived some physical quantities; temperature dependent work function, for example, $\phi = a + bT^2$ ($a = 14 \pm 1$ K^2, $b = 0.5 \pm 0.2$) and τ_0 = 67 μs.

Application of external, electric as well as magnetic field or stress induces various modifications of the property of the electron-hole drop.[21)-24)] Influence of magnetic fields on the electron-hole drop has been studied in several kinds of measurements, luminescence, and magnetoplasma absorption. Photoluminescence in magnetic fields was first observed by Alekseev et al.[25)] The luminescence line of electron-hole drops is split into two peaks and shift to higher energy. Such behavior of magnetoluminescence was investigated by Martin et al. in more detail.[26)] All the peaks are fitted by the calculation including the complicated valence band structure in magnetic fields. But 10 % mass renormalization was necessary in order to interpret their experimental results consistently. They also derived the variation of the ground state energy and the carrier pair density in magnetic fields. The ground state energy increases from $\sim$ 6 meV at B = 0 to $\sim$ 12 meV at 14 T. The carrier pair density also increases from $n_0 = 2.3 \times 10^{17}$ cm^{-3} to $n_0 = 7.5 \times 10^{17}$ cm^{-3} for the same field range. The increase of the ground state energy and the carrier pair density was calculated by Chui,[27)] Büttner[28)] and Keldysh and Onischenko.[29)] Recently more detailed studies of luminescence in magnetic fields have been done by Störmer and Martin,[30)] and also by Skolnick and Bimberg.[31)]

Murzin et al. observed plasma resonance of drops in magnetic fields.[32)] The splitting of absorption peak was well explained by a simple calculation and more detailed treatment of the theory with hole quantum effect has recently been given by Kononenko and Murzin.[33)]

Plasma resonance can be observed at the photon energy of ∿ 8.7 meV. In magnetic fields, several peaks of magnetoplasma resonance have been studied in the lower photon energy range. It was first observed by Fujii and Otsuka[34,35] and then Gavrilenko et al. performed an excellent experiment in the low energy region and fitted two peaks of magnetoplasma resonance with 10 % mass renormalization.[36] They also found the resonance by magnetic waves. The peak positions were satisfactorily interpreted by Ford et al.'s theory.[37,38]

One phenomenon peculier to the Fermi liquid is the magneto-oscillation. Magneto-oscillatory behavior has been observed at a few kinds of measurements in magnetic fields of several Tesla.[31,32) 34,35) 39)-48] Magneto-oscillations similar to the de Haas-van Alphen or Shvbnikov-de Haas effect in metals were discovered by two groups; namely, Bagaev et al.[39] and Murzin et al..[32] Both groups proposed that variation of the work function is responsible for the oscillations. Keldysh and Silin opposed the proposal and suggested instead the dependence of the carrier pair density on the magnetic field as the principal mechanism of the oscillations.[49] Their theoretical predictions were demonstrated by Betzler et al. in the time-resolved measurements of the integrated intensity of drop luminescence.[40)-44] Nowadays it is generally accepted that magneto-oscillations of luminescence are due to oscillatory carrier pair density.

Several reports on magneto-oscillations of far-infrared absorption are available so far. There has been only a small amount of information about their origin, however. Hensel et al.

suggest that the magneto-oscillations observed in far-infrared absorption are also attributable to the variation of carrier pair density induced by magnetic fields.[9] According to them, the integrated resonant absorption is just proportional to ω_p^2; i.e., to the carrier pair density n, where ω_p is the plasma freqency. The total number of pairs in EHD is governed by the total decay rate Cn^2. Here C is some constant. Thus the quantum efficiency for absorption in the far-infrared various as $C^{-1}n^{-1}$. One expects the absorption to decrease at an increase of n, which occurs when the Landau level crosses the Fermi level.

Impurity effect to electron-hole drop is also an interesting problem. Luminescence of drops in doped germanium was first observed by Alekseev et al. systematically. Fundamental properties of drops, carrier pair density and ground state energy are not affected in the impurity concentrations up to $\sim 10^{16}$ cm^{-3}.[50] But Alekseev et al. reported that excitation threshold for drop creation is lowered by doping impurities. Another phenomenon associated with doping is appearance of the zero phonon line. This line has been observed by many experimentalists.[50)-52)]

In far-infrared absorption measurements Timusk and Silin observed peak shift of plasma resonance induced by doping and interpreted the phenomenon by formation of small droplets in the vicinity of impurities.[53] Rose et al., on the other hand, proposed increase of EHD radius by impurities as the origin of the peak shift.[54] Zayats et al. agree with this opinion.[55]

This thesis consists of three main themes, the first is the decay kinetics of electron-hole drops and excitons, the second is

the magneto-oscillations of far-infrared absorption and the third is impurity effects to the far-infrared absorption.

In Chapter II, the theory will be given of the exciton system in germanium in association with the band structure; isolated excitons, electron-hole drops, and their behavior in magnetic fields.

In Chapter III, our experimental procedures are presented. They are divided in two setups.

In Chapter IV, experimental results and their analyses are given.

In Chapter V, magneto-oscillations and impurity effects are mainly discussed.

In Chapter VI, some obtained knowledge about critical temperature and work function is given. Origin of the magneto-oscillation in FIR absorption becomes clear. Some conclusions related to impurities are also presented.

II. Theoretical Background

II-1. Band Structure of Germanium

Germanium is an indirect gap semiconductor; the valence band maximum is separated from the conduction band minimum in the k space (see Fig. 1). The conduction band minima are located at the L points of the Brillouin zone, making four equivalent valleys. Electrons residing in these conduction band minima have been investigated by microwave cyclotron resonance.[1] The energy contour of the conduction electrons is an ellipsoid, whose principal axis is parallel to the [111] type direction. Taking the principal axis as the z-axis, the energy of electron can be written by

$$\varepsilon(k) = \frac{\hbar^2}{2m_t}(k_x^2 + k_y^2) + \frac{\hbar^2}{2m_\ell} k_z^2 \quad ; \qquad (2\text{-}1)$$

where transverse mass m_t is 0.08152 m_0, longitudinal mass m_ℓ is 1.588 m_0, and m_0 = 9.109 x 10^{-28} g (free electron mass).[1]

On the other hand, the valence band maximum occurs at Γ_{25}' point in the center of Brillouin zone. It splits into two levels according to spin orbit interaction, one is Γ_7^+ and the other is Γ_8^+. The energy of Γ_7^+ is lower than Γ_8^+ level. The splitting is so large that we can ignore the presence of Γ_7^+ level. The Γ_8^+ level has four-fold degeneracy. The structure of the valence band has been studied by microwave cyclotron resonance.[1] In a classical approach, the energy surface of holes can be written as

$$E_{\pm}(k) = Ak^2 \pm [B^2k^4 + C^2(k_x^2k_y^2 + k_y^2k_z^2 + k_z^2k_x^2)]^{1/2} \qquad (2\text{-}2)$$

The parameters A, B, and C have been precisely determined by cyclotron resonance experiments; to be $A = 13.38 \frac{\hbar^2}{2m_0}$, $B = 8.48 \frac{\hbar^2}{2m_0}$, $C = 13.15 \frac{\hbar^2}{2m_0}$.[1] As seen from Eq. (2-2), two kinds of holes with different masses exist and we call them heavy and light holes. We often use the spherical approximation; in which the warped valence bands are replaced by spherical bands with heavy hole mass $m_{hh} = 0.387\ m_0$ and light hole mass $m_{\ell h} = 0.042\ m_0$.

In magnetic fields the conduction band is quantized into Landau levels. The splitting between adjacent Landau levels is given, in terms of the cyclotron mass m_c, by

$$\left(\frac{1}{m_c}\right)^2 = \frac{\cos^2\theta}{m_t^2} + \frac{\sin^2\theta}{m_t m_\ell} \quad ; \qquad (2\text{-}3)$$

where θ is the angle between the direction of the magnetic field and that of the principal axis of the ellipsoidal energy surface. The number of kinds of electrons with different cyclotron masses thus depends on the direction of the magnetic field.

The variation of energy of holes due to magnetic fields has been studied in detail by Hensel and Suzuki by means of microwave cyclotron resonance.[1] The structure of the valence band in magnetic fields is very complicated and the spacings between adjacent Landau levels are not the same as in the case of electrons (see Fig. 2).

The top of the valence band has the symmetry of Γ_8^+ and the total angular momentum J = 3/2. The four Bloch states $|M_J>$,

where $M_J = \pm \frac{1}{2}, \pm \frac{3}{2}$, are coupled to one another. The eigen-vectors are described as

$$\psi = \sum_n \sum_{M_J} a_n(M_J) u_n |M_J> \quad . \qquad (2\text{-}4)$$

Here u_n's are the harmonic oscillation states with the quantum number n = 0, 1, 2, $\cdots$. They classify the Landau levels by the scheme (N_n, K^{π}). Two quantum numbers are necessary to uniquely identify each eigenstate : N, the Landau quantum number for the envelope function, and its subscript n, which is required to distinguish the four states of the same N. The quantum number K (K = 0, $\cdots$, ν-1) embodies the ν-fold rotational symmetry of the crystal about the direction of magnetic field B with π being parity of the envelope function. Various kinds of transitions between these states are possible. Among them the strongest is M_0 transition which occurs in the absence of warping and at $k_H = 0$. The selection rule of this transition is $\Delta N = \pm 1$, $\Delta\pi$ yes and $\Delta K = \pm 1$.

II-2. Exciton

An electron and a hole form an exciton by Coulomb force. In germanium, it has a long lifetime of the order of microsecond. Though the exciton in germanium resembles a hydrogen atom, it has several different properties, the masses of the components are more or less very alike and smaller than the free electron mass. Moreover, the exciton is embedded in a dielectric. As a result the Bohr radius a_0 of the exciton in germanium is 127 Å,

which is much larger than that of a hydrogen atom and the energy scale of the exciton shrinks by three orders compared with that of the hydrogen atom. The ionization energy of the exciton in germanium is only $\sim$ 3.8 meV so that the far-infrared absorption study is a good tool for investigating the exciton states. Unlike the case of hydrogen, there are two kinds of holes and anisotropy of electron mass. In fact, two species of excitons can be observed associated with heavy and light holes. The binding energies of these are 4.17 and 3.25 meV, respectively.[56] Three techniques have been used to obtain the exciton binding energy, far-infrared photoconductance, far-infrared absorption and interband absorption in the near infrared. They give us the values of 4.15, 3.8, and 3.6 meV, respectively.

II-3. Electron-Hole Drop

The electron-hole drop is a metallic liquid which has a finite life time. Existence of the electron-hole drop can be examined by calculating the ground state energy of the many particle system. Such calculation was done by several theoreticians.[57)-61)] Here we will review the calculation by Brinkman and Rice.[59)] The total energy of the electron-hole drop is the sum of kinetic, exchange and correlation energies.

If the energy band of electrons and holes are spherical and nondegenerate, the kinetic and exchange energies are easily calculated and the results are

$$E_{kin} = \frac{2.21}{r_s^2} \left(= \frac{3}{5} \frac{\hbar^2 k_F^2}{2M_{ex}}\right) \qquad (2\text{-}5)$$

$$E_{exch} = -\frac{1.832}{r_s} \left(= -\frac{3e^2 k_F}{2\pi\varepsilon_0}\right) \quad ; \tag{2-5}$$

where r_s is the average spacing between carriers with unit being the Bohr radius of exciton a_0 and M_{ex} is the reduced mass ($M_{ex}^{-1} = m_e^{-1} + m_h^{-1}$), k_F is the Fermi wavevector, ε_0 is the dielectric constant of germanium. The correlation energy is difficult to calculate and there exist some different ways to evaluate it. Brinkman and Rice adoped Hubbard's procedure of the random phase approximation.[62] These calculated results are shown in Fig. 3.

As seen from Fig. 3, the ground state energy of the drop is always higher than that of an exciton. For isotropic non-degenerate bands, accordingly, it seems that the exciton gas phase is more stable than the metallic phase.

In germanium, however, the valence band is degenerate and the energy surface of electron is ellipsoid. The ground state energy for the drop system is different from the case of a spherical non-degenerate band structure. The exact numerical calculation of the Hartree-Fock energy has been carried out by Brinkman et al.[57),59] Their result is

$$E_{HF} = E_{kin} + E_{exch} = \frac{0.468}{r_s^2} - \frac{1.136}{r_s} \quad . \tag{2-6}$$

The correlation energy of the drop in germanium has been calculated by several groups. Brinkman et al., as stated before,

used the random phase approximation modified by Hubbard and neglected the degeneracy of the valence band in their calculation. Their calculated results are shown in Fig. 4. Combescot and Nozières[58] used the Nozières-Pines approximation[63] and Vashishta et al.[60,61] took the generalized Singwi-Tosi-Land-Sjölander scheme.[64] Their numerical results are also shown in Fig. 4. As a result, the complicated band structure has turned out to favor the stability of electron-hole drops. The basic parameters; i.e., carrier pair density, ground state energy and work function, are shown in Table I.

Electrons and holes within the electron-hole drop are different from those outside in the sense that they are strongly affected by other carriers. According to the Landau Fermi liquid theory, the quasi-particle which is excited from the liquid has the mass different from that of a free carrier owing to the many body effect. The masses of the carriers in the drop are modified because of the effect as calculated by Rice,[65] and Rösler and Zimmermann.[66] The calculated results by Rice are as follows:

$$m_t^* = 1.10\, m_t \quad , \quad m_\ell^* = 0.99\, m_\ell \quad ;$$
$$m_{\ell h}^* = 1.10\, m_{\ell h} \quad , \quad m_{hh}^* = 1.14\, m_{hh} \quad . \qquad (2\text{-}7)$$

II-4. Thermodynamics of the Exciton System in Germanium

The features of electron-hole drops and excitons have been described at absolute zero temperature. When the temperature is

not zero, the system which contains electrons, holes, excitons and electron-hole drops, has to be treated by thermodynamics. At low temperatures, there are few free carriers and hence excitons and electron-hole drops can be considered to exist in quasi-thermal equilibrium. As temperature becomes higher, excitons dissociate thermally and electron-hole drops become unstable. Above the critical temperature, there remain only free carriers and excitons in the crystal.

In order to describe the phase diagram of this exciton system, we will first calculate the temperature dependence of the carrier pair density in electron-hole drops.[67]

The free energy per carrier pair $F(n, T)$ can be expanded in powers of the temperature as

$$F(n, T) = E_G(n) - \frac{1}{2}\gamma(n)(k_B T)^2 \quad ; \tag{2-8}$$

where the coefficient $\gamma(n)$ is proportional to the density of quasi-particle states at the Fermi level. The temperature dependence of the carrier pair density $n(T)$ can be obtained by minimizing the free energy and is

$$n(T) = n_0 + \frac{1}{2}(\gamma'/E_G'')(k_B T)^2 \quad . \tag{2-9}$$

The primes denote derivatives with respect to density evaluated at $n = n_0$.

On the other hand, the exciton density can be calculated by the condition that the chemical potentials of excitons and

electron-hole drops are equal to each other. The partition function for a single exciton can be written as

$$Z = \int_0^\infty dE\, D_{ex}(E)\, \exp[-(E - \varepsilon_x)/k_B T] \quad ; \tag{2-10}$$

where $D_{ex}(E)$ is the exciton density of states and ε_x is the binding energy of exciton. The free energy per exciton can be obtained from this partition function as

$$F(n_{ex}) = - k_B T \ln(Ze/n_{ex}) \quad . \tag{2-11}$$

We can calculate the chemical potential of excitons having the mass M_{ex} and degeneracy ν_{ex}

$$\mu_{ex} = - \varepsilon_x + k_B T \ln\{\frac{n_{ex}}{\nu_{ex}} (\frac{2\pi\hbar^2}{M_{ex} k_B T})^{3/2}\} \quad . \tag{2-12}$$

The density of excitons can be evaluated by equating μ_{ex} with the chemical potential of electron-hole drops as

$$n_{ex}(T) = \nu_{ex} (\frac{M_{ex} k_B T}{2\pi\hbar^2})^{3/2} \exp(- \frac{\phi}{k_B T} - \frac{1}{2}\gamma k_B T) \quad . \tag{2-13}$$

This is correct only at very low temperatures. For temperatures $T > 2$ K, the nonparabolicity of the exciton band has to be considered.

By using $n(T)$ and $n_{ex}(T)$, the phase diagram can be described as shown in Fig. 5.

The critical temperature of the electron-hole drop has been

calculated by many theoreticians.

II-5. Rate Equations

In an exact sense, the exciton system in germanium is not in thermal equilibrium, since free carriers, excitons and electron-hole drops all have finite lifetimes. The number of free carriers as well as excitons, and the carrier pair number in an electron-hole drop can change in time. We can express the time variation of the number of each species by the rate equations.[68] One is written as

$$\frac{d\nu}{dt} = n_{ex} b\nu^{2/3} - \frac{\nu}{\tau_0} - aT^2\nu^{2/3} \exp\left[-\frac{\phi(\nu)}{k_B T}\right] \quad , \qquad (2\text{-}14)$$

where ν is the number of carriers in a single electron-hole drop, n_{ex} is the density of excitons, b is some constant, τ_0 is the total lifetime of an electron-hole drop and $\phi(\nu)$ is a work function with a being the so-called Richardson-Dushuman type constant. The first term on the right-hand side expresses the back flow of excitons onto the electron-hole drop. The second term is the recombination of carriers within the drop. And the third term gives the evaporation rate of excitons from the surface of the drop. Carriers in the drop can recombine in three different ways; recombination via impurities, radiative recombination and Auger recombination. Then the total lifetime can be given by

$$1/\tau_0 = 1/\tau_{imp} + 1/\tau_{rad} + 1/\tau_{Aug} \quad . \qquad (2\text{-}15)$$

The recombination of carriers in the drop via impurities is less effective than the recombination of excitons via impurities owing to the bottle necking of impurity centers. The radiative recombination always takes place with a phonon, since germanium is an indirect gap semiconductor. The third process of recombination is the Auger recombination. The process in which three particles play around with a phonon participation is most effective. In that case an electron and a hole recombine and give up their energy and momentum to the third particle. The Auger lifetime can be written as

$$1/\tau_{Aug} = Cn^2 \quad . \tag{2-16}$$

For germanium, Betzler and others obtained the values for the constant $C = 4 \times 10^{-31}$ cm^6 sec^{-1} and for the lifetime $\tau_A = 50$ μs.[69] The coefficient a of exciton evaporation can be calculated by the equation

$$a = \nu_{ex}\left(\frac{3}{4\pi n_0}\right)^{2/3} \frac{M_{ex}k_B^2}{\pi\hbar^3} \quad . \tag{2-17}$$

Westervelt et al.[19] obtained the value of $a = 15 \times 10^9$ sec^{-1} K^{-2}, while Hensel et al. $a = 4 \times 10^9$ sec^{-1} K^{-2}.[17] The rate equation for excitons can be written as

$$\frac{dn_{ex}}{dt} = G_{ex} + aN_dT^2\nu^{2/3}e^{-\phi/k_BT} - bn_{ex}\nu^{2/3}N_d - n_{ex}/\tau_{ex} \quad ; \tag{2-18}$$

where G_{ex} is the generation rate of excitons, N_d is the number of

electron-hole drops in unit volume, τ_{ex} is the lifetime of an exciton. The first term is the generation of excitons by excitation light. The second term expresses the exciton evaporation. The third term is exciton backflow to an electron-hole drop. The forth term is the recombination of excitons.

II-6. Excitons in a Magnetic Field

Like a hydrogen atom the each level of an exciton splits into Zeeman levels in the magnetic field. First we will consider the energy levels of the exciton in a magnetic field for a simple band structure; namely, isotropic non-degenerate band. In that case the Hamiltonian of the exciton can be expressed as[70]

$$H = -\frac{\hbar^2}{2M_{ex}}\{\frac{1}{\rho}\frac{\partial}{\partial\rho}(\rho\frac{\partial}{\partial\rho}) + \frac{1}{\rho^2}\frac{\partial^2}{\partial\phi^2} - \frac{ie\hbar}{2c}(\frac{1}{m_\ell} - \frac{1}{m_h'})H\frac{\partial}{\partial\phi} + \frac{\omega_c^2}{8M_{ex}}\rho^2 - \frac{\hbar^2}{2M_{ex}}\frac{\partial^2}{\partial z^2} - \frac{e^2}{\varepsilon_0\sqrt{\rho^2 + z^2}}\quad ; \tag{2-19}$$

where the magnetic field is applied in the Z direction; $\rho = \sqrt{x^2 + y^2}$, ω_c is the cyclotron frequency, and ε_0 is the dielectric constant of germanium. The Schrödinger equation for this Hamiltonian cannot be solved analytically. In the two limiting cases the solution can be obtained. One is for zero magnetic field, when the solution of this equation is the same as the case of a hydrogen atom. Then

the solution can be written as

$$\phi_{n\ell m} = N_0 \, e^{-\frac{1}{2}\rho} \, \rho^{\ell} \, L_{n+\ell}^{2\ell+1}(\rho) \, P_{\ell}^{m}(\cos\theta) \, e^{im\phi} \quad ; \qquad (2\text{-}20)$$

where N_0 the normalization constant, and $L_n^m(\rho)$ and $P_\ell^m(\cos\theta)$ are associated Laguerre and associated Legendre polynomials, respectively. The other case is for the high field limit, when the Schrödinger equation is soluble. The eigenstate is given by[71,72]

$$\Phi_{NM} = C \, \sigma^{\frac{1}{2}|M|} \, e^{-\frac{1}{2}\sigma} \, L_{N+\frac{1}{2}(|M| - M)}^{|M|}(\sigma) \, e^{iM\phi} e^{ikZ} ; \qquad (2\text{-}21)$$

where $\sigma = \rho^2$ and C the normalization constant.

At the magnetic fields where the Coulomb term cannot be neglected, we have to solve the following equation[72]:

$$\left(\frac{P_z^2}{2M_{ex}} + V_{NM}(z)\right) F_{NM\nu}(z) = \varepsilon_{NM\nu}(z) \, F_{NM\nu}(z) \; ;$$

where (2-22)

$$V_{NM}(z) = \int \Phi_{NM}^{*}(\rho,\phi) \, \frac{-e^2}{\varepsilon_0 \sqrt{\rho^2 + z^2}} \, \Phi_{NM}(\rho,\phi) \, d\rho d\phi \quad .$$

There is a relation between the set of quantum number (n, ℓ, m) and (N, M, ν) as shown in Table II.

The oscillator strength of the transition from the ground state has been calculated by using various trial functions.[73] It turns out that for the transitions between the donor-like levels, the transition between the ground and the $2P_{+1}$ state is strongest. Upon increase of the magnetic field, the same

probability increases while the transition probability between the ground and $2P_{-1}$ states decreases. For the transitions between the acceptor-like levels, we must exchange $2P_{+1}$ and $2P_{-1}$.

II-7. Electron-Hole Drops in the Magnetic Field

Keldysh and Silin calculated the influence of a magnetic field on the Helmholtz free energy of EHD and reported that the carrier pair density oscillates in magnetic fields.[49] We will introduce the outline of their theory for the purpose of comparison with our experimental results. The carrier pair density n is calculated from the condition that the free energy becomes minimum, viz., $\partial F(n, H)/\partial n = 0$, where $F(n, H)$ is the free energy as a function of carrier pair density n in the presence of a magnetic field H. For such low magnetic fields as $\hbar\omega_c \ll E_F$, where E_F is the Fermi energy, the free energy and the carrier pair density are written as

$$F(n, H) = F_0(n) + \Delta F(n, H) \qquad (2\text{-}23)$$

and

$$n = n_0 + \Delta n(H) \ , \qquad (2\text{-}24)$$

respectively, where $F_0(n)$ and n_0 are zero field values with $\Delta F(n, H)$ and $\Delta n(H)$ being the correction due to the field.

The condition of making the free energy minimum yields the magnetic field dependent term of the carrier pair density

$$\Delta n(H) = -\left.\frac{\partial \Delta F}{\partial n}\right)_{n=n_0} \Bigg/ \left.\frac{\partial^2 F_0}{\partial n^2}\right)_{n=n_0} . \tag{2-25}$$

The free energy of EHD in zero magnetic field is written in the form

$$F(n, 0) = F_0(n) = an^{2/3} + dn^{1/3} , \tag{2-26}$$

neglecting the correlation term. Here a and d are constants. The correction to the carrier pair density due to the field can be expressed as

$$\Delta n(H) = -\frac{9n_0^2 \left.\frac{\partial \Delta F}{\partial n}\right)_{n=n_0}}{2F_0(n_0)} . \tag{2-27}$$

Since $F_0(n_0)$ is negative, the field where $\Delta n(H)$ becomes maximum is the same as that where $\partial \Delta F/\partial n)_{n=0}$ becomes maximum. Next we should calculate $\partial \Delta F/\partial n$ explicitly. The oscillatory part of the kinetic and exchange terms of the electron free energy is written

$$\Delta F^{osc}(n, H) = \frac{3}{2^{7/2}} \frac{\mu}{\pi^2} \frac{1}{\eta} \sum_{i=1}^{\eta} \left(\frac{\hbar\omega_i}{\mu}\right)^{5/2} \sum_{j=1}^{\infty} \{\frac{(-1)^j}{j^{5/2}} S(\frac{2\pi^2 jkT}{\hbar\omega_i})$$

$$\cos(2\pi j A_e \frac{\mu}{\hbar\omega_i} - \frac{\pi}{4}) + 4R_e^{1/2} \frac{\mu j}{\hbar\omega_i} A_e^{1/2} \psi(\frac{m_t}{m_\ell}) S(\frac{2\pi^2 jkT}{\hbar\omega_i}) \tag{2-28}$$

$$\sin(2\pi j A_e \frac{\mu}{\hbar\omega_i} - \frac{\pi}{4})\} ;$$

where η is the number of valleys, $\omega_i = eH/m_i c$ is the cyclotron frequency of the carrier in i-th valley, $\mu = \hbar^2(3\pi^2 n)^{2/3}/2m_d \eta^{2/3}$, $S(x) = x/\sinh x$, $A_e = E_F/\mu$, $R_e = m_d e^4/2\varepsilon_0{}^2\hbar^2\mu$ and $m_d = (m_t{}^2 m_\ell)^{1/3}$ is the density-of-states effective mass of electrons. $\Psi(\gamma)$ is a function which takes into account the effect of the non-sphericity of the electron valleys on the exchange energy. The first term is due to the kinetic energy and the second due to the exchange energy. At low magnetic fields, the oscillation amplitude of the exchange term is larger than that of the kinetic term. When the magnetic field is applied along [100] direction, the relative correction to the density $\Delta n(H)/n_0$ becomes as large as 0.33 at 1 T.

Equations (2-27) and (2-28) lead to the oscillatory part of the density $\Delta n(H)$ which is proportional to

$$g(H) = \sum_{i=1}^{\eta} (\hbar\omega_i)^{1/2} \sum_{j=1}^{\infty} \frac{(-1)^j}{j^{1/2}} S\left(\frac{2\pi^2 jkT}{\hbar\omega_i}\right) \cos\left(2\pi j \frac{E_F}{\hbar\omega_i} - \frac{\pi}{4}\right) \qquad (2\text{-}29)$$

We have first examined the convergence of g(H) prior to the numerical calculation. If the summation over j is carried out up to the eleventh term, the error is less than 1 percent. The result of the numerical calculation of $\Delta n(H)$ for B // [100] with E_F = 2.5 meV and at 2 K is shown in Fig. 6. From this result, the fields of carrier pair density maxima are given by

$$E_F = (\ell + \beta)\hbar\omega_i \quad ; \qquad (2\text{-}30)$$

where ℓ is integer and the phase factor β is 0.534. Since the magnetic fields of the Fermi level crossing the Landau levels are calculated by Eq. (2-30) with $\beta = 0.5$, the crossing field should come very close to the magnetic field of the density maximum. We have also calculated Δn for B // [111] as shown in Fig. 7. The heavier cyclotron mass electron contributes much to the magneto-oscillation of density. A large dip appears neat 4 T between the fields where the $\ell = 0'$ and $\ell = 1'$ Landau levels of heavier cyclotron mass electron intersect the Fermi level. Here the primes on the Landau quantum numbers indicate the association with the heavier cyclotron mass electron at the B // [111] geometry. We will use unprimed numbers for the lighter electron.

Until now we have assumed that the Fermi energy keeps constant in magnetic fields. There is a possibility that the Fermi energy also oscillates. In order to obtain information about the magneto-oscillations of both the carrier pair density and the Fermi energy, one more equation is necessary. This equation can be derived from the integral of the density of states. At zero temperature the integral can easily be evaluated to give the carrier pair density in the case of the [100] magnetic field direction; namely,

$$n = \frac{2\sqrt{2}}{\pi^2}\left(\frac{eH}{\hbar^2 c}\right)\frac{m_t\sqrt{m_\ell}}{m_c}\sum_{\ell}\left(E_F - (\ell + \tfrac{1}{2})\hbar\omega_i \pm \tfrac{1}{2}g^*\mu_B H\right)^{1/2} \quad , \qquad (2\text{-}31)$$

where g* is the effective g value and μ_B is the Bohr magneton. We calculate the carrier pair density by this equation with assumption E_F = constant + $\frac{1}{2}\hbar\omega_c$. The result is shown in Fig. 8. The minima of carrier pair density occur just at the crossing fields. Theoretically the sequent equations (2-27) and (2-31) have to be solved.

At high magnetic field, increase of the carrier pair density in electron-hole drops has been reported. Keldysh and Onishchenko predict the magnetic field dependent carrier pair density in a strong magnetic field as follows[29]:

$$n(H) = \left(\frac{eHa_0^2}{\hbar c}\right)^{8/7} a_0^{-3} \quad . \tag{2-32}$$

In their model electrons and holes are assumed to have an equal mass m_{eff}.

The shape of an electron-hole drop is deformed by a magnetic field.[74] This is due to recombination magnetization. At low temperatures, evaporation of excitons from the surface of a drop is not frequent. Excitons rather come into the drop by backflow and carriers in drops recombine in several ways. The carriers flow from the surface into the center of the drop. In magnetic field carriers which travel along the direction of the magnetic field do not feel any force but the carriers going along other directions are influenced by the Lorentz force. As a result, the shape of the drop becomes an ellipsoid of revolution.

II-8. Far-Infrared Absorption

The problem of scattering and absorption of electro-magnetic

waves by small conducting spheres was first calculated by Mie.[75)-77)] He solved the Maxwell equations under the boundary condition of sphere which is isotropic and has a scalar dielectric constant. The results of Mie's calculation are as follows. The extinction cross-section is given by[78,79)]

$$Q_{ext} = Q_{abs} + Q_{scat} \tag{2-33}$$

with

$$Q_{ext} = \frac{2\pi}{k_0^2} \sum_n (2n + 1)\ \mathrm{Re}({}^{e}B_n + {}^{m}B_n) \tag{2-34}$$

and

$$Q_{scat} = \frac{2\pi}{k_0^2} \sum_n (2n + 1)\,(|{}^{e}B_n|^2 + |{}^{m}B_n|^2) \quad ; \tag{2-35}$$

where

$${}^{e}B_n = \frac{\varepsilon^* j_n(kR)\,[k_0 R\, j_n(k_0R)]' - j_n(k_0R)\,[kR\, j_n(kR)]'}{\varepsilon^* j_n(kR)\,[k_0 R\, h_n^{(1)}(k_0R)]' - h_n^{(1)}(k_0R)\,[kR\, j_n(kR)]'} \tag{2-36}$$

and

$${}^{m}B_n = \frac{j_n(kR)\,[k_0 R\, j_n(kR)]' - j_n(k_0R)\,[kR\, j_n(kR)]'}{j_n(kR)\,[k_0 R\, h_n^{(1)}(k_0R)]' - h_n^{(1)}(k_0R)\,[kR\, j_n(kR)]'} \quad . \tag{2-37}$$

The functions $j_n(Z)$ and $h_n^{(1)}(Z)$ are the n-th order spherical Bessel and first kind Hankel functions, respectively. The superscripts e and m denote absorption for electric and magnetic waves, respectively. The quantity ε^* is the dielectric function inside the drop divided by that outside. We further write R for the

average radius of a drop, and k and k_0 for the propagation constants inside and outside the drops, respectively.

In our case the radius of a drop is several micrometers and the wavelength of far-infrared radiation is 70 to 513 μm. The wavelength of FIR is much longer than the radius. The expression for the extinction cross-section is then greatly simplified :

$$Q_{ext} = 4\pi k_0 R^3 \left\{ \mathrm{Im}\left[\frac{\varepsilon^* - 1}{\varepsilon^* + 2} + \frac{(k_0 R)^2}{15} \left(\frac{\varepsilon^* - 1}{\varepsilon^* + 2}\right) \times \left(\frac{\varepsilon^{*2} + 27\varepsilon^* + 38}{\varepsilon^*(2\varepsilon^* + 1)}\right)\right] - \frac{2}{3}(k_0 R)^3 R_e \left(\frac{\varepsilon^* - 1}{\varepsilon^* + 2}\right)^2 \right\} \quad . \tag{2-38}$$

In the Rayleigh limit, where $kR, k_0 R \ll 1$, the term of R^3 is dominant and the extinction cross-section can be written

$$Q_{ext} = 4\pi k_0 R^3 \, \mathrm{Im} \frac{\varepsilon^* - 1}{\varepsilon^* + 2} \quad . \tag{2-39}$$

By using this extinction cross-section, we find the absorption coefficient of EHD to be

$$\alpha = \frac{4\pi\omega}{c} R^3 N_d \varepsilon_0^{1/2} \mathrm{Im}\left(\frac{\varepsilon^* - 1}{\varepsilon^* + 2}\right) \quad ; \tag{2-40}$$

where N_d is the number of EHD in unit volume. Next we consider the dielectric function of an electron-hole drop. The dielectric function ε is defined as follows :

$$\vec{D} = \overleftrightarrow{\varepsilon} \vec{E} \quad , \tag{2-41}$$

where the dielectric function $\overleftrightarrow{\varepsilon}$ is a tensor in general. It can be calculated from the conductivity tensor by using the equation

$$\overleftrightarrow{\varepsilon} = 1 - \frac{4\pi i}{\omega} \overleftrightarrow{\sigma} \quad . \tag{2-42}$$

In the isotropic system, the dielectric constant can be written as

$$\varepsilon^* = 1 - \frac{\omega_p^2}{\omega(\omega + i/\tau)} \quad ; \tag{2-43}$$

where τ is the relaxation time and ω_p is the plasma frequency. In the case of no damping, or $\tau \to \infty$, we can estimate the frequency of plasma resonance for an electron-hole drop by using equations (2-40) and (2-43); or we have

$$\varepsilon^* = 1 - \frac{\omega_p^2}{\omega} = -2 \, , \tag{2-44}$$

$$\omega = \omega_p/\sqrt{3} \quad .$$

In reality, both electrons and holes have anisotropic masses in germanium, so that it is not easy to calculate the frequency of plasma resonance. We first consider the anisotropy of electron mass. In germanium the energy surface of an electron is

$$\varepsilon(k) = \frac{1}{2m_t} (k_x^2 + k_y^2) + \frac{1}{2m_\ell} k_z^2 \quad . \tag{2-45}$$

The group velocity of the electron is given by

$$\vec{v} = \frac{1}{\hbar} \operatorname{grad}_k \varepsilon(k)$$

$$= \frac{1}{\hbar} \left(\frac{k_x}{m_t}, \frac{k_y}{m_t}, \frac{k_z}{m_\ell}\right) \quad . \tag{2-46}$$

The equation of motion $\frac{d\vec{k}}{dt} = \frac{1}{\hbar} e\vec{E}$ can be written in components as

$$m_t \left(\frac{dv_x}{dt} + \frac{1}{\tau}\right) = eE_x \quad ,$$

$$m_t \left(\frac{dv_y}{dt} + \frac{1}{\tau}\right) = eE_y \quad , \tag{2-47}$$

$$m_\ell \left(\frac{dv_z}{dt} + \frac{1}{\tau}\right) = eE_z \quad .$$

We can obtain the conductivity from these equations as follows:

$$\overleftrightarrow{\sigma} = \begin{pmatrix} \frac{1}{m_t} & & 0 \\ & \frac{1}{m_t} & \\ 0 & & \frac{1}{m_\ell} \end{pmatrix} \frac{ne^2}{\left(i\omega - \frac{1}{\tau}\right)} \quad . \tag{2-48}$$

If the [001] direction is taken as Z axis, four valleys are equivalent. The mass tensor can be written as

$$\overleftrightarrow{\left(\frac{1}{m^*}\right)} = \begin{pmatrix} \frac{1}{3m_t} + \frac{2}{3m_\ell} & 0 & \frac{2\sqrt{2}}{3}\left(\frac{1}{m_t} - \frac{1}{m_\ell}\right) \\ 0 & \frac{1}{m_t} & 0 \\ \frac{2\sqrt{2}}{3}\left(\frac{1}{m_t} - \frac{1}{m_\ell}\right) & 0 & \frac{2}{3m_t} + \frac{1}{3m_\ell} \end{pmatrix} \tag{2-49}$$

The total conductivity is obtained by including the contribution from all valleys, or

$$\sigma = \frac{ne^2}{m_e^{opt}} \frac{1}{i\omega - \frac{1}{\tau}} \quad ; \tag{2-50}$$

where m_e^{opt} is the optical mass of electron and given by $m_e^{opt} = 3/(2/m_t + 1/m_\ell)$. Next we will consider influence of the complicated valence band structure on the dielectric function.[54] An angle dependent mass of the i-th band is defined as

$$\begin{aligned} e^i_{\vec{k}} &= k^2/2m_i(\theta, \phi) \\ &= Ak^2 \pm [B^2k^4 + C^2(k_x^2k_y^2 + k_z^2k_x^2 + k_y^2k_z^2)]^{1/2} \quad ; \end{aligned} \tag{2-51}$$

where $e^i_{\vec{k}}$ denotes the eigenvalue of the i-th band with wave vector $\vec{k}$. The dielectric function within the random-phase approximation (RPA) is as follows :

$$\begin{aligned} \varepsilon^*(\omega) = 1 - \lim_{q\to 0} \frac{4\pi}{2} \sum_{\vec{k}} \sum_{ij} |\rho^{ij}_{\vec{k},\vec{k}+\vec{q}}|^2 \, 2\theta(e^i_F - e^i_k) \\ [1 - \theta(e^i_F - e^{ij}_{\vec{k}+\vec{q}})] \times \frac{e^i_{\vec{k}+\vec{q}} - e^i_{\vec{k}}}{\omega(\omega + i\delta) - (e^i_{\vec{k}+\vec{q}} - e^i_{\vec{k}})^2} \quad ; \end{aligned} \tag{2-52}$$

where e^i_F is the Fermi energy for holes and the indices i and j are summed over the bands. The quantity δ is a positive infinitesimal. Finally, $|\rho^{ij}_{\vec{K},\vec{k}+\vec{q}}|^2$ denotes the matrix element of the density operator between the $\vec{k}$-th state of the i-th band and

the $(\vec{k} + \vec{q})$-th state of the j-th band. The dielectric function can be divided into two parts : one is due to the intervalence band transition and the other the intraband transition :

$$\varepsilon^*(\omega) = 1 - \frac{4\pi}{\omega(\omega + i\delta)} \sum_{\vec{k},j} \frac{\theta(e_F^i - e_{\vec{k}}^i)}{m_i(\theta, \phi)} + \varepsilon^*_{inter}(\omega) \quad . \qquad (2\text{-}53)$$

The effective plasma frequency $\tilde{\omega}_p$ is defined as

$$\tilde{\omega}_p^2 = 4\pi \sum_{\vec{k},i} \frac{\theta(e_F^i - e_{\vec{k}}^i)}{m_i(\theta, \phi)} = 4\pi n(1/m_e^{opt} + 1/m_h^{plas}) \quad ; \qquad (2\text{-}54)$$

where the hole-plasma mass m_h^{plas} is numerically evaluated to be

$$m_h^{plas} = 0.224\ m_0 \quad . \qquad (2\text{-}55)$$

The interband contribution is also calculated as shown in Fig. 9.

II-9. Dielectric Function in Magnetic Fields

Kononenko calculated the dielectric function of EHD in magnetic fields, which is rather complicated due to the anisotropy of the electron energy surface.[80] He assumed the spherical valence bands with light hole and heavy hole. For B // [111], the result is as follows:

$$\varepsilon_{\pm}^* = 1 - 3\left\{\frac{\omega_{01}^2}{\omega(\omega + i/\tau) \mp \omega_{cl}} + \frac{\omega_{03}^2(\omega + i/\tau \pm \frac{m_{e3}}{m_{c3}}\omega_{c3})}{\omega\{(\omega + i/\tau)^2 - \omega_{c3}^2\}} + \frac{\omega_{oh}^2}{\omega(\omega + i/\tau \mp \omega_{ch})} + \frac{\omega_{o\ell}^2}{\omega(\omega + i/\tau \mp \omega_{c\ell})}\right\} \quad ; \qquad (2\text{-}56)$$

where

$$\omega_{01}^2 = \frac{4\pi e^2}{3\varepsilon_0}\frac{n_1}{m_t}, \qquad \omega_{03}^2 = \frac{4\pi n_3}{m_{e3}};$$

$$\omega_{c1} = \frac{eH}{m_t c}, \qquad \omega_{c3} = \frac{eH}{m_{c3} c};$$

$$m_{c3} = \sqrt{\frac{9m_\ell m_t^2}{m_\ell + 8m_t}}, \qquad m_{e3}^{-1} = \frac{4}{9m_\ell} + \frac{5}{9m_t};$$

$$\omega_{oh}^2 = \frac{4\pi e^2}{3\varepsilon_0}\frac{n_h}{m_{hh}}, \qquad \omega_{o\ell}^2 = \frac{4\pi e^2}{3\varepsilon_0}\frac{n_\ell}{m_{\ell h}};$$

$$\omega_{ch} = -\frac{eH}{m_{hh} c}, \qquad \omega_{c\ell} = -\frac{eH}{m_{\ell h} c};$$

n_1, n_3, n_h and n_ℓ are the densities of one-valley electron, three-valley electron, heavy hole and light hole, respectively.

The calculated results of $\varepsilon_\pm$ at 420 μm are shown in Fig. 10. This simple treatment of the valence bands is not adequate to explain the observed magnetoplasma absorption. More realistic structure of the valence bands is necessary to be taken into account. If the dielectric function is not scalar, the values of ε_+ and ε_- are usually employed in the analysis of the absorption by the spherical obstacles. This is called the Cardona approximation.

The generalization is given by Ford and Werner of the classic Mie scattering problem to the case where the dielectric constant is a tensor having axial symmetry.[81] The amplitudes of the scattered spherical waves are found to be expressible in the form of a series of ratios of determinants. Their result gives

Mie's theory in the case of scalar dielectric function and leads to their previous result[38] in the Rayleigh limit, which is given by

$$P_{mag} = \frac{1}{2}\omega \, \mathrm{Im}\, \vec{M} \cdot \vec{B}_1^* \, ,$$

$$P_{elect} = \frac{1}{2}\omega \, \mathrm{Im}\, \vec{P} \cdot \vec{E}_1^* \qquad (2\text{-}57)$$

with

$$\vec{M} = \frac{R^5}{30}\left(\frac{\omega}{c}\right)^2 \sum_{m=-1}^{+1} \frac{\varepsilon_m^{(eff)}}{1 - \frac{21}{2}\left(\frac{\omega R}{c}\right)^2 \varepsilon_m^{(eff)}} \hat{e}_m^* \cdot \vec{B}_1 \, \hat{e}_m \qquad (2\text{-}58)$$

and

$$\vec{P} = -\frac{1}{2}R^3 \sum_{m=-1}^{+1} \left(1 - \frac{3\varepsilon_m}{\varepsilon_m + 2 - \frac{1}{5}(\omega R/c)^2 \varepsilon_m}\right) \hat{e}_m^* \cdot \vec{E}_1 \, \hat{e}_m \, ; \qquad (2\text{-}59)$$

where

$$\varepsilon_{m=\pm 1}^{(eff)} = 2\varepsilon_{\pm 1}\, \varepsilon_0 / (\varepsilon_{\pm} + \varepsilon_0) \qquad (2\text{-}60)$$

and

$$\varepsilon_{m=0}^{(eff)} = 2\varepsilon_{+1}\, \varepsilon_{-1} / (\varepsilon_{+1} + \varepsilon_{-1}) \qquad (2\text{-}61)$$

with ε_m defined by

$$\varepsilon_{\pm 1} = \varepsilon_{xx} + i\varepsilon_{xy} \, ,$$

$$\varepsilon_0 = \varepsilon_{zz} \, . \qquad (2\text{-}62)$$

Here, P_{elect} and P_{mag} are the mean powers absorbed by the sphere,

E_1 and B_1 are electric and magnetic fields of incident radiation, respectively.

II-10. Magneto-Oscillation of FIR Absorption

We will calculate the influence of the carrier pair density on the far-infrared absorption coefficient. In the Rayleigh limit, the absorption coefficient by EHD with the radius R is given by

$$\alpha = \frac{4\pi\omega}{c} R^3 N_d \varepsilon_0^{1/2} \mathrm{Im}\left(\frac{\varepsilon^* - 1}{\varepsilon^* + 2}\right) \quad . \tag{2-63}$$

Here N_d is the number of EHD in unit volume. As the electron-hole pair number ν in one EHD is related to the carrier pair density n by $4\pi R^3 n/3 = \nu$, the absorption coefficient α can be written

$$\alpha = 3 \frac{\omega\nu}{cn} N_d \varepsilon_0^{1/2} \mathrm{Im}\left(\frac{\varepsilon^* - 1}{\varepsilon^* + 2}\right) \quad . \tag{2-64}$$

The relation between ν and n becomes definite if one knows the drop radius R which is attainable from the kinetic equations for EHD and excitons. Since the evaporation of excitons from EHD can be neglected at low temperatures, the rate equations in steady state are written as follows :

$$\frac{dn_{ex}}{dt} = G_{ex} - b\, n_{ex} \nu^{2/3} N_d - \frac{n_{ex}}{\tau_{ex}} = 0 \tag{2-65}$$

and

$$\frac{d\nu}{dt} = b\, n_{ex}\, \nu^{2/3} - \frac{\nu}{\tau_0} = 0 \tag{2-66}$$

In the limit of high excitation, where $G_{ex} >> n_{ex}/\tau_{ex}$, one obtains

$$\nu = \frac{G_{ex}}{N_d} \tau_0 \quad . \tag{2-67}$$

The absorption coefficient is rewritten by this relation as follows :

$$\alpha = \frac{3\omega}{c} \varepsilon_0^{1/2} \frac{G_{ex}\tau_0}{n} \mathrm{Im}\left(\frac{\varepsilon^* - 1}{\varepsilon^* + 2}\right) \quad . \tag{2-68}$$

Neglecting the recombination at impurities, one can write the inverse total lifetime as

$$\frac{1}{\tau_0} = Bn + Cn^2 \quad ; \tag{2-69}$$

where B and C are constants. According to Betzler et al., the coefficients B and C are 3×10^{-14} cm^3 s^{-1} and 4×10^{-31} cm^6 s^{-1}, respectively.[40] If we write G(n) for $\mathrm{Im}[(\varepsilon^* - 1)/(\varepsilon^* + 2)]$, the absorption coefficient can be written as

$$\alpha = A \frac{G(n)}{n^2(B + Cn)} , \qquad \text{with } A = \frac{3\omega}{c} \varepsilon_0^{1/2} G_{ex} \quad . \tag{2-70}$$

The correction $\Delta n(H)$ of the carrier pair density induces the variation $\Delta\alpha(H)$ of the absorption coefficient, whose ratio to the zero field value α_0 is

$$\frac{\Delta\alpha}{\alpha_0} = \left(-2 - \frac{Cn_0}{B + Cn_0} + \frac{G'(n_0)}{G(n_0)} n_0\right) \frac{\Delta n(H)}{n_0} \tag{2-71}$$

First we calculate $G'(n_0)/G(n_0)$. For zero magnetic field

ε^* takes the form

$$\varepsilon^* = 1 - \frac{\omega_p^2}{\omega(\omega + \frac{i}{\tau})} \quad ; \tag{2-72}$$

where ω_p is the plasma frequency, which is given by $\omega_p^2 = 4\pi e^2 n_0/\varepsilon_0 (1/m_e^{opt} + 1/m_h^{plasma})$. In terms of Eq. (2-72), $G'(n_0)/G(n_0)$ can be written

$$\frac{G'(n_0)}{G(n_0)} = \frac{\omega^4 - \frac{1}{9}\omega_p^4 + \omega^2/\tau^2}{\{(\omega^2 - \frac{1}{3}\omega_p^2)^2 + \omega^2/\tau^2\} n_0} \quad . \tag{2-73}$$

The relative variation of the absorption coefficient then becomes

$$\frac{\Delta\alpha}{\alpha_0} = (-2 - \frac{Cn_0}{B + Cn_0} + \frac{\omega^4 - \frac{1}{9}\omega_p^4 + \omega^2/\tau^2}{\{(\omega^2 - \frac{1}{3}\omega_p^2)^2 + \omega^2/\tau^2\}}) \frac{\Delta n(H)}{n_0} \quad . \tag{2-74}$$

Making use of the values $n_0 = 2.1 \times 10^{17}$ cm^{-3}, $B = 3 \times 10^{-14}$ cm^3 s^{-1} and $C = 4 \times 10^{-31}$ cm^6 s^{-1}, we next calculate $\tilde{\alpha}(\omega) = (\Delta\alpha/\alpha_0)/(\Delta n(H)/n_0)$ as a function of ω for various damping constants as shown in Fig. 11. As can be seen from this figure, $\tilde{\alpha}(\omega)$ undergoes a drastic change near the plasma resonance frequency $\omega_p/\sqrt{3}$ (138 μm), and its sign reverses itself for small damping constant $\hbar/\tau$, causing inversion between peaks and dips of the oscillation. With $\hbar/\tau = 2$ meV, for example, $\tilde{\alpha}(\omega)$ is changing from -6.1 at 171 μm to +2.2 at 119 μm. At the magnetic fields satisfying Eq. (2-30), the far-infrared absorption is indeed minimized for 171 μm.

II-11. Magneto-Oscillation of Luminescence and Time Dependent Oscillation Amplitude

The total luminescence intensity is given by

$$I = Bn\nu \quad . \tag{2-75}$$

From Eqs. (2-67) and (2-69), the total luminescence intensity under the steady excitation will have the form

$$I \propto \frac{1}{B + Cn} \quad . \tag{2-76}$$

When n changes from n_0 to $n_0 + \Delta n(H)$, the relative variation of I is

$$\frac{\Delta I}{I_0} = - \frac{Cn_0}{B + Cn_0} \frac{\Delta n}{n_0} = -0.74 \frac{\Delta n}{n_0} \quad . \tag{2-77}$$

Comparing Eq. (2-74) with Eq. (2-77), we find that the dips of far-infrared absorption for 171 μm corresponds to those of luminescence intensity and the oscillation amplitude of far-infrared absorption is several times as large as that of luminescence intensity.

We will next consider the time dependence of the oscillation amplitude of far-infrared absorption and that of luminescence intensity. Betzler et al. calculate the oscillation amplitude of the total luminescence at time t after shutting off the excitation to be[40)]

$$\frac{\Delta I}{I_0} = - \{-1 + n_0 (B + 2Cn_0) t\} \frac{\Delta n}{n_0} \quad . \tag{2-78}$$

As $\Delta I/I_0$ is zero at $t = 20$ μs, the content of the curly bracket should then vanish, whence the inversion of peaks and dips occurs.

In the case of far-infrared absorption, EHD retains its stationary form during the long pulse excitation; then, after shutting off excitation, EHD decays according to the equation

$$\frac{d\nu}{dt} = - \frac{\nu}{\tau_0} \quad . \tag{2-79}$$

The solution of this simple equation is

$$\nu = \nu(0) \exp(-t/\tau_0) \quad . \tag{2-80}$$

The absorption coefficient is given by

$$\begin{aligned} \alpha(t) &= A \frac{\nu}{n} G(n) = A \frac{\nu(0) \exp(-t/\tau_0)}{n} G(n) \\ &= \alpha(0) \exp(-t/\tau_0) \quad . \end{aligned} \tag{2-81}$$

The change in pair density n influences $\alpha(t)$ through the relation

$$\frac{\Delta\alpha(t)}{\alpha(t)} = \frac{\Delta\alpha(0)}{\alpha(0)} + \frac{\Delta \exp(-t/\tau_0)}{\exp(-t/\tau_0)} \quad . \tag{2-82}$$

From Eqs. (2-69) and (2-71) we have

$$\frac{\Delta\alpha(t)}{\alpha(t)} = -\frac{\Delta n}{n_0}\left\{2 + \frac{Cn_0}{B + Cn_0} - n_0\frac{G'(n_0)}{G(n_0)} + n_0(B + 2Cn_0)t\right\} . \quad (2\text{-}83)$$

For 171 μm and at low magnetic fields, one obtains

$$\frac{\Delta\alpha(t)}{\alpha(t)} = -\frac{\Delta n}{n_0}\{a_1 + a_2 t\} , \quad (2\text{-}84)$$

with $a_1 = 6.1$ and $a_2 = 4.2 \times 10^4\ s^{-1}$.

Equation (2-84) leads us to the conclusion that the inversion of peaks and dips of oscillation does not occur in the far-infrared experiment. It is further seen that the time dependent part of the oscillation amplitude is much smaller in magnitude than the total oscillation amplitude.

II-12. Plasmon Damping

Several different mechanisms are counted for the relaxation of carriers in the electron-hole drop.[33] We first find single-particle processes —— collisions of carriers with each other, with the phonons, with the impurities, and with the EHD boundaries. We then find collective relaxation processes in which the plasmon transfers all its energy to the photon (radiative damping) or to an individual carrier (Landau damping). Among these processes, elelctron-hole scattering and Landau damping are most important. First we will consider electron-hole scattering which was treated by several authors. Landau calculated the damping of zero sound in the Fermi liquid and obtained the damping factor[82]

$$\gamma = \gamma_{c\ell}\left[1 + \left(\frac{\hbar\omega}{2\pi K_B T}\right)^2\right] , \qquad (2\text{-}85)$$

when $E_F >> \hbar\omega \gtrsim k_B T$.

For $\hbar\omega \gtrsim E_F$, one finds some theories, one of which was given by Lee-Whiting.[83] They calculated the loss of electrons travelling through a degenerate free electron gas. Their result is such that the damping becomes maximum near twice at the Fermi energy and the amount of damping is about the Fermi energy. At very high frequencies the damping falls off as $(\hbar\omega)^{-3/2}$.

A calculation of the conductivity of an electron-hole plasma was recently developed by Tzoar and Platzman using the temperature dependent Green's-function formalism.[84] They evaluated the frequency dependence of the resistivity for several r_s values and electron-hole mass ratio, considering isotropic bands. Zarate et al. applied the theory of Tzoar and Platzman to the case of germanium.[85] Not only the anisotropy of the conduction band but also intervalence band transition is included in their calculation. Their results are shown in Fig. 12. They compared their calculated results with their experimental results. The calculated damping is smaller by a factor of 1.4 than the experimental. They believe the discrepancy to have been caused by the static approximation taken in their calculation.

Another effective damping is the Landau damping. It was first pointed out by Kononenko and Murzin.[33] EHD has finite

radius and so plasmon has uncertainty of wavevector by $\hbar/R$. The plasmon with large wavenumber damps fast. The damping constant is given by

$$\gamma_L \approx \frac{e^2}{R} \frac{(E_F)^{3/2}(E_F + \omega_p/\sqrt{3})^{1/2}}{\frac{1}{3}\omega_p^2} \tag{2-86}$$

For EHD with R = 2 μm, this constant can be evaluated to be 1 meV.

III. Experimental Procedure

The samples used in this experiment are pure, Sb-doped and In-doped Ge. Impurity concentrations of Sb-doped samples are 5.1×10^{13}, 1.3×10^{14}, 8.6×10^{14} and 4.5×10^{15} cm^{-3} and that of In-doped one is 8×10^{15} cm^{-3}. Sample dimensions are $3 \times 4 \times (0.5 \sim 1.5)$ mm^3, having some variety in thickness. The sample surfaces were first polished mechanically with Syton or alumina powder and then chemically etched in the solution of CP-4.

We use two kinds of experimental set-up (see Fig. 13 and Fig. 14). The heart of the first kind set-up consists of a pulsed far-infrared laser and a xenon flash lamp, while the second consists of an optically pumped laser and an argon ion laser. Both systems will be described to some detail.

The xenon flash lamp has a pulse width of $\sim$ 1 μs and the repetition rate is 15 or 10 Hz. The total energy yield per pulse is expected to be of the order of 10^{-1} Joule. Light from the lamp has strong spikes peaking at the wavelength of 0.87 μm (1.4 eV), 0.91 μm (1.4 eV) and 0.98 μm (1.3 eV) and those photon energies are near the band gap energy of germanium (0.98 eV). It is expected then that the quantum efficiency to produce high density of electrons and holes is sufficiently large.

In the first kind of experimental set-up, we use pulsed molecular far-infrared laser. This laser cavity consists of Pyrex glass tube and two concave mirrors. The diameter of the tube is 8 cm and the distance between two mirrors is 2 m. The radius of curvature of the mirrors is 4 m and one mirror is

placed on the translational base and the alignment of making two mirrors pararell can be made by three micrometers attached to the holder of the other mirror. This is done by He-Ne laser. In order to minimize the fluctuation in distance between the two mirrors, we use invar rods on account of their very low thermal expansion coefficient. The back pressure of the cavity is several tens of milli-torr, which is obtained by 300 ℓ/min rotary pump. The gases used for laser oscillation are H_2O, D_2O, HCN and DCN, the pressure of which is kept $\sim$ 200 m Torr. The gas flows during the operation. The value of this flow is controlled by a needle valve between the cavity and the gas container. In order to excite the oscillation medium, we use high voltage discharge.

For electrodes, a stainless-steel corn is used as cathode while a copper tube as anode. The voltage of the pulse is 6 kV, the duration is 100 μs and the repetition rate is 20 or 30 Hz. By this excitation we obtain laser pulse with the pulse width of 50 μs. The output radiation comes from the 2 mm coupling hole in the center of the concave mirror and through the mylar window. The beam is guided by brass light pipe into the window of cryostat. As a result we have several lines of far-infrared radiation, 84 (D_2O), 119 (H_2O), 172 (D_2O), 190, 195 (DCN), 220 (H_2O), 311, and 337 μm (HCN). We can distinguish the lines by translating the mirror and tunable detector.

The sample is placed in the 7 T or 5 T superconducting magnet. The 7 T magnet is a solenoid with the bore diameter of 12 mm. One of the two 5 T magnets is a solenoid while the other

is a rotatable split coils. All the 5 T magnets have the bore of 20 mm diameter. The excitation light is guided onto the surface of sample by a silica rod whose diameter is 3 mm. For a detector we use Sb-doped Ge (the impurity concentration is 1.3×10^{14} cm^{-3}) and n-InSb placed in the persistent current driven superconducting magnet (see Fig. 15). The signal from the detector is amplified by video-amplifier with the bandwidth up to 500 kHz, and then is averaged in boxcar integrators. In order to eliminate the effect of the laser fluctuations, use is made of a logarithmic amplifier which gives us the ln A/B-type output. The repetition of the pulsed FIR laser is 20 or 30 Hz and that of excitation light is 10 or 15 Hz so that the absorption by photo-excited carriers occurs at every other FIR pulse. Two boxcar integrators are used and the gate of one boxcar is open in the time of no absorption. The positions of the two gates can be moved simultaneously by the time delay circuit. Two signals from the boxcar integrators are divided between them and transformed into a logarithm. The output power after going through the sample with thickness d and absorption coefficient α is reduced by $\bar{e}^{\alpha d}$. The signal from the logarithmic amplifier is directly proportional to the absorption coefficient. The data are recorded by an XY recorder.

Most of the experiments are made below 4.2 K. A rotary pump is used to obtain the temperature lower than 4.2 K. The temperature is monitored by Hg manometer. For the measurements above 4.2 K, we use the double tube cryostat, whose sample holder is shielded by vacuum room from the liquid helium and

the temperature is monitored by Au-Fe thermocouple. The temperature is varied from 4.2 to 20 K by the use of a heater.

In the second kind of experimental set-up, an argon ion laser is employed for excitation light. Its power is about 3 W and the wavelength is 5145 Å. Long time stabilization is achieved by a feed-back system. The laser beam is chopped by acoustic optical modulator. The pulsewidth is 0.2 msec and the repetition rate is 180 Hz. After reflections at flat mirrors, the excitation light is focused onto the glass rod by a convex lens. This glass rod is specially made and has double cores in order to minimize the transmission loss. Other apparatus in the cryostat are the same as used in the before-mentioned set-up.

The source of far-infrared radiation is optically pumped far-infrared laser (see Fig. 16). This type laser was invented by Chang and Bridges in 1970.[86)-88)] As one can obtain many high power lines in the wavelength region of 40 μm ∿ 1.8 mm, it has become more popular than a discharge type laser. It consists of two parts, one is a CO_2 laser and the other FIR cavity. We have used two CO_2 lasers, one is home-made and the other a commercial unit. The first CO_2 laser, or the home-made one, has a pyrex tube whose length is 1.1 m and inner diameter is 15 mm. In order to prevent heating, the glass tube is covered by water jacket. The gas for laser oscillation is mixed one. $He : N_2 : CO_2 = 80 : 15 : 5$. It has three electrodes and the voltage of excitation is 8 kV and current is 40 mA. The radius of curvature of an gold coated inner mirror is 8 m. For a Brewster window we use KCl. The grating is employed in order to select the wavelength.

We used the grating with 90 grooves per mm. The first order diffraction beam goes back to the inner mirror for laser oscillation and the zeroth order beam comes out of the grating as the output. In order to prevent the thermal damage of grating and obtain high peak power, internal chopping is efficient. The duty ratio of this chopper is 10 and the repetition rate is 80 or 60 Hz. The CO_2 laser oscillates at about 100 different wavelengths. Each line is denoted by the quantum number of CO_2 molecule for example 9 R (20), 10 P (16), etc..

The beam of the CO_2 laser is reflected twice by plane mirrors and focused into the coupling hole of FIR cavity by concave mirror with radius of curvature of 60 cm. FIR cavity is 1 m long and the diameter is 10 cm. It has two mirrors, one is plane brass mirror, and the other concave brass mirror with R = 2 m. Both of them have a 3 mm coupling hole. The plane mirror is translational and the angle of the concave mirror can be aligned by three micrometers. The distance between two mirrors is fixed by invar rods. The window for input is KCl and that for output is polystylene.

The gases used for laser oscillation are CH_3OH, CH_3OD, CD_3OD, CH_3NH_2 and CH_3COOH. The pressure of gas is about 50 $\sim$ 150 m Torr. The wavelengths and the kinds as well as pressures of gases are tabulated in Table III. The commercial CO_2 laser has two ZnSe Brewster windows and the output beam is derived from concave half mirror made of ZnSe. The power of each line is 10 $\sim$ 20 W. At the use of this commercial unit, all the KCl windows have been replaced by ZnSe windows and the concave

mirror, with which the radiation of the CO_2 laser is focused in, has been replaced by ZnSe lens.

The mechanical vibration gives fatal fluctuation of output FIR power. Combination of granite with rubber has been successful in obtaining enough stability.

In this system we use a 2 channel Boxcar integrator whose gates are open before and during the absorption.

IV. Experimental Result

IV-1. Temperature Dependence of Spectra

In our experiments, three kinds of signals, magnetoplasma absorption by EHD, inter-discrete level absorption by exciton and cyclotron resonance of free-carriers, are observed. The typical data are shown in Fig. 17. With decrease of temperature, the dominant signal is taken turns by free hole, exciton and EHD in this order.

The cyclotron resonance of free hole is complicated because it reflects the complex structure of the valence band. The detailed study of quantum cyclotron resonance was done by Hensel and Suzuki[1] in the microwave region, while in far-infrared absorption a little information has been obtained. Muro and Nisida assigned the hole quantum cyclotron resonance observed in far-infrared region.[45]

The sharp peak at 7 K shown in Fig. 17 corresponds to the transition $2_0 \rightarrow 1_1$, after the use of the notation of Hensel and Suzuki.[1] The information necessary for assignment is obtained by changing temperature and comparing the intensity of absorption peaks. The linewidth of this quantum cyclotron resonance is dominated by electron-hole, hole-hole and hole-exciton scattering at this temperature.

The assignment of excitonic peaks is more difficult than that of hole quantum cyclotron resonance. This was tried by Fujii and Otsuka,[34] and Muro and Nisida.[45] The dependence of the peak positions on the wavelength of incident radiation helps us assign these excitonic peaks. The features of exciton absorption

lines are shown in Fig. 18 for various wavelengths.

The magnetic fields of excitonic peaks are plotted in Fig. 19. As seen from this figure, the large peak of exciton observed at 119 μm is parallel to the hole cyclotron resonance line $2_0 \rightarrow 1_1$ in magnetic fields. It seems that the excitonic peak corresponds to the transition 2_0 to 1_1 of the hole which composes the exciton. Since this transition corresponds to $1S \rightarrow 2P_-$ transition, the oscillator strength is the largest among the allowed transitions. The intensity of this absorption peak increases with magnetic field. This fact has been explained in II. Fujii obtained good agreement between experiment and calculation in which he used the Kohn-Luttinger type wave function for the ground state trial function and Yafet-Keys-Adams type function for the excited state.[90] In Fig. 19 his experimental results and our newly observed data are shown.

The absorption by EHD shown in Fig. 17 is plasma resonance. As mentioned in II, the plasma resonance of EHD occurs at $\lambda = 138$ μm in the simple theory, which is calculated by the equation $\varepsilon^* = -2$. As 119 μm is near this wavelength, a large amount of absorption can be expected in zero magnetic field. In magnetic fields, Ford et al.'s theory gives us the absorption by EHD.[38] The detailed structure of this absorption will be discussed below by using their theory. The magnetoabsorption by EHD at 119 μm is very broad. This is due mainly to the frequency dependent damping of plasmon by electron-hole scatterings.

IV-2. Ionization of Excitons

More detailed temperature dependence of exciton and free hole is shown in Fig. 20. Temperature dependence of the intensity of the hole quantum lines is slightly different from each other. The linewidth of a quantum line broadens at temperatures higher than 10 K. The broadening seems to be due to hole-phonon scatterings. The linewidth is plotted in Fig. 21 as a function of temperature. The summary of this experiment is described in Fig. 22. As seen in this figure, free carriers and excitons exist above 5 K and below 4 K EHD and excitons mainly exist. Above 5 K, excitons dissociate thermally into free electrons and holes, so that this figure gives us an idea of the binding energy of exciton —— 2.8 meV. This value is somewhat lower than the recently calculated value of light mass exciton —— 3.25 meV.

Below 4 K, few free carriers are left and the number of excitons decreases with decreasing temperature. We can obtain only a part of the phase diagram, since the absolute value of the exciton density is difficult to estimate.

IV-3. Critical Temperature of EHD

It is well known that the critical temperature of EHD is about 6 K. We will show the drastic change of some physical properties associated with this phase transition. Figure 23 shows the typical variation of absorption in low magnetic field at 119 μm in the course of changing temperature. It forces us to imagine the phase transition near 5 K. The absorption at temperatures higher than 5 K is due to inter-valence band transition. The second evidence of this phase transition

is the temperature dependence of exciton density. Figure 24 shows the result of an experiment, which gives us a kink near 6.3 K. At temperatures higher than 6.3 K, the exciton density strongly depends on temperature. The last evidence is observed in decay kinetics. We monitor the exciton peak and the background signal observed at 119 μm. The result is shown in Fig. 25. At the temperatures below 6 K, both the exciton signal and the background reveal non-exponential decay. Above 6 K, both of them decay exponentially. When electron-hole drops exist, terms of evaporation and backflow contribute to the non-exponential decay. From these three experimental results, one can conclude that the critical temperature is about 6 K. The theoretical values of the critical temperature ranges in 5 ∿ 8.7 K and the observed value in luminescence is 6.5 K.[91] Our value thus seems to be reasonable.

Character of the first order gas-liquid transition is shown in Fig. 26. As the intensity of excitation increases, the absorption by EHD increases somewhat but the exciton signal shows little change. This feature shows that for exciton densities higher than the critical density the transition to EHD occurs so promptly that the exciton density practically keeps constant.

IV-4. Kinetics of Coexisting Excitons and EHD

The decay kinetics of EHD and excitons can be studied by the signals observed at 84 and 119 μm. Typical traces of magneto-absorption are shown in Fig. 27 for the wavelength of 84.3 μm at various delay times.

The peak near 5 T is the same exciton line as observed at 119 μm and we take it as the monitoring signal for the exciton system. Absorption due to EHD appears as a broad background near the magnetic field of 5 T. The EHD absorption decays steadily with time, while the excitonic transition seems to stay nearly flat for a certain initial period of time after the light pulse. This feature is shown in Fig. 28 as obtained for 3.6 K. The general trend is nearly independent of excitation power and to some extent of temperature. The variation of the exciton signal with temperature is shown in Fig. 29.

A simple explanation for the existence of the plateau of the exciton signal is that during the existence of EHD, free excitons are provided from EHD through evaporation, thus tending to keep the amount of excitons from decreasing.

The rapid decay of the excitonic signal in Fig. 28 after $\sim$ 50 μs then indicates disappearance of EHD.

We shall confine our analysis within the plateau region. The requirement n_{ex} = constant, or $\dot{n}_{ex} = 0$ yields

$$n_{ex} = aN_d T^2 \nu^{2/3} \exp(-\phi/kT)/(1/\tau_{ex} + bN_d \nu^{2/3}) \quad , \qquad (4\text{-}1)$$

Since ν is time dependent, constancy of n_{ex} is guaranteed only if $1/\tau_{ex} \ll b\nu^{2/3}$, when

$$n_{ex} = (a/b) T^2 \exp(-\phi/kT) \quad . \qquad (4\text{-}2)$$

Since $b \propto \langle v_{ex} \rangle \propto T^{1/2}$, where $\langle v_{ex} \rangle$ is the thermal velocity of

the exciton, one may expect

$$n_{ex} \propto T^{3/2} \exp(-\phi/kT) \quad . \tag{4-3}$$

Comparison with experimental observation yields the value of 14.7 K for the work function ϕ.

The ϕ value thus derived cannot be temperature dependent as in our former analysis and is somewhat lower in absolute magnitude.[20] Perhaps the present analysis is too crude for precisely deriving a physical quantity. The above derivation is just to see the general adequacy of our decay-kinetics treatment, which is valid only for the time interval during which n_{ex} is nearly constant and further under some convenient assumptions.

The apparent decay time of the EHD signal varies from 11.5 μs at 4.2 K to 24 μs at 3.3 K. This is not the internal electron-hole recombination time τ_0. The relative abundance of excitons at higher temperatures tends to shorten the apparent decay time of EHD.

Whenever ν is small, τ_{ex} is directly observable through the time variation of the exciton signal. The exciton evaporation from EHD, however, cannot entirely be neglected at higher temperatures and this tends to make the apparent exciton lifetime longer. One finds, for example, 6 μs of the excitonic decay time at 3.3 K and 10 μs of that at 4.2 K.

IV-5. Magneto-plasma Resonance of EHD

At 2 K the main signal observed in far-infrared absorption is plasma resonance by electron-hole drops.

Typical resonance traces are shown in Fig. 30 for several wavelengths. For pure Ge, observed peaks are classified into seven branches. We denote them D_1 to D_7. The magnetoplasma resonance of EHD is analyzed by Ford et al.'s theory.[38)]

For B // [111] there are two kinds of valleys of electrons and two kinds of holes in a simple model. The density of electrons residing at each valley and that of each kind of holes do not keep constant in magnetic fields. We calculate them according to the following equations :

$$n_{d1} = \frac{2^{1/2} eH}{\hbar^2 c} \frac{\sqrt{m\ell}\, m_t}{m_c} \sum_{\ell} (E_F - (\ell + \tfrac{1}{2})\hbar\omega_{c1} \pm g_1^* \mu_B H)^{1/2} \qquad (4\text{-}4)$$

and

$$n_{d3} = 3 \frac{2^{1/2} eH}{\hbar^2 c} \frac{\sqrt{m\ell}\, m_t}{m_c} \sum_{\ell} (E_F - (\ell + \tfrac{1}{2})\hbar\omega_{c3} \pm g_3^* \mu_B H)^{1/2} \qquad (4\text{-}5)$$

with

$$n_d = n_{d1} + n_{d3} \; ; \qquad (4\text{-}6)$$

where the subscripts 1 and 3 denote the "one valley", whose axis is directed along the magnetic field, and the "three equivalent valleys", respectively. For heavy and light holes it is assumed that the Fermi surface is spherical. The same analyses as to the electrons in the drop are applied to the holes in the drop. The derived values of $n_{\ell 1}/n$, and $n_{\ell h}/n$ are shown in Fig. 31.

We calculate the peak position including mass renormalization

and give it by dotted line and broken line in Fig. 32. In our assignment, D_2, D_3 and D_7 are resonances by electric waves, while D_1 that by magnetic waves. D_4, D_5 and D_6 are independent of laser frequency. We ascribe them to the magneto-oscillation of drops. In the previous paper[46,47] we assigned D_2 to magnetic dipole resonance and both D_1 and D_3 to electric dipole resonances after observing the decay process of absorption at 337 μm. We have measured the lifetimes of D_2 and D_3 for several wavelengths in order to test the above conclusion. The decay profiles of magnetoplasma resonance for 420 μm are shown in Fig. 33. From the time-resolved observation of D_2 and D_3 for some wavelengths, we obtain lifetimes of D_2 and D_3 at different strengths of magnetic field (see Fig. 34). The lifetime certainly depends on the magnetic field but there is no difference in lifetime between D_2 and D_3. It is very likely then that both D_2 and D_3 are electric dipole resonances in contradictions with our previous conclusion.

The linewidth of magnetoplasma resonance gives us the damping of plasma oscillation. Fujii observed the temperature dependence of peak D_3 at 337 μm.[46] And he concluded that it depends on temperature in the form of $a + bT^2$ and the width is due mainly to electron-hole scattering. We examine this result at 513 μm, at the wavelength of which the peak is well separated from other peaks. It leads to the same conclusion as Fujii's. We also investigate the wavelength dependence of linewidth of magneto-plasma resonance. Figure 35 shows the results. The linewidth of D_3 increases with frequency of far-infrared radiation;

while that of D_2 gets minimum near the wavelength of 400 μm. The behavior of linewidth of D_3 can be understood by electron-hole scattering but the behavior of D_2 is not clear.

The peak height of the magnetoplasma resonance gives us the magnetic field dependence of the carrier pair density. The observed peak height is shown in Fig. 36. It decreases at higher magnetic fields. This indicates increase of the carrier pair density. The tendency was predicted by Keldysh and Onishcenko[29] and has actually been observed in luminescence measurements.

IV-6. Magneto-oscillation of EHD

The observed magneto-oscillations in the far-infrared absorption by EHD in the course of excitation are shown in Fig. 37 for the wavelength of 171 μm. These signals are similar to the magneto-oscillations in the integrated intensity of the recombination photoluminescence line or to those in the integrated far-infrared magnetoabsorption. The dips in absorption occur at the magnetic fields near which the Landau levels with indicated quantum numbers of the light cyclotron mass electron intersect the Fermi level. We can calculate the Fermi energy E_F from these data with the help of Eq. (2-30). It is true that E_F depends a little on direction and strength of the magnetic field. But at low magnetic fields, E_F is found to be 2.5 meV without consideration of mass renormalization. This value of the Fermi energy yields a carrier pair density of $n = 2.3 \times 10^{17}$ cm^{-3}. If the possible mass renormalization is included ($m_t^* = 1.15\ m_t$, $m_\ell^* = 0.96\ m_\ell$),[92] E_F and n reduce to 2.2 meV and to 2.1×10^{17} cm^{-3},

respectively.

There are some peaks and dips of magnetoabsorption above 2 T. As the peaks of magnetoplasma resonance start overlapping there with magneto-oscillations, assignment of the oscillations becomes difficult. We presume that both the dip near 3.5 T for B // [111] and the one near 4 T for B // [110] correspond to the $\ell = 0$ Landau level of the light mass electron crossing the Fermi level, and that the large peak denoted by D_4 corresponds to the density minimum between 4 and 5 T shown in Fig. 7. This large peak is observed over the entire range of laser wavelength from 171 to 513 μm. For wavelengths shorter than 171 μm, we cannot observe it, however. This fact can be explained by the calculation developed in II. The oscillation amplitude decreases promptly as the laser wavelength becomes shorter than the wavelength corresponding to the plasma resonance.

The feature in magneto-oscillation observed at the wavelength of 119 μm is different from that observed at 171 μm. Magneto-oscillatory signals at this wavelength are observed by rotating the magnetic field around a fixed crystallographic axis [110]. The results are shown in Fig. 38. The magnetic field positions for the occurrence of dips change like hole quantum cyclotron resonance rather than electron cyclotron resonance on rotating the magnetic field. This fact indicates that the observed oscillatory signals arise from hole quantum effects on magneto-plasma resonance as Kononenko and Murzin insist.[33]

The way of calculation by Kononenko and Murzin is as follows.[33] They took into account the real quantum spectra obtained in Ref . 1)

of the holes in the magnetic field. In the course of computation with each of the filled j-th Landau subband (at fixed n and H) was associated its own type of isotropic carriers, and consequently, its own Drude-type term. This procedure is equivalent to taking account of the transitions of the carriers within the heavy- and light-hole branches.

Allowance for the actual structure of the valence band of Ge in a magnetic field permitted them to give a fairly good account of both the locations of the maxima and the structure of the measured spectra of the magneto-plasma resonance in EHD.

Their peaks D_{p1} and D_{p2} are also found in our measurements but we have more detailed structure (see Fig. 38 for D_{p1}). Accordingly it is necessary to adopt a more realistic structure of the valence band.

The damping feature of oscillation amplitude as observed for B // [100] and shown in Fig. 39 is almost the same as that calculated, suggesting that the broadening of each Landau level due to collisions is small in comparison with broadening by temperature. The effect of collision broadening is taken into account by a damping factor, which was first introduced by Dingle.[93] This damping factor can be written as $\exp(-2\pi^2 kT_D/\hbar\omega_i)$ with T_D being called the Dingle temperature. Thus the collision- and temperature-broadenings produce similar type effects on the oscillations. Our calculation explains the experimentally observed damping well by simply setting our temperature parameter equal to 2.0 K, the experimental bath temperature. This is indeed showing that the collision-broadening is negligible in comparison

with temperature-broadening; in other words, the Dingle temperature can be ignored. As a matter of fact, the experimental result of RF mobility, $\mu = (0.5 \text{ —— } 2) \times 10^6 \text{ cm}^{-2} \text{ v}^{-1} \text{ s}^{-1}$, gives us $\hbar/\tau = 10^{-3}$ meV. This value is much smaller than $k_B T = 0.17$ meV.

It is shown in Fig. 30 and in Fig. 40 that magneto-oscillations are also observed at wavelengths 184 to 233 μm for B // [111] and 146 to 184 μm for B // [100] in the same magnetic field range as that for 171 μm. The magnetic fields whose dips occur are independent of laser wavelength (see Fig. 41). This makes us confident that the observed oscillations are not fine structures of a magnetoplasma resonance. The oscillation amplitudes start decreasing for the laser frequency somewhat higher than the plasma resonance frequency $\omega_p/\sqrt{3}$. One can expect that again from the numerical results shown in Fig. 11. The magneto-oscillations cannot be observed for wavelengths longer than 295 μm in pure germanium. That is due partly to decrease in relative oscillation amplitude $\tilde{\alpha}(\omega)$ and partly to decrease in the absorption coefficient.

The ratio of the oscillation amplitude to the total absorption is about 0.16 at B = 1 T and for B // [100]. In the calculation by Keldysh and Silin,[49] one finds $\Delta n/n_0 = 0.33$ at B = 1 T for [100] direction. Combined with Eq. (2-74), the relative change of the absorption coefficient $\Delta\alpha/\alpha_0$ is predicted to be - 1.9 at 171 μm. This value is much larger in magnitude than the experimental value 0.16.

The decay profiles of magneto-oscillation at 171 μm are shown in Fig. 42 for B // [100]. Inversion of dips and peaks of

oscillations as such reported by Betzler et al. in luminescence measurements[40] is not observed for all three typical field directions. The ratio of oscillation amplitude to the total absorption changes little in the course of decay after shutting off the excitation light. (As shown in Fig. 43, it depends on the direction of magnetic field though the reason is not clear until now.) This result is not surprising, since Eq. (2-84) tells us that the time dependent part of the oscillation is smaller in magnitude, say for $t < 100$ μs, than the time independent part.

The lifetime of EHD in a magnetic field is obtained from the time resolved absorption of 171 μm radiation on the assumption that absorption is proportional to the volume of EHD. This assumption is justified in the case of small droplets. The decay of the absorption coefficient is exponential in time and lifetime can be calculated easily. The lifetime of EHD in a magnetic field is shown in Fig. 44. It is changing so much as 42 to 20 μs in 0 to 4.5 T for B // [100] but only 36 to 30 μs in 0 to 6 T for B // [111]. This behavior resembles the luminescence results reported by Skolnick and Bimberg.[31] They interpret the difference of lifetime between B // [100] and B // [111] by that of carrier pair density. It was shown to follow from the considerably higher electron and hole densities of states for B // [001] than for B // [111]. For $E_F = 5$ meV and B // [001], the number of states N increases as $B^{0.6}$ from 5 to 20 T and as $B^{0.3}$ for B // [111] over the same field range. Such increase of density of states results in reduction of the kinetic energy, which leads to stabilization of EHD and a strong increase, for nearly constant

Fermi energy, of the carrier pair density with magnetic field.

IV-7. Impurity Effects

We further observe some impurity effects on far-infrared absorption by EHD. We first present experimental results of magneto-oscillations in doped Ge. Magneto-oscillations in pure and Sb-doped Ge at the wavelength of 171 μm are shown in Fig. 45. The dip positions of the oscillations for 171 to 513 μm are the same for impurity concentrations up to 8.6×10^{14} cm^{-3} (see Fig. 41), suggesting that no change of carrier pair density occurs for such a low doping level. This fact has been confirmed also by Benôit á la Guillaume and Voos[52] through luminescence measurement. In the meantime, theoretical calculation supporting the experimental observation is made by Smith.[95]

The low field peak of the envelope on which magneto-oscillations occur shifts to higher magnetic field with the increase of impurity concentration. In time-resolved measurements, this peak position moves to the lower magnetic field in the course of decay as shown in Fig. 46. These properties are not affected by any kind of impurity.

Doping impurities decreases the oscillation amplitude. In fact, the sample with Sb concentration of 4.5×10^{15} cm^{-3} does not show any magneto-oscillation at low magnetic fields. The relative oscillation amplitude $\Delta\alpha/\alpha_0$ is plotted against impurity concentration in Fig. 47. It decreases with increasing impurity concentration.

In the time-resolved absorption measurements for doped

samples, we do not observe any such inversion between dips and peaks as observed in the luminescence measurement reported by Karuzskii et al.[44] The lifetime in zero magnetic field depends on the impurity concentration as shown in Fig. 48. Another new finding is that the decay constant in zero magnetic field decreases upon the doping heavier than 1.5×10^{14} cm^{-3}. Such decrease of lifetime has not been reported in the luminescence measurement.[18]

The FIR absorption traces for doped samples are shown in Fig. 49 for 420 μm. Magneto-oscillations can be observed at low magnetic fields. The dips of these oscillations occur at the same magnetic fields as those observed for the pure sample at 171 μm (see Fig. 41). Some peaks of magneto-plasma resonance are discernible also for doped samples. The magnetic fields of the peaks for lightly doped samples are a little higher than those for pure germanium. At heavier doping, namely at 4.5×10^{15} cm^{-3}, the peak D_3 apparently shifts in opposite direction, however. A similar tendency is recognizable for In-doped sample. The reason for this phenomenon is not clear at present.

The peak positions of magnetoplasma resonances from the same Sb-doped sample ($N_{Sb} = 5.1 \times 10^{13}$ cm^{-3}) are shown in Fig. 50 and Fig. 51 for several wavelengths of the FIR laser.

The linewidth of magnetoplasma resonance becomes somewhat broader on doping impurities. The line-width of D_3 is plotted against impurity concentration in Fig. 52. The width increases rather abruptly upon light doping and then gradually with the increase of doping. The width of the corresponding magnetoplasma

resonance is broader for the Sb-doped sample than for the In-doped at the same order of concentration.

We also observe the impurity effect of EHD formation. As seen in Fig. 53, doping impurities induces the fast apparent increase of absorption by EHD. Formation of EHD has been studied by using nanosecond pulse excitation. The pair number after shutting off the short pulse is written as

$$\nu = A(e^{-\frac{t}{\tau_0}} - e^{-\frac{t}{\tau_R}}) , \qquad (4.7)$$

where τ_R is the rise-time. Use is made of the pulsewidth of 0.2 ms and the rise time of 0.1 μs. The response time of the detector system is 3 μs. If the sample is excited from t = 0 to t = t_0, the generated pair number in EHD is

$$\tilde{\nu} = \int_0^{t_0} \nu(t)dt = -\tau_0(e^{-t_0/\tau_0} - 1) + \tau_R(e^{-t_0/\tau_R} - 1) . \qquad (4.8)$$

The observed data are fitted by this equation. For Ge/Sb (N_{Sb} = 4.5 x 10^{15} cm^{-3}) τ_0 has been estimated to be 10 μs. This is much shorter than the decay lifetime 28.5 μs. It means that during the course of EHD formation, swift recombination occurs in the vicinity of impurities.

IV-8. Thin Sample Measurement

When the density of excitons increases up to a certain level, the gas-liquid transition takes place. Meanwhile, possibility has been discussed for another phase transition, namely, the

Mott transition of excitons. We have tried to examine this possibility. The samples used for this purpose are thin pure germanium plates whose thickness are 150 ∿ 700 μm. In order to generate as many carriers as possible, the light for excitation is generated by a Q switched YAG laser as well as by a xenon flash lamp. We monitor the exciton signal as observed at 119 μm. The result is shown in Fig. 54. As the excitation becomes stronger, the exciton signal becomes small. It certainly indicates that generation of too many excitons induces the ionization of excitons into free electrons and holes. But if the Mott transition really occurs in this system, the exciton signal would suddenly disappear. We have never observed such a phenomenon.

Instead of the Mott transition associated change, a sharp peak has been observed at low magnetic fields (Fig. 55). It becomes sharper with decreasing wavelength and temperature. Near 4.2 K, this peak becomes maximum in height. Above 4.2 K it broadens and shifts to higher magnetic fields. Judging from the temperature dependence, we consider that it is related to excitons. But until now it is not clear why such a sharp peak appears only upon the intense excitation.

V. Discussions

Three kinds of experiments suggest that the critical temperature of electron-hole drops is about 6 K. The observed density of excitons as well as the decay kinetics of EHD coexisting with excitons reveals a sudden change near 6 K, though the amount of the EHD absorption signal itself changes only gradually in the vicinity of the critical temperature. Our value of critical temperature is the first one by far-infrared absorption. In the measurement of luminescence or current burst in the p-n junction, the values of 6 to 8 K have been reported
The phase diagram of the exciton system in magnetic fields has never been investigated. From our experimental results it can be said that the critical temperature T_c is not affected so much by magnetic fields up to 5 T.

From the time-resolved far-infrared absorption we conclude that two peaks of magnetoplasma resonance, D_2 and D_3, have the same origin and are electric dipole resonances. This forces us to admit the mass renormalization[36,37) 65,66) 92)] because the calculation using free carrier mass cannot explain the observed magnetic field positions of these magnetoplasma resonances. As our experimental results agree well with the results obtained by Gavrilenko et al.[36)] and Yamanaka et al.,[92)] the same mass renormalization will have to be utilized to interpret our data.

So far the way of analysis of magneto-oscillation of EHD has been rather ambiguous. In fact, Bagaev et al.[39)] and Murzin et al.[32)] analyzed their data by assuming that dips of luminescence

as well as far-infrared absorption correspond to the level crossing, while Skolnick and Bimberg insisted that the peaks of luminescence correspond to the crossing.[31),48)] That is because the former assumed a constant carrier pair density while the latter a constant Fermi energy. In order to eliminate this partition of assignment, we have made some calculation on the basis of Keldysh and Silin's theory and found simultaneous variation of carrier pair density and Fermi energy. It leads to the conclusion that dips occur near the crossing field though not exactly at the position.

The electron Fermi energy E_F = 2.2 meV and the carrier pair density $n_0 = 2.1 \times 10^{17}$ cm^{-3} calculated from our experimental results at low magnetic fields agree well with the value obtained from various measurements at zero magnetic field. For example, Thomas et al. obtained $n_0 = (2.38 \pm 0.05) \times 10^{17}$ cm^{-3} in luminescence measurements and Murzin et al. $n_0 = (1.97 \pm 0.05) \times 10^{17}$ cm^{-3} in far-infrared resonant absorption.

The idea of density oscillation gives us a clue to solve further problems; e.g., frequency dependent amplitude of magneto-oscillation and the origin of the large peak near 5 T for B // [111]. The proposal that the magneto-oscillation is due to oscillation of the work function is unable to explain the frequency dependent amplitude, since the oscillation of EHD radius induced by variation of the work function should be independent of the frequency of FIR radiation. Moreover, absorption by EHD decays exponentially at 2 K so that the term of evaporation contributes to the decay of EHD much less than the recombination.

It is true that there still remain some other possibilities for interpreting magneto-oscillations of FIR absorption; e.g., in terms of change in plasmon damping in the presence of a magnetic field. Such a mechanism fails to explain the oscillations observed in luminescence measurement. The magneto-oscillations of FIR absorption can thus be explained most likely in terms of the oscillation of carrier pair density. Contribution of plasmon damping, if any, is considered relatively small.

In our previous paper,[46] the origin of the large peak, which appears near 5 T for B // [111] (see Fig. 37) and designated D_4 or D_9, was considered to be arising from the transfer of electrons between one- and three-valleys. Such an idea was based on the fact that the transfer of electrons caused a small anomaly of the real part of the dielectric constant near 5 T. Indeed this anomaly could be enhanced by introducing anisotropy of the relaxation time to such an extent as to explain the large peak. But Skolnick and Bimberg in the meantime observed the corresponding peak at the same magnetic field in their luminescence measurement.[31),48)] The experimental result of luminescence has nothing to do with dielectric constant. Thus in order to explain the common phenomenon observed both in FIR absorption and in luminescence, the mechanism proposed in our previous paper must now be abandoned. Skolnick and Bimberg insist that the peak is due to the density variation when the lowest Landau level of the light cyclotron mass electron crosses the Fermi level. But our calculation shows that only dips and not peaks can very nearly correspond to the crossing field. The large peak may rather be

considered as a beat between the density oscillation of light cyclotron mass electron and that of heavy cyclotron mass electron.

When the oscillation amplitude of FIR absorption at 171 μm is compared with that of luminescence, the former is larger than the latter. This fact is explained by Eq. (2-74) and Eq. (2-77). In our calculation the amplitude ratio between FIR absorption and luminescence is about 8. When our FIR data are compared with Skolnick and Bimberg's luminescence data, the ratio is about 5. We further compare our results with Betzler et al.'s,[40] in which the magneto-oscillations of luminescence obtained just after shutting off the excitation should be expected equal to those of the carrier pair density (put $t = 0$ in Eq. (2-84)). Their experimental results of $\Delta n/n_0$ is about 0.05 near 1.7 T for B // [100], while our result of $\Delta\alpha/\alpha_0$ is about 0.23. The relative oscillation amplitude $\Delta I/I_0$ in the steady excitation is calculated to be 0.04 from Eq. (2-77). The amplitude ratio $(\Delta\alpha/\alpha_0)/(\Delta I/I_0)$ then becomes 6. This is almost the same as the value of 5 which is derived with the help of Skolnick and Bimberg's result. Thus our tentative adoption of Skolnick and Bimberg's result for combination with ours will have rather general validity.

For coefficients of radiative recombination B and Auger recombination C, Betzler et al.'s experimental values have been adopted. One should note, however, that Skolnick and Bimberg also derived these coefficients from luminescence measurements. According to them $B = (7 \pm 3) \times 10^{-14}$ s^{-1} cm^3 and $C = (8 \pm 2) \times 10^{-32}$ s^{-1} cm^6 in magnetic field.[31] By using these parameters, one can obtain the relative oscillation amplitudes of luminescence

and FIR absorption as $\Delta I/I_0 = -0.19\,\Delta n/n_0$ and $\Delta\alpha/\alpha_0 = -5.6\,\Delta n/n_0$, respectively. The ratio $(\Delta\alpha/\alpha_0)/(\Delta I/I_0)$ then becomes 29, which is much too large in comparison with the experimental value 5. Betzler et al.'s values of B and C thus seem to be more favorable for interpreting the experimental result.

According to our calculation for 119 μm, the crossing field should nearly correspond to the peak of absorption for $\hbar/\tau = 2$ meV. That is indeed opposite to the case for 171 μm. Unfortunately, this prediction cannot be verified experimentally on account of the interference by the hole quantum effect on plasma resonance. Apart from that, the dips or peaks question in itself is rather sensitive to the time constant of the plasmon damping τ. The variation of τ with the probe laser wavelength in fact considerably affects the matter. Our experimental observation of much smaller oscillation amplitude at 119 μm than at 171 μm tells us that $\hbar/\tau$ should be larger than 2 meV at 119 μm. For such a short damping time, there would possibly arise a chance that dips and peaks again change places (see Fig. 11).

There are some reports concerning the frequency dependent relaxation time by two groups : Kononenko and Murzin obtained $\hbar/\tau \sim 1$ meV for $\hbar\omega = 10$ meV from the magnetoplasma resonance at $B = 2 \sim 2.5$ T,[33] while Zarate et al. calculated $\hbar/\tau \sim 2.7$ meV for $\hbar\omega = 10$ meV at zero magnetic field.[85] Our experimental results quantitatively agree with Zarate et al's.

The lifetime calculated from the decay of magnetoplasma resonance peaks D_2 and D_3 is different from that obtained from magneto-oscillations. For B // [111], the lifetime obtained from

D_2 and D_3 varies from 35 to 20 μs as the magnetic field changes from 1 to 3.5 T (Fig. 44). On the other hand, the lifetime of EHD obtained from the data of magneto-oscillations varies only from 36 to 30 μs in the sweep of magnetic field from zero to 6 T. The reason of this discrepancy is not clear at this moment.

Increase of EHD radius due to doping impurities has been reported in some literatures.[53)-55),96)] In the Rayleigh limit, where the EHD radius R is much smaller than the wavelength of the incident radiation, the absorption coefficients can be simply calculated by Eq. (2-40). Increase of R induces a deviation from the Rayleigh limit and it is necessary to include the higher order terms of R. Rose et al.[54)] and Zayats et al.[55)] as well calculated the absorption coefficient by EHD with large radii. According to the numerical calculation by Zayats et al., the absorption coefficient at the frequency of plasma resonance is proportional to R^3 for $R \lesssim 1$ μm, to R^5 for $1 \lesssim R \lesssim 5$ μm and to R^2 for $R \gtrsim 5$ μm as seen from Fig. 3 in reference 55.

Influence of the EHD radius on plasma resonance is also calculated by the same groups cited above. Both claim that the frequency of plasma resonance becomes lower with increasing EHD radius. In the Rayleigh limit the plasma resonance of EHD takes place at $\varepsilon^* = -2$ as seen from Eq. (2-40). When the EHD radius increases, however, the condition for resonance should be different from $\varepsilon^* = -2$. The new condition can be estimated from the numerical results of Rose et al.; namely, ε^* is - 2.4 for R = 1 μm and $\hbar\omega$ = 8.5 meV, - 5.2 for R = 7 μm and $\hbar\omega$ = 6.3 meV, - 11.3 for R = 15 μm and $\hbar\omega$ = 4.4 meV and so on. The value of ε^* corresponding

to resonance decreases from - 2 with the increase of R.

The dielectric function at 171 μm is shown in Fig. 56 for B // [111]. One finds that the increase of EHD radius induces the peak shift of magnetoplasma resonance to higher magnetic field. It seems that all the peaks of magnetoplasma resonance shift to higher magnetic field upon the light doping of impurities. That is typically shown in Fig. 51. The radius of EHD estimated from peak positions of magnetoplasma resonance is about 20 μm for the $N_{Sb} = 5.1 \times 10^{13}$ cm^{-3} sample. It is true that at 420 μm, as mentioned before, the peak shift is practically unobservable for heavily doped samples (see for example the peak D_3 in Fig. 49). Even for these heavily doped samples, however, a considerable shift has been found at 171 μm (Fig. 45).

In the time resolved measurement appears a subsidiary evidence supporting the idea that the larger radius causes the peak shift toward the higher magnetic field. For the $N_{Sb} = 4.5 \times 10^{15}$ cm^{-3} sample, the changing peak position observed at 171 μm in the course of decaying after switching off the excitation (Fig. 46) should be connected with the shrinking radius. The radius decreasing with time will certainly induce the change of the resonance condition and make the peak shift, on the contrary to the increasing radius case, to the lower magnetic field. That is exactly what is observed. A similar tendency has been observed also for other samples.

The decrease of lifetime shown in Fig. 48 is also explicable by the increase of radius. When the radius of EHD increases, the absorption coefficient becomes proportional to R^5 instead of

to R^3. So that the apparent lifetime decreases.

One should admit that the decrease of relative oscillation amplitude upon doping impurities shown in Fig. 47 may be explained either by increase of R or by considering the effect of bound excitons. Increase of R makes the plasma shift to lower frequency. As is seen from the experimental results shown in Fig. 40, the relative oscillation amplitude decreases for frequencies higher than the plasma resonance frequency $\omega_p/\sqrt{3}$. Making the plasma resonance frequency lower is equivalent to raising the FIR frequency and hence the observed relative oscillation amplitude would decrease upon doping impurities. On the other hand, if a monotonic absorption by bound excitons is added to the absorption by EHD, the apparent relative oscillation amplitude would also decrease.

The linewidth of magnetoplasma resonance increases upon the doping of impurities. One should, however, note that while the first light doping causes a large line broadening, further increase of doping does not influence the linewidth so much. Two reasons are considered for line broadening due to impurities. One is the carrier-impurity scattering and the other is inhomogeneous broadening based on the distribution of the radii of EHD. At the pure sample, the linewidth of magnetoplasma resonance is due mainly to electron-hole scatterings. The relaxation times due to electron-electron scatterings and electron-impurity scatterings in metal are calculated by Pines.[97] He gives $(1/\tau)_{e\text{-}e} = \{80(kT)^2/r_s{}^3E_F{}^2\} \times 10^{15}\ s^{-1}$ and $(1/\tau)_{e\text{-imp}} \simeq (80n_i/r_s{}^3n) \times 10^{15}\ s^{-1}$, where n_i is impurity concentration. For $E_F \sim 2$ meV

and T = 2 K, the factor $(k_B T/E_F)^2$ becomes $\sim$ 0.01. For the contribution of the electron-impurity scattering to be of the same order as that of the electron-electron scattering, n_i should be larger than 2×10^{15} cm^{-3}. The rather abrupt rise of linewidth in the lower impurity concentration range, accordingly, should be interpreted in a different way. One speculation would be to introduce the idea of inhomogeneous broadening due to the distribution of EHD radii caused by impurities.

It is interesting enough to note that for the same doping level influence of impurities on the oscillation amplitude and on the half-width of magnetoplasma resonance is smaller for In-doped sample than for Sb-doped sample. One can find two possible mechanisms to interpret this fact. One is the difference in radius distribution between Sb- and In-doped samples and the other is the different cross sections of the carrier-impurity scattering between donors and acceptors. A decisive conclusion will be drawn only after repeating more sophisticated experiments.

VI. Conclusions

Various properties of electron-hole drops are investigated by far-infrared absorption in this thesis; the main results consist of critical temperature of EHD, decay kinetics of excitons and EHD, magneto-oscillation of EHD and impurity effects on some features of EHD.

Critical temperature is obtained by three different kinds of information : First, the plasma absorption by EHD increases abruptly near 5 K. Second, the exciton absorption corresponding to the transition between two discrete levels has a kink in the vicinity of 6.3 K. Finally, the decay profiles of the exciton peak and EHD absorption are non-exponential below 6.0 K and exponential at temperatures higher than 6.6 K. These facts indicate the critical temperature of EHD is $\sim$ 6 K, which agrees well with the value obtained in luminescence measurements.

We observe the decays of exciton and EHD at various temperatures simultaneously. Exciton absorption keeps constant in rather long time after shutting off excitation in spite of rapid decay of EHD. The constancy of the exciton peak in time allows us an estimation of the work function —14.7 K, which is somewhat lower than the value by other kinds of experiments.

Magneto-oscillations of electron-hole drops are well explained by the oscillation of electron-hole pair density. The main reasons for this conclusion are as follows :

1. The Fermi energy which is calculated from the magnetic fields of dips agrees well with other experimental results.
2. Damping of oscillation amplitude is the same as evaluated

by the numerical calculation based on the Keldysh - Silin's theory.

3. The oscillation amplitude in 171 μm absorption is several times as large as that of photo-luminescence and this can be interpreted by our calculation.

4. The decrease of oscillation amplitude above the frequency of plasma resonance is also explained by our calculation.

5. Variation of the relative oscillation amplitude with time of far-infrared absorption is much smaller than that of luminescence. Our calculation gives an explanation to this fact, too.

All these aspects of the far-infrared magneto-oscillation can be explained in terms of density oscillation in the electron-hole drop.

Impurity effects for EHD are also discussed in the present paper. The dip positions of magneto-oscillations are not affected by doping impurities up to $N_{Sb} = 4.5 \times 10^{15}$ cm^{-3}, or $N_{In} = 8 \times 10^{15}$ cm^{-3}. This fact leads to the constant carrier-pair density in the range of impurity concentration investigated.

Increase of the EHD radius due to impurities can be concluded by the following reasons; peak shift of magneto-plasma resonance, decrease of apparent lifetime, increase of linewidth of magneto-plasma resonance, and decrease of amplitude in magneto-oscillation.

Increase of the EHD radius forces us to calculate higher order terms of Mie's scattering theory. Decrease of the apparent lifetime can be explained by taking the contribution from higher order terms into account.

These terms also induce a change of the resonance condition from $\varepsilon^* = -2$, giving an explanation to the peak shifts of magnetoplasma resonances and decrease of the amplitude in magnetooscillation. Moreover, the distribution of radii of EHD might explain increase of linewidth of magnetoplasma resonance.

References

1) For typical measurements, only some representative works of band structures and relaxation times for germanium are shown. For effective mass of electrons; B. W. Levinger and D. R. Frankl: J. Phys. Chem. Solids 20 281 (1961). For band parameters of valence bands; J. C. Hensel and K. Suzuki: Phys. Rev. B9 4219 (1974) and K. Suzuki and J. C. Hensel: Phys. Rev. B9 4184 (1974). For relaxation times; M. Fukai, H. Kawamura, K. Sekido and I. Imai: J. Phys. Soc. Jpn. 19 288 (1964), E. Otsuka, K. Murase and I. Iseki: J. Phys. Soc. Jpn. 19 1579 (1964) and H. Kawamura, H. Saji, M. Fukai, K. Sekido and I. Imai: J. Phys. Soc. Jpn. 19 288 (1964).

2) S. Zwerdling, B. Lax, L. M. Roth and K. J. Button: Phys. Rev. 114 80 (1959).

3) E. M. Gershenzon: Proc. Int. Conf. Phys. Semicond. 12th, Stuttgart p.355. Teubner, Stuttgart, (1974).

4) M. A. Lampert: Phys. Rev. Lett. 1, 450 (1958).

5) J. R. Haynes: Phys. Rev. Lett. 17, 860 (1966).

6) V. M. Asnin and A. A. Rogachev: Zh. Eksp. Teor. Fiz., Pis'ma Red. 7, 464 (1968) [JETP Lett. 7, 360 (1968)].

7) L. V. Keldysh: Proc. Int. Conf. Phys. Semicond., 9th, Moscow p.1303 (1968).

8) For reviews see, e.g., T. M. Rice: in Solid State Physics, edited by H. Ehrenreich, F. Seitz and D. Turnbull (Academic, New York, 1978) Vol. 32, p.1.

9) J. C. Hensel, T. G. Phillips and G. A. Thomas; in Solid State Physics, edited by H. Ehrenreich, F. Seitz and D. Turnbull (Academic, New York, 1978) Vol. 32, p.88.

10) Y. E. Pokrovskii and K. I. Svistunova: Zh. Eksp. Teor. Fiz., Pis'ma Red. 9, 435 (1969) [JETP Lett. 9, 261 (1969)].

11) Y. E. Pokrovskii and K. I. Svistunova: Zh. Eksp. Teor. Fiz., Pis'ma Red. 13, 297 (1971) [JETP Lett. 13, 212 (1971)].

12) V. S. Vavilov, V. A. Zayats and V. N. Murzin: Zh. Eksp. Teor. Fiz., Pis'ma Red. 10, 304 (1969) [JETP Lett. 10 192 (1969)].

13) V. M. Asnin, A. A. Rogachev and N. I. Sablina: Zh. Eksp. Teor. Fiz., Pis'ma Red. 11, 162 (1970) [JETP Lett. 11, 99 (1970)].

14) C. Benôit à la Guillaume, M. Voos, F. Salvan, J. M. Laurant and A. Bonnot: C. R. Acad. Sci. 272, 236 (1971).

15) P. S. Gladkov, B. G. Zhurkin and N. A. Penin, Fiz. Tekh. Poluprovodn. 6, 1919 (1972) [Sov. Phys. Semicond. 6, 1649 (1973)].

16) J. C. Hensel and T. G. Phillips: Proc. Int. Conf. Phys. Semicond., 11th, Warsaw p.671, PWN, Warsaw, (1972).

17) J. C. Hensel, T. G. Phillips and T. M. Rice: Phys. Rev. Lett. 30 227 (1973).

18) C. Benôit à la Guillaume, M. Voos and F. Salvan: Phys. Rev. B5, 3079 (1972).

19) R. M. Westervelt, T. K. Lo, J. L. Staehli and C. D. Jeffries: Phys. Rev. Lett. 32, 1051 (1974).

20) K. Fujii and E. Otsuka: Solid State Commun. 14 763 (1974).

21) C. Benoit à la Guillaume, M. Voos and F. Salvan: Phys. Rev. B5, 3079 (1972).

22) V. S. Bagaev, T. I. Galkina and O. V. Gogolin: Proc. Int. Conf. Semicond., 10th, Cambridge, Mass. CONF-700801, p.500. USAEC Div. Tech. Inf., Springfield, Virginia, (1970).

23) T. Ohyama, T. Sanada and E. Otsuka: Phys. Rev. Lett. 33 647 (1974).

24) J. P. Wolfe, W. L. Hansen, E. E. Haller, R. S. Markiewicz, C. Kittel and C. D. Jeffries: Phys. Rev. Lett. 34 1292 (1975).

25) A. S. Alekseev, V. S. Bagaev, T. I. Galkina, O. V. Gogolin, N. A. Penin, A, N. Semenov and V. G. Stopachinskii: Zh. Eksp. Teor. Fiz., Pis'ma Red. 12, 203 (1970) [JETP Lett. 12, 140 (1970)].

26) R. W. Martin, H. L. Störmer, W. Rühle and D. Bimberg: J. Lumin. 12/13, 645 (1976).

27) S. T. Chui: Phys. Rev. B9, 3438 (1974).

28) H. Büttner: Proc. Int. Conf. Phys. Semicond., 12th, Stuttgart, p.81. Teubner, Stuttgart, (1974).

29) L. V. Keldysh and T. A. Onishchenko: Pis'ma Zh. eksper. teor. Fiz. 24 70 (1976) [Sov. Phys. JETP Lett. 21 197 (1975)].

30) H. L. Störmer and R. W. Martin: Phys. Rev. B20 4213 (1979).

31) M. S. Skolnick and D. Bimberg: Phys. Rev. B21 4624 (1980).

32) V. N. Murzin, V. A. Zayats and V. L. Kononenko: Fiz. Tverd. Tela (Leningrad) 15, 3634 (1973) [Sov. Phys. Solid State 15, 2421 (1974)].

33) V. L. Kononenko and V. N. Murzin: Zh. Eksp. Teor. Fiz. 75, 124 (1978) [Sov. Phys. JETP 48 61 (1978)].

34) K. Fujii and E. Otsuka: J. Phys. Soc. Jpn. 38 742 (1975).

35) K. Fujii and E. Otsuka: Proc. Eur. Congr. Mol. Spectrosc., 12th, Strasbourg, 1975 p.143. Elsevier, Amsterdam, 1976.

36) V. I. Gavrilenko, V. L. Kononenko, T. S. Mandelshtam and V. N. Murzin: Zh. Eksp. Teor. Fiz. Pis'ma Red. 23, 701 (1976) [JETP Lett. 23, 645 (1976)].

37) V. I. Gavrilenko, V. L. Kononenko, T. S. Mandelshtam, V. N. Murzin and S. A. Saunin, Pis'ma Zh. Eksp. Teor. Fiz. 25, 102 (1977) [JETP Lett. 26, 96 (1977)].

38) G. W. Ford, J. K. Furdyna and S. A. Werner: Phys. Rev. B12 1452 (1975).

39) V. Z. Bagaev, T. I. Galkina, N. A. Penin, V. B. Stopachinskii and M. N. Churaeva: Pis'ma Zh. Eksp. Teor. Fiz. 16, 120 (1972) [JETP Lett. 16, 83 (1972)].

40) K. Betzler, B. G. Zhurkin and A. L. Karuzskii: Solid State Commun. 17, 577 (1975).

41) A. L. Karuzskii, K. W. Betzler, B. G. Zhurkin and B. M. Balter: Zh. Eksp. Teor. Fiz. 69, 1088 (1975) [Sov. Phys. JETP, 42, 554 (1976)].

42) K. Betzler, B. G. Zhurkin and A. L. Karuzskii: Phys. Stat. Sol. (b) 70, K109 (1975).

43) A. L. Karuzskii, K. W. Betzler, B. G. Zhurkin and B. M. Batler: Pis'ma Sh. Eksp. Teor. Fiz. 22, 65 (1975) [JETP Lett. 22, 29 (1975)].

44) A. L. Karuzskii, K. W. Betzler, B. G. Zhurkin and V. P. Aksenov: Fis. Tverd. Tela 17, 3104 (1975) [Sov. Phys. Solid State 17, 2058 (1976)].

45) K. Muro and Y. Nisida: J. Phys. Soc. Jpn. 40, 1069 (1976).

46) H. Nakata, K. Fujii and E. Otsuka: J. Phys. Soc. Jpn. 45, 537 (1978).

47) H. Nakata, K. Fujii, T. Ohyama and E. Otsuka: J. Mag. Mag. Mat. 11, 127 (1979), H. Nakata and E. Otsuka: to be published in Proc. Int. Conf. Phys. Semicond., 15th, Kyoto, (1980).

48) D. Bimberg and M. S. Skolnick: Solid State Commun. 32, 1311 (1979).

49) L. V. Keldysh and A. P. Silin: Fiz. Tverd. Tela 15, 1532 (1973), [Sov. Phys. Solid State, 15, 1027 (1973)].

50) A. S. Alekseev, V. S. Bagaev, T. I. Galkina, O. V. Gogolin and N. A. Penin: Fiz. Tverd. Tela (Leningrad) 12, 3516 (1970) [Sov. Phys. Solid State 12, 2855 (1971)].

51) E. Göbel, R. W. Martin, M. H. Pilkuhn and R. Sauer: Proc. Int. Conf. Phys. Semincond., 11th, Warsaw p.691. PWN, Warsaw, 1972.

52) C. Benôit à la Gvillaume and M. Voos: Solid State Commun. 11, 1585 (1972).

53) T. Timusk and A. Silin: Phys. Stat. Sol (b) 69, 87 (1975).

54) J. H. Rose, H. B. Shore and T. M. Rice: Phys. Rev. B17, 752 (1978).

55) V. A. Zayats, V. N. Murzin, I. N. Salganik and K. S. Shifrin: Zh. Eksp. Teor. Fiz. 73, 1422 (1977) [Sov. Phys. JETP 46, 748 (1977)].

56) A. Frova, G. A. Thomas, R. E. Miller and E. O. Kane: Phys. Rev. Lett. 34, 1572 (1975).

57) W. F. Brinkman, T. M. Rice, P. W. Anderson and S. T. Chui: Phys. Rev. Lett. 28, 961 (1972).

58) M. Combescot and P. Noziéres: J. Phys. C5. 2369 (1972).

59) W. F. Brinkman and T. M. Rice: Phys. Rev. B7, 1508 (1973).

60) P. Bhattacharyya, V. Massida. K. S. Singwi and P. Vashishta: Phys. Rev. B10, 5127 (1974).

61) P. Vashishta, S. G. Das and K. S. Singwi: Phys. Rev. Lett. 33 911 (1974).

62) J. Hubbard: Proc. Roy. Soc. London. Ser. A 243, 336 (1957).

63) P. Noziéres and D. Pines: Phys. Rev. 111, 442 (1958).

64) K. S. Singwi, M. P. Tosi, R. H. Land and A. Sjölander: Phys. Rev. 176, 589 (1968).

65) T. M. Rice: Nuovo Cimento B 23, 226 (1974).

66) M. Rösler and R. Zimmermann: Phys. Status Solidi B 67, 525 (1975).

67) D. Pines and P. Noziéres: "Quantum Theory of Fluids". Benjamin, New York, 1973.

68) Y. E. Pokrovskii and K. Svistunova: Proc. Int. Conf. Phys. Semicond., 12th Stuttgart p.71. Teubner, Stuttgart, 1974.

69) K. Betzler: Proc. Oji Semin. Phys. Highly Excited States in Solids, Tomakomai, Jpn., 1975 p.211, Springer-Verlag, Berlin and New York, 1976.

70) R. J. Elliott and R. Loudon: J. Phys. Chem. Solids 15 196 (1960).

71) R. F. Wallis and H. J. Bowlden: J. Phys. Chem. Solids 7 78, (1958).

72) H. Hasegawa and R. E. Howard: J. Phys. Chem. Solids 21 179 (1961).

73) W. S. Boyle and R. E. Howard: J. Phys. Chem. Solids 19 181 (1961).

74) V. L. Kononenko: Fiz. Tverd. Tela 19 3010 (1977) [Sov. Phys. Solid State 19 1762 (1977)].

75) G. Mie: Ann. Phys. (France) 25 377 (1908).

76) M. Born and E. Wolf: "Principle of Optics" (Pergman Press, New York, 1970) p.633.

77) J. A. Stratton: "Electromagnetic Theory" (McGraw-Hill Book Company, New York and London, 1941) p.201.

78) T. A. Evans and J. K. Furdyna: Phys. Rev. B 8 1461 (1973).

79) F. G. Galleener, T. A. Evans and J. K. Furdyna: Phys. Rev. Lett. 29 728 (1972).

80) V. L. Kononenko: Fiz. Tverd. Tela 17, 3264 (1975) [Sov. Phys. Solid State, 17 2146 (1976)].

81) G. W. Ford and S. A. Werner: Phys. Rev. B 18 6752 (1978).

82) L. D. Landau: Zh. Eksp. Teor. Fiz. 32 59 (1957) [Sov. Phys. JETP 5 101 (1957).

83) G. E. Lee-Whiting: Proc. Roy. Soc, (London) A 212 362 (1952).

84) N. Tzoar and P. M. Platzman: Linear and Non-Linear Electron Transport in Solids, ed. J. T. De Vreese and V. E. VanDoren (Plenum, N. Y.) p.199 1976.

85) H. G. Zarate, J. P. Carbotte and T. Timusk: Phys. Rev. B 21 4649 (1980).

86) T. Y. Chang and T. J. Bridges: Optics Commun. 1 423 (1970).

87) T. Y. Chang, T. J. Bridges and E. G. Burkhardt: Appl. Phys. Lett. 17 249 (1970).

88) T. Y. Chang, T. J. Bridges and E. G. Burkhardt: Appl. Phys. Lett. 17 357 (1970).

89) H. Nakata and E. Otsuka: Solid State Physics 10 553 (1975).

90) K. Fujii: PhD Thesis, Osaka University 1977, unpublished.

91) G. A. Thomas, T. M. Rice and J. C. Hensel: Phys. Rev. Lett. 33, 219 (1974).

92) M. Yamanaka, K. Muro and S. Narita: J. Phys. Soc. Jpn. 47, 1168 (1979).

93) R. B. Dingle: Proc. Roy. Soc. A211, 517 (1952).

94) A. S. Kaminskii, Ya. E. Pokrovskii and A. E. Shidkov: Zh. Eksp. Teor. Fiz. 72, 1960 (1977) [Sov. Phys. JETP 45, 1030 (1977)].

95) D. L. Smith: Solid State Commun. 18, 637 (1976).

96) M. A. Washington, J. M. Worlock and M. Voos: Solid State Commun. 33, 549 (1980).

97) D. Pines, Elementary Excitations in Solids (W. A. Benjamin, New York, 1964), p.277.

Table I Ground State Parameters in Ge

	BRAC[57]	CN[58]	VDS[61]
n_0 (cm^{-3})	1.8×10^{17}	2.0×10^{17}	2.2×10^{17}
$-E_G$ (meV)	5.3	6.1	5.9
ϕ (meV)	1.15	1.95	1.75

Table II Relation between (n, ℓ, m) and (N, M, ν)

	(n, ℓ, m)	(N, M, ν)
1S	(1, 0, 0)	(0, 0, 0)
$2P_{-1}$	(2, 1, -1)	(0, -1, 0)
$2P_{+1}$	(2, 1, 1)	(1, 1, 0)
$2P_0$	(2, 1, 0)	(0, 0, 1)

Table III Obtained Lines of Optically Pumped Far-Infrared Laser

WAVELENGTH (μm)	GAS	GAS PRESSURE (m Torr)	INPUT	OUTPUT * (mV)
96.5	CH_3OH	100	9R(10)	10
103.1	CH_3OD	170	9P(30)	20
118.8	CH_3OH	150	9P(36)	100
145.7	CH_3OD	170	9P(30)	20
163.0	CH_3OH	100	10R(38)	40
170.6	CH_3OH	150	9P(36)	100
184.0	CD_3OD	180	10R(24)	25
191.6	CH_3OH	250	10R(10)	10
215.4	CH_3OD	150	9R(14)	10
232.9	CH_3OH	100	9R(10)	10
251.1	CH_3OH	100	10R(38)	40
294.8	CH_3OD	130	9R(8)	20
299.0	CD_3OD	180	10R(24)	25
305.7	CH_3OD	130	9R(8)	20
392.1	CH_3OH	150	9P(36)	100
393.6	HCOOH	120	9R(18)	60
418.6	HCOOH	300	9R(22)	100
423.6	HCOOH	130	9R(20)	30
513.0	HCOOH	120	9R(28)	30

*) Output voltage of pyroelectric detector.

FIGURE CAPTIONS

Fig. 1 The calculated band structure of germanium. [From T. M. Rice reference 8) p6].

Fig. 2 Valence-band Landau levels in Ge calculated at $k_H = 0$. The Landau levels are classified by (N_n, K^{π}). [From J. C. Hensel and K. Suzuki : Phys. Rev. B9 4219 (1974)].

Fig. 3 The ground-state energy (in units of the exciton Rydberg) of the EHD vs. interparticle spacing (in units of the exciton Bohr radius for the ideal band structure (equal isotropic electron and hole masses). [BRAC : W. F. Brinkman, T. M. Rice, P. W. Anderson, and S.-T. Chui. Phys. Rev. Lett. 28, 961 (1972); VBS : P. Vashishta, P. Bhattacharyya, and K. S. Singwi, Phys. Rev. Lett. 30, 1248 (1973); IH : M. Inoue and E. Hanamura, J. Phys. Soc. Jpn. 35 643 (1973)].

Fig. 4 The ground-state energy of the EHD in Ge vs. interparticle spacing in exciton units. [BRAC : W. F. Brinkman, T. M. Rice, P. W. Anderson, and S.-T. Chui, Phys. Rev. Lett. 28 961 (1972); VDS : P. Vashishta, S. G. Das, and K. S. Singwi, Phys. Rev. Lett 33 911 (1974)].

Fig. 5 The phase diagram of EHD in Ge. The solid curve is the universal phase diagram which can be joined smoothly to the curve obtained from Eq. (2-9).

Fig. 6 Correction n of the carrier pair density calculated at 2 K as a function of magnetic field which is applied along the [100] direction for a fixed Fermi energy 2.5 meV.

Fig. 7 Calculated correction of the carrier pair density for B // [111], where the numbers 0, 1, 2 and 3 are the Landau quantum numbers of the one-valley electron (lighter electron) and the primed numbers 1' and 2' are those of the three-valley electron (heavier electron).

Fig. 8 Calculated carrier pair density for B // [100] by using the density-of-states integral. The Fermi level is assumed to be parallel to the lowest Landau level.

Fig. 9 The real ($\delta\varepsilon_1$) and imaginary ($\delta\varepsilon_2$) parts of the dielectric function due to interband transitions between the heavy and light hole bands. The interband absorption has a sharp onset at 3 meV (J. H. Rose, H. B. Shore and T. M. Rice : Phys. Rev. B17, 752 (1978)).

Fig. 10 The real part of dielectric function for the wavelength of 420 μm and carrier pair density of $n = 2.1 \times 10^{17} cm^{-3}$.

Fig. 11 The calculated value of relative oscillation amplitude $\tilde{\alpha}(\omega) = (\Delta\alpha/\alpha_0)/(\Delta n/n_0)$ is given as a function of FIR frequency for various damping constants $\hbar/\tau$.

Fig. 12 Frequency dependent damping due to electron-hole collisions in the EHD. The calculated curve, solid line, uses a static approximation but includes both the anisotropy and the degeneracy of the valence band (H. G. Zarate, J. P. Carbotte, and T. Timusk : Phys. Rev. B21 4649 (1980)). Some experimental measurements are also shown. Magneto-plasma resonance linewidths are stars (Ref. 37)) open circles (Ref. 36)) and squares (Ref. 45)). The single solid circle is a

typical linewidth obtained from the far-infrared plasma resonance (Ref. 33)).

Fig. 13 Block diagram for time-resolved magneto-absorption measurement. In this measurement, pulsed FIR laser and xenon flush lamp are employed.

Fig. 14 Block diagram of our experimental set-up. In this measurement, an optically pumped laser and an argon ion laser are employed.

Fig. 15 The lower part of the cryostat. Black polyethlene sheets are to cut off the undesirable shorter wavelength radiations.

Fig. 16 Optically pumped FIR laser.

Fig. 17 The typical data of magneto-absorption. The wavelength of FIR radiation is 119 μm.

Fig. 18 Typical absorption spectra at 4.2 K observed at several wavelengths in B // [111] during the steady excitation. The E_{x1}^{h} and E_{x2}^{h} lines are nearly parallel to the cyclotron energies of free holes CR_h $(2_0 \rightarrow 1_1)$ and $CR_h(1_0 \rightarrow 2_1)$, respectively. The E_{x1}^{e} and E_{x2}^{e} lines are also nearly parallel to the cyclotron energies of the one valley electrons CR_e^1 and the other three valley elelctrons CR_e^3, respectively.

Fig. 19 Magnetic fields where the transitions between the exciton levels occur are shown for the energy of far-infrared radiation.

Fig. 20 Absorption spectra at the temperatures higher than the liquid helium temperature. These are obtained 30 μs

after the excitation. The assignment is after Muro (Doctor thesis (1975)).

Fig. 21 Temperature dependence of the observed inverse relaxation time of holes.

Fig. 22 Temperature dependence of 119 μm absorption by free hole ($2_0 \rightarrow 1_1$), exciton E^h_{x1} and EHD. The gradient of free hole signal gives us the ionization energy of an exciton 2.8 meV.

Fig. 23 Plasma absorption by EHD measured at 0.64 T and at 20 μs after the light pulse is traced as a function of temperature. A bend indicative of the critical temperature is obvious.

Fig. 24 Temperature dependence of exciton absorption. A kink corresponding to the critical temperature is observed near 6.3 K.

Fig. 25 Decay profiles of the absorption lines for the wavelength of 84 μm. Excitonic absorption is E^h_{x1} line at 4.9 T and EHD absorption is non-resonant background. Sudden change occurs between 6.0 and 6.6 K.

Fig. 26 The excitation dependence of exciton and EHD absorption. The exciton signal shows little change for varying excitation power as indicated on the right. The relative excitation powers are shown in numbers.

Fig. 27 Absorption traces of the exciton signal at different delay-times after photo-excitation, on top of the plasma absorption due to EHD, which appears as a non-resonant broad background.

Fig. 28 Joint decay profiles of exciton and EHD absorption signals. EHD absorption is measured at the foot of the exciton signal. One may note the nearly time-independent n_{ex} between 10 and 35 μs of delay time.

Fig. 29 Temperature variation of the exciton decay profile.

Fig. 30 Magneto-absorption by EHD in pure Ge obtained at the geometry B // [111] is shown for various FIR wavelengths. Numbers 1 and 2 indicate the Landau numbers of the light electron. Peaks of magneto-plasma resonances are denoted by D_1, D_2 etc.. D_4 is the large peak near 5 T mentioned in the text.

Fig. 31 Ratio of the density of one-valley electrons (whose valley axis is along [111] direction) to the total electron density in the drop, and ratio of the density of light holes to the total hole density in the drop.

Fig. 32 Comparison of the calculated and observed peak positions of the absorptions by the electron-hole drops for the incident radiation frequencies are shown. Experimentally observed peak positions are shown by the solid circles. Calculated peak positions for the electric and magnetic dipole resonances are shown by broken and dotted lines, respectively.

Fig. 33 Time resolved magneto-absorption traces of EHD in pure germanium obtained at the FIR wavelength of 420 μm.

Fig. 34 Lifetimes of EHD obtained from magneto-plasma resonances D_2 and D_3.

Fig. 35 The frequency dependence of the damping constant of the plasma oscillations in EHD in Ge.

Fig. 36 The frequency dependence of peak height for D_2 and D_3.

Fig. 37 Far-infrared absorption by EHD. The numbers at the dips of oscillation indicate the Landau quantum numbers of the light cyclotron mass electron.

Fig. 38 The change of FIR absorption for 119 μm with rotating magnetic field.

Fig. 39 Calculated and experimental magneto-oscillation of EHD.

Fig. 40 Magneto-absorption by EHD in pure Ge obtained at the geometry B // [100] is shown for various FIR wavelengths. Numbers 1, 2 and 3 indicate the Landau number of the light electron.

Fig. 41 The dip positions in magnetic field of magneto-oscillations are given at the geometry of B // [111] for a pure and various doped germanium crystals. ○ - Pure Ge, ● - Ge/Sb : $N_{Sb} = 5.1 \times 10^{13}$ cm^{-3}, Δ - Ge/Sb : $N_{Sb} = 1.3 \times 10^{14}$ cm^{-3}, ▲ - Ge/Sb : $N_{Sb} = 8.6 \times 10^{14}$ cm^{-3}, □ - Ge/In : $N_{In} = 8.0 \times 10^{15}$ cm^{-3}.

Fig. 42 Time-resolved magneto-oscillation observed for 171 μm after the end of 0.2 ms excitation. Delay-times are indicated on the right.

Fig. 43 Time dependence of the relative oscillation amplitude $\Delta\alpha/\alpha_0$ of $\ell = 1$ magneto-oscillation at the geometriés of B // [111] and B // [100].

Fig. 44 The lifetime of EHD in pure Ge obtained at the 171 μm measurement is shown as a function of magnetic field for two geometries.

Fig. 45 Magneto-oscillations of FIR absorption at 171 μm in

pure and Sb-doped samples. The Sb concentrations are indicated.

Fig. 46 The decay profile of 171 μm absorption by EHD in a Sb doped sample (N_{Sb} = 4.5 x 10^{15} cm^{-3}) after shutting off the excitation light. The delay times are given on the right.

Fig. 47 The relative oscillation amplitude (ratio of the ℓ = 1 oscillation amplitude to the zero field absorption) as a function of impurity concentration.

Fig. 48 The apparent lifetime at zero magnetic field obtained from the 171 μm measurement is given against impurity concentration. Optical measurement[52] does not show any indication of concentration dependence within the range shown here.

Fig. 49 FIR absorption by EHD in pure and doped germanium for 420 μm. The number 1 indicates the dips of oscillation due to the ℓ = 1 Landau level of the light electron.

Fig. 50 Magneto-absorption by EHD in Sb-doped germanium (N_{Sb} = 5.1 x 10^{13} cm^{-3}) obtained for several FIR wavelengths.

Fig. 51 Positions of magnetoplasma resonance peaks in pure and Sb-doped germanium (N_{Sb} = 5.1 x 10^{13} cm^{-3}).

Fig. 52 Linewidths of magneto-plasma resonance D_3 at 420 μm for pure, Sb- and In-doped samples.

Fig. 53 Absorption profiles just after the onset of excitation for Sb- and In-doped samples.

Fig. 54 Far-infrared absorption for thin and thick samples.

Fig. 55 Temperature dependence of a sharp peak in low magnetic field for a thin sample.

Fig. 56 Calculated dielectric function $\varepsilon_{\pm}$ for the frequency of the incident radiation wavelength 171 μm with an infinite relaxation time and n = 2.1 x 10^{17} cm^{-3}. The densities of one valley electrons and light holes are 0.25 n and 0.035 n, respectively.

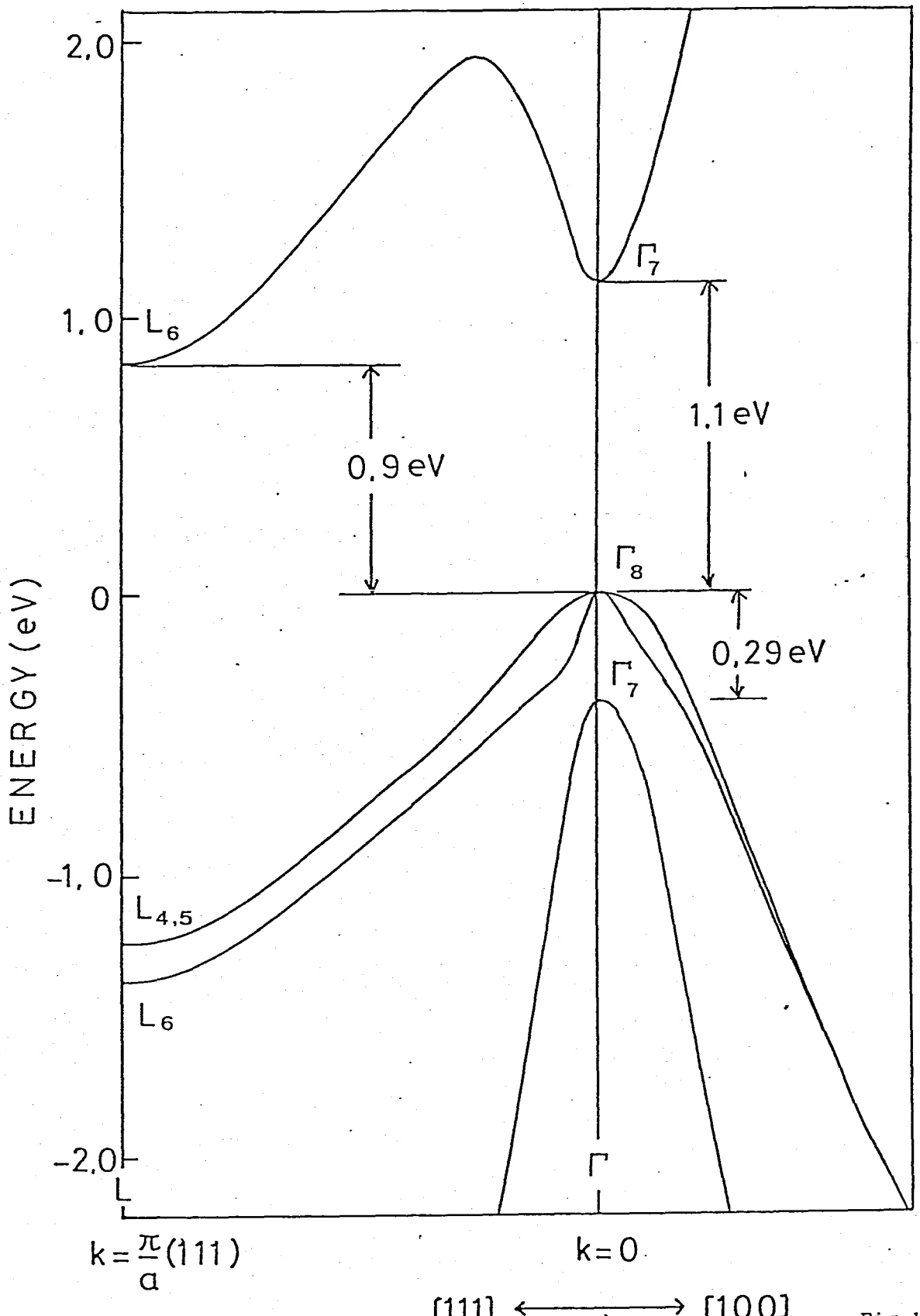
2.0
1.0
0
-1.0
-2.0
ENERGY (eV)
L6
Γ7
1.1 eV
0.9 eV
Γ8
0.29 eV
Γ7
L4,5
L6
Γ
L
k = π/a (111)
k = 0
[111] ⟷ [100]

Fig.1

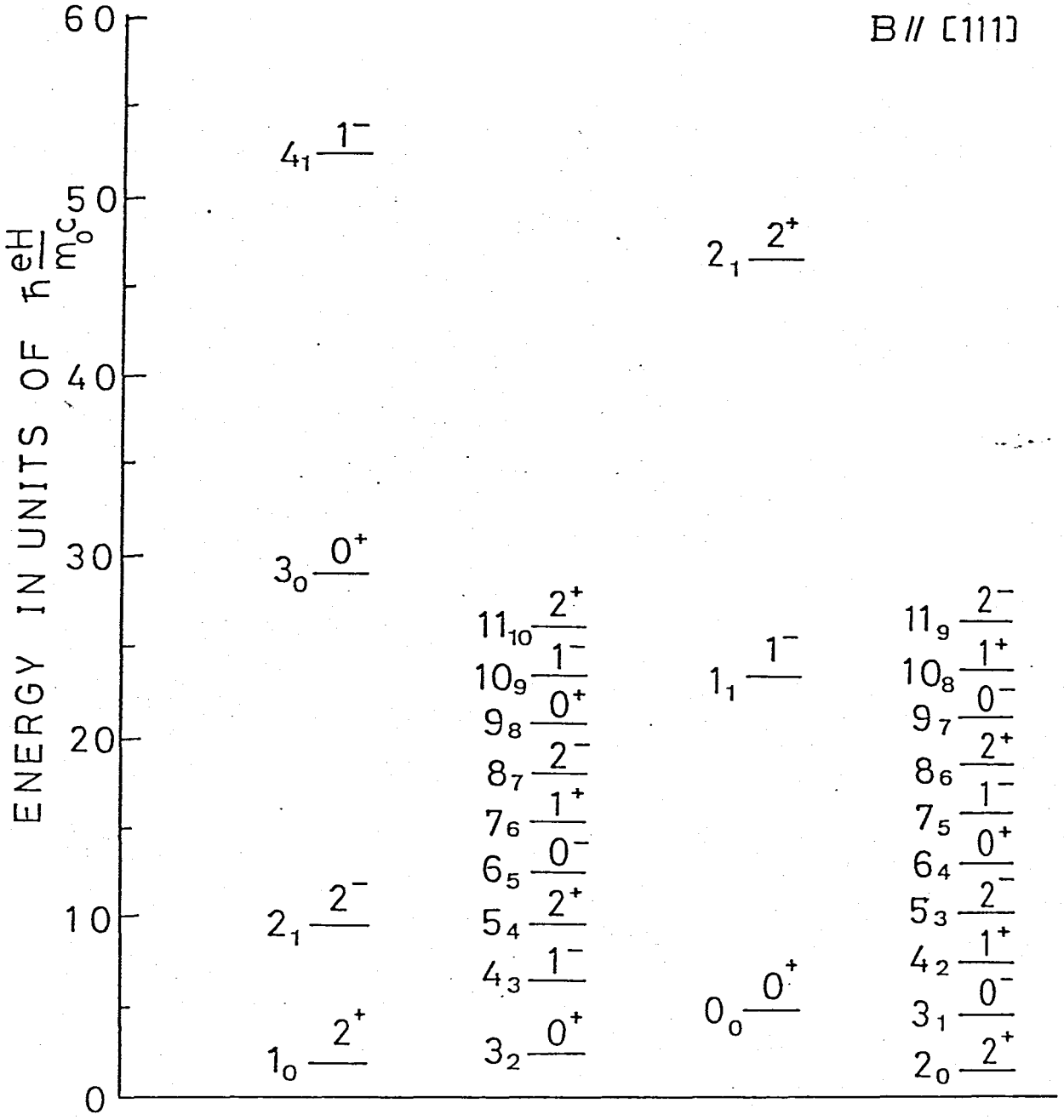
B // [111]
ENERGY IN UNITS OF $\hbar\frac{eH}{m_0c}$
60
50
40
30
20
10
0
4_1 1^-
3_0 0^+
2_1 2^-
1_0 2^+
11_{10} 2^+
10_9 1^-
9_8 0^+
8_7 2^-
7_6 1^+
6_5 0^-
5_4 2^+
4_3 1^-
3_2 0^+
2_1 2^+
1_1 1^-
0_0 0^+
11_9 2^-
10_8 1^+
9_7 0^-
8_6 2^+
7_5 1^-
6_4 0^+
5_3 2^-
4_2 1^+
3_1 0^-
2_0 2^+

Fig.2

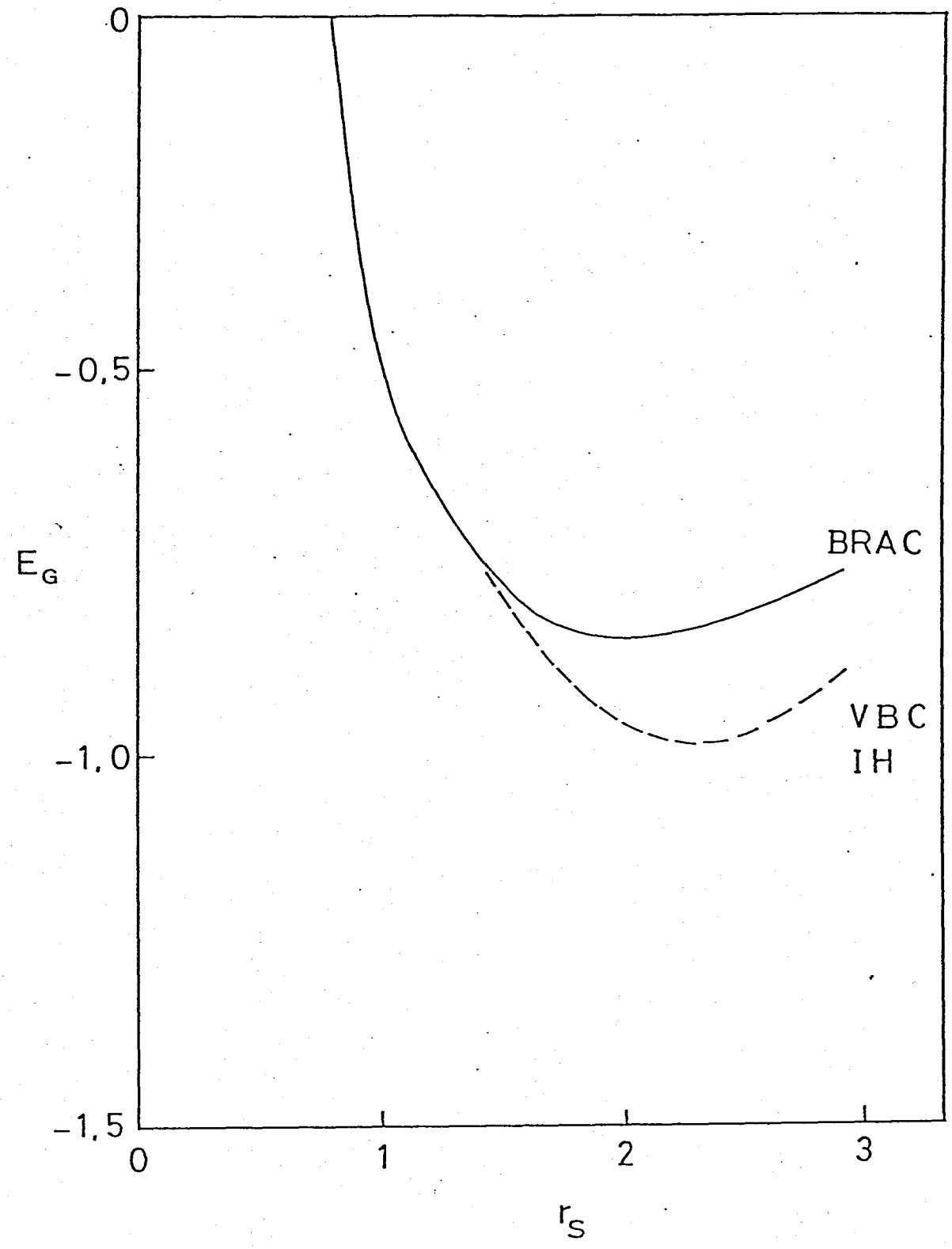

Fig.3

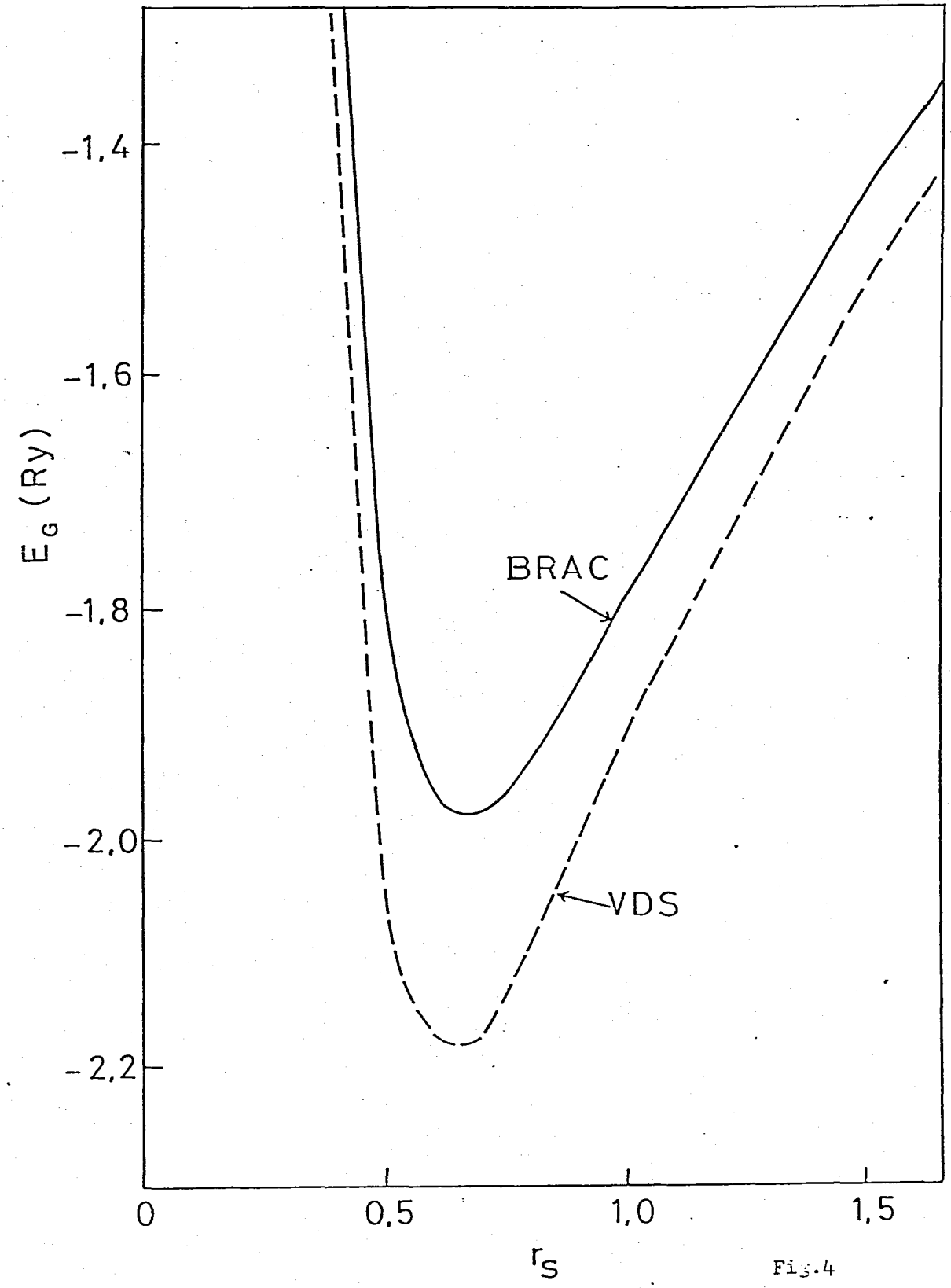

Fig.4

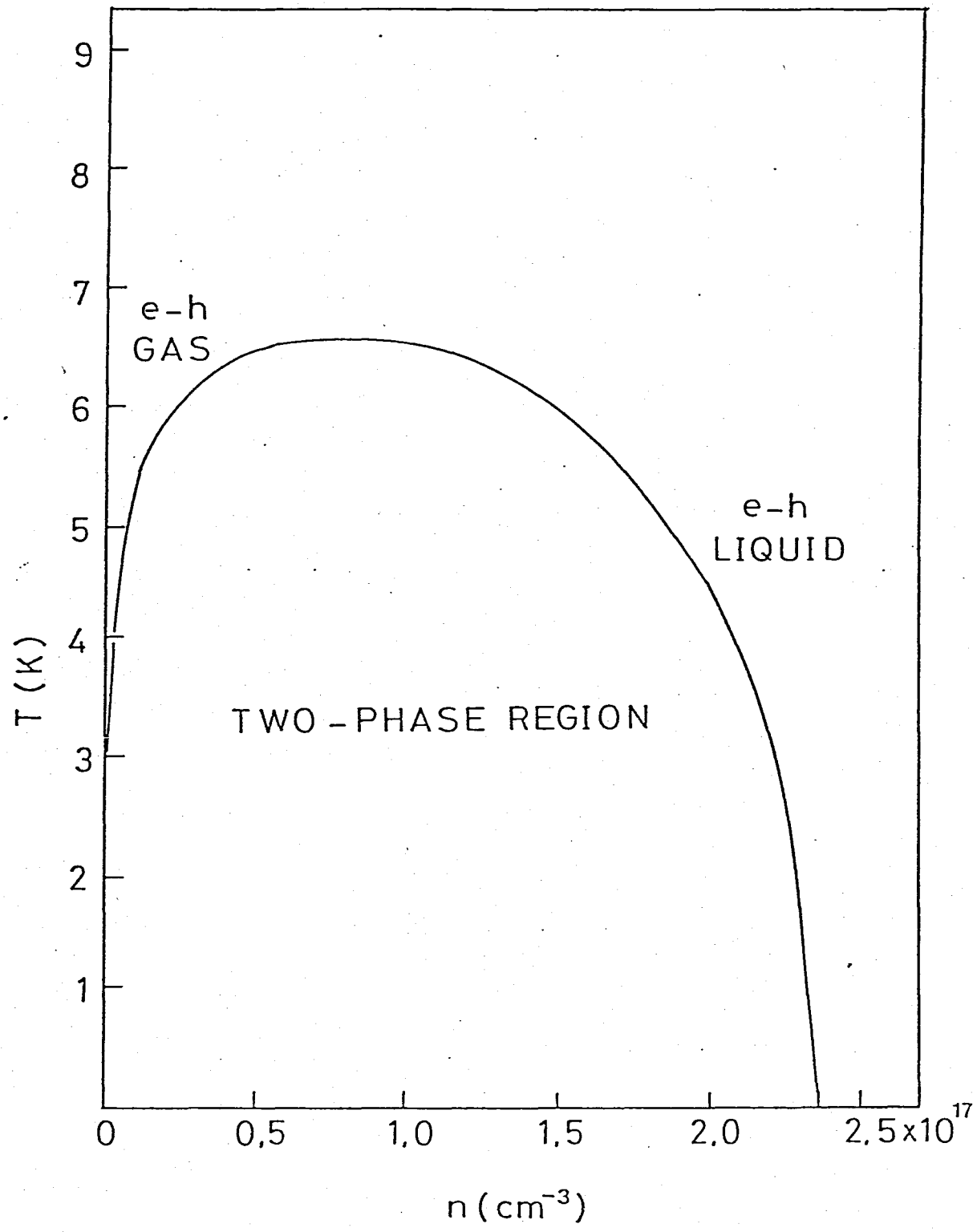
9
8
7
6
5
4
3
2
1
T (K)
e-h
GAS
e-h
LIQUID
TWO-PHASE REGION
0
0,5
1,0
1,5
2,0
2,5x10^17
n (cm^-3)

Fig.5

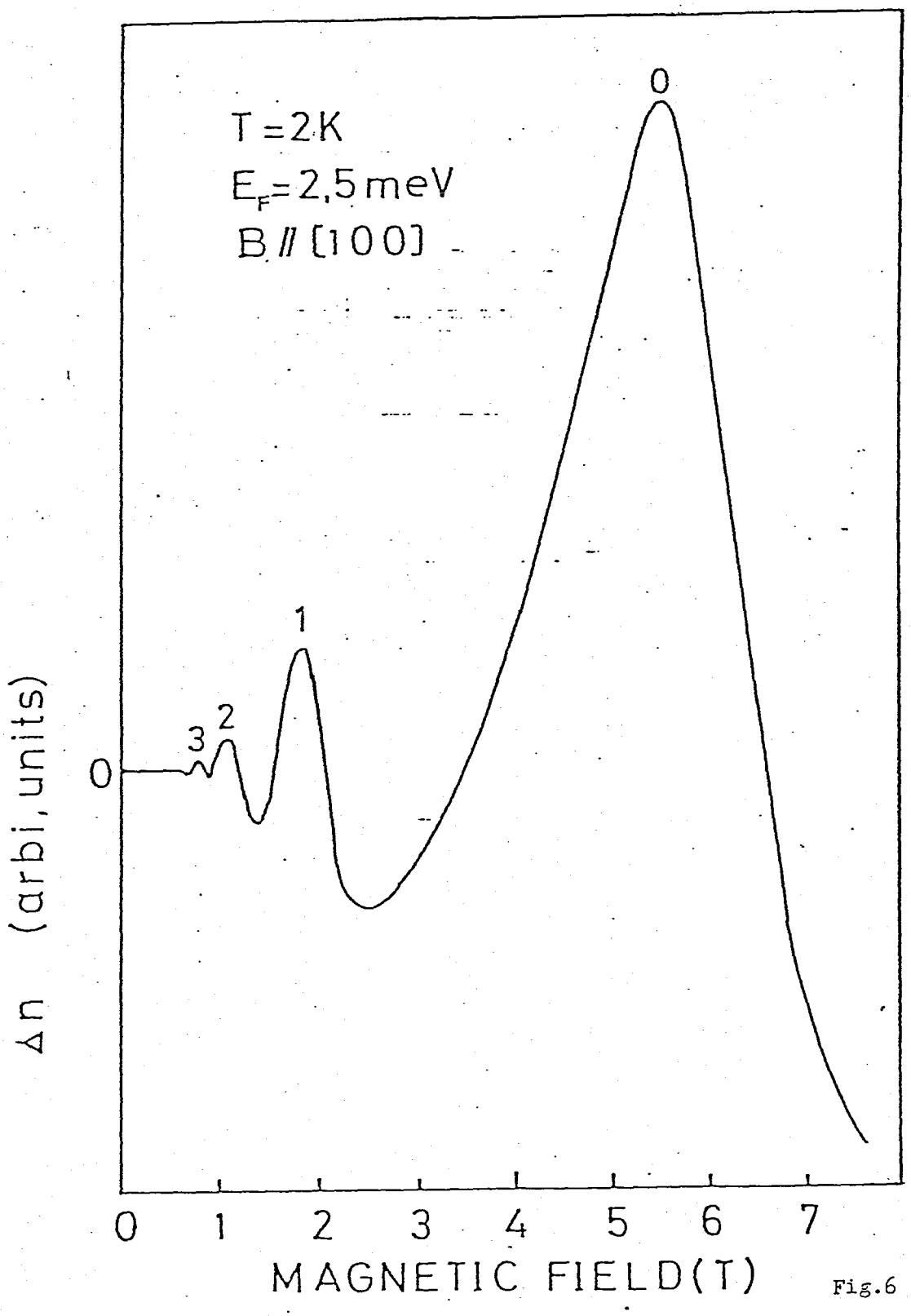
T = 2K
E_F = 2,5 meV
B // [100]
0
1
2
3
0
Δn (arbi, units)
0 1 2 3 4 5 6 7
MAGNETIC FIELD(T)

Fig.6

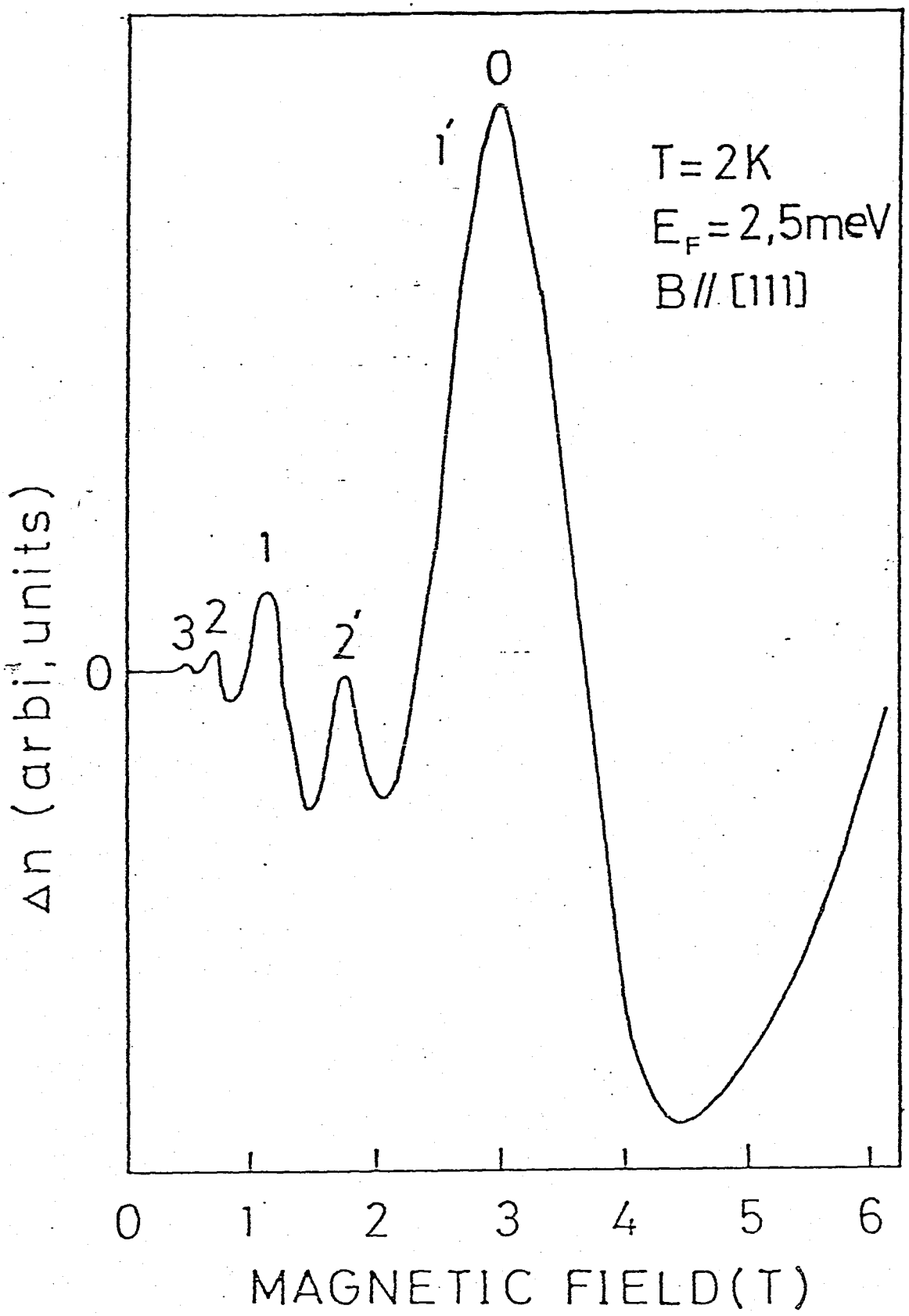
0
1'
T = 2K
E_F = 2,5meV
B // [111]
1
3 2
2'
0
Δn (arbi, units)
0 1 2 3 4 5 6
MAGNETIC FIELD (T)

Fig.7

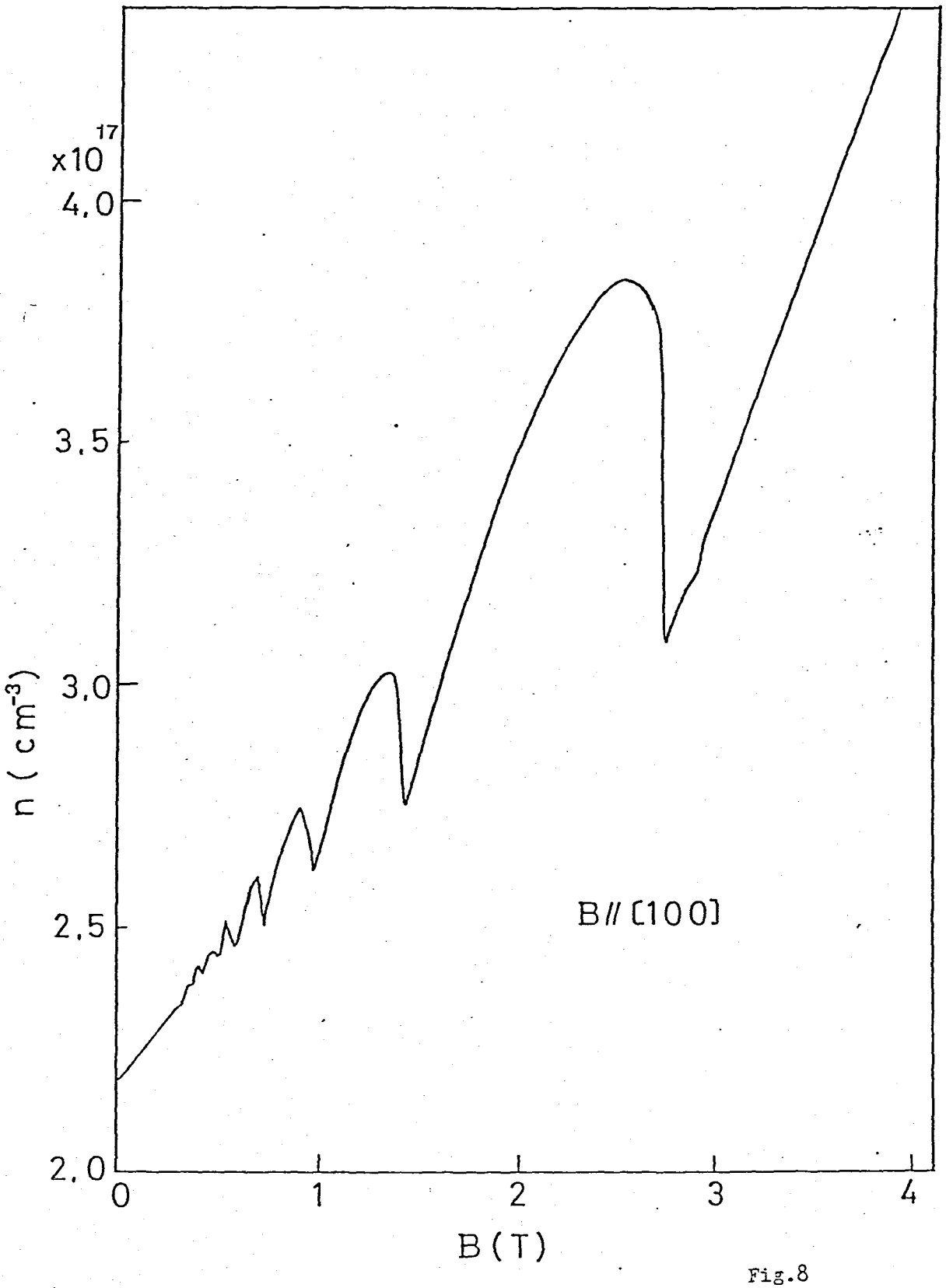

Fig.8

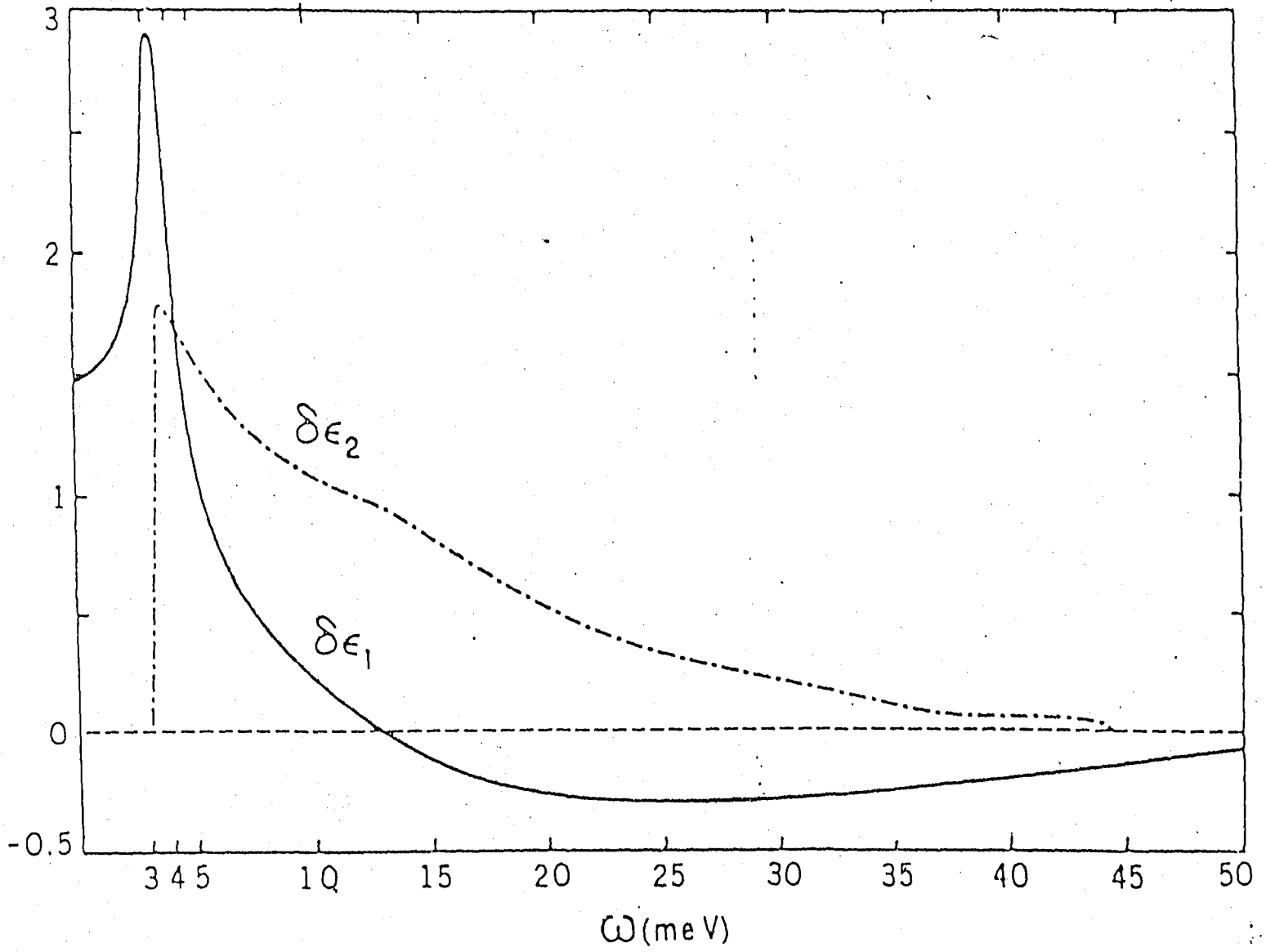
3
2
1
0
-0.5
$\delta\epsilon_2$
$\delta\epsilon_1$
3 4 5
10
15
20
25
30
35
40
45
50
ω(meV)

Fig. 9

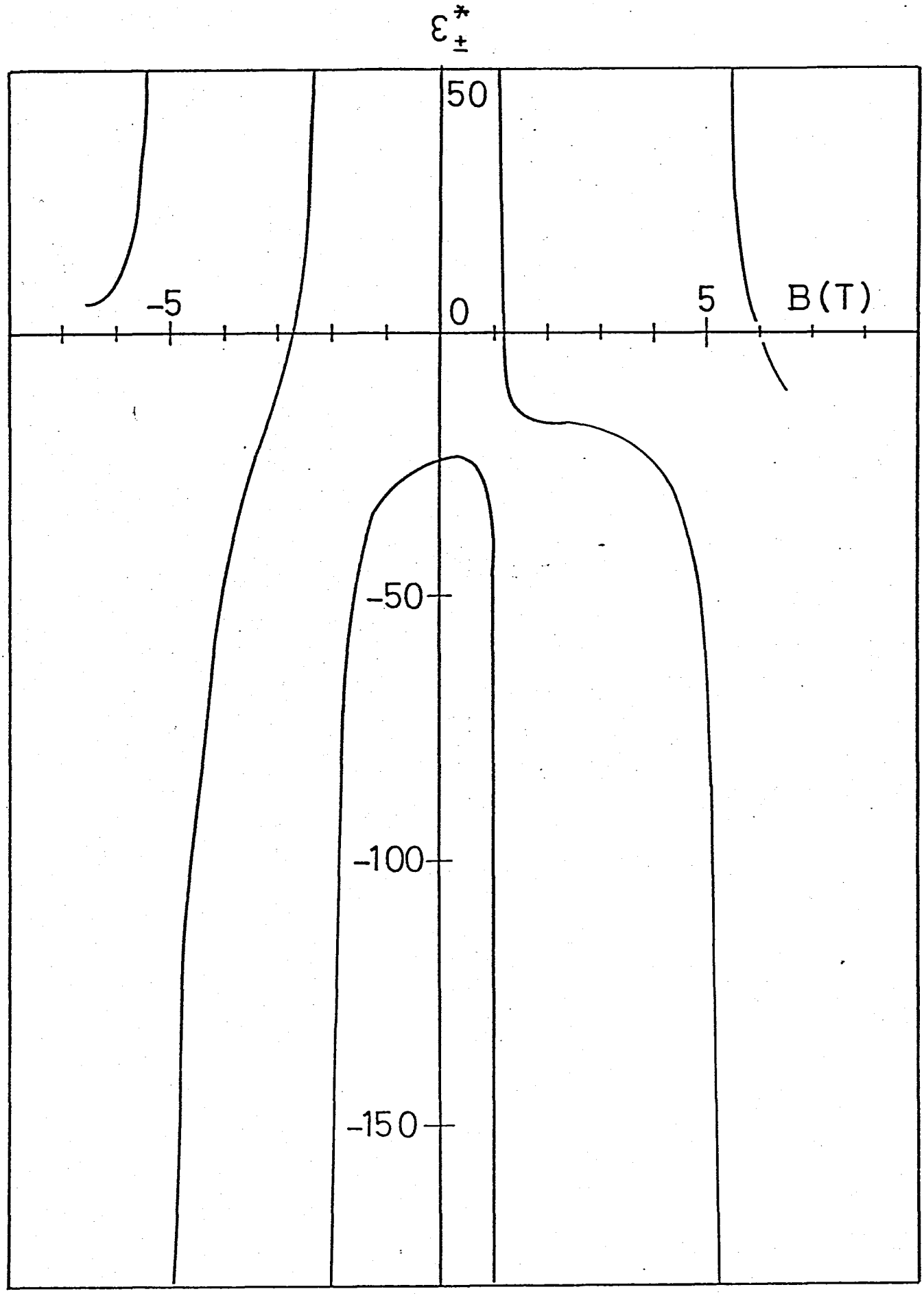

Fig.10

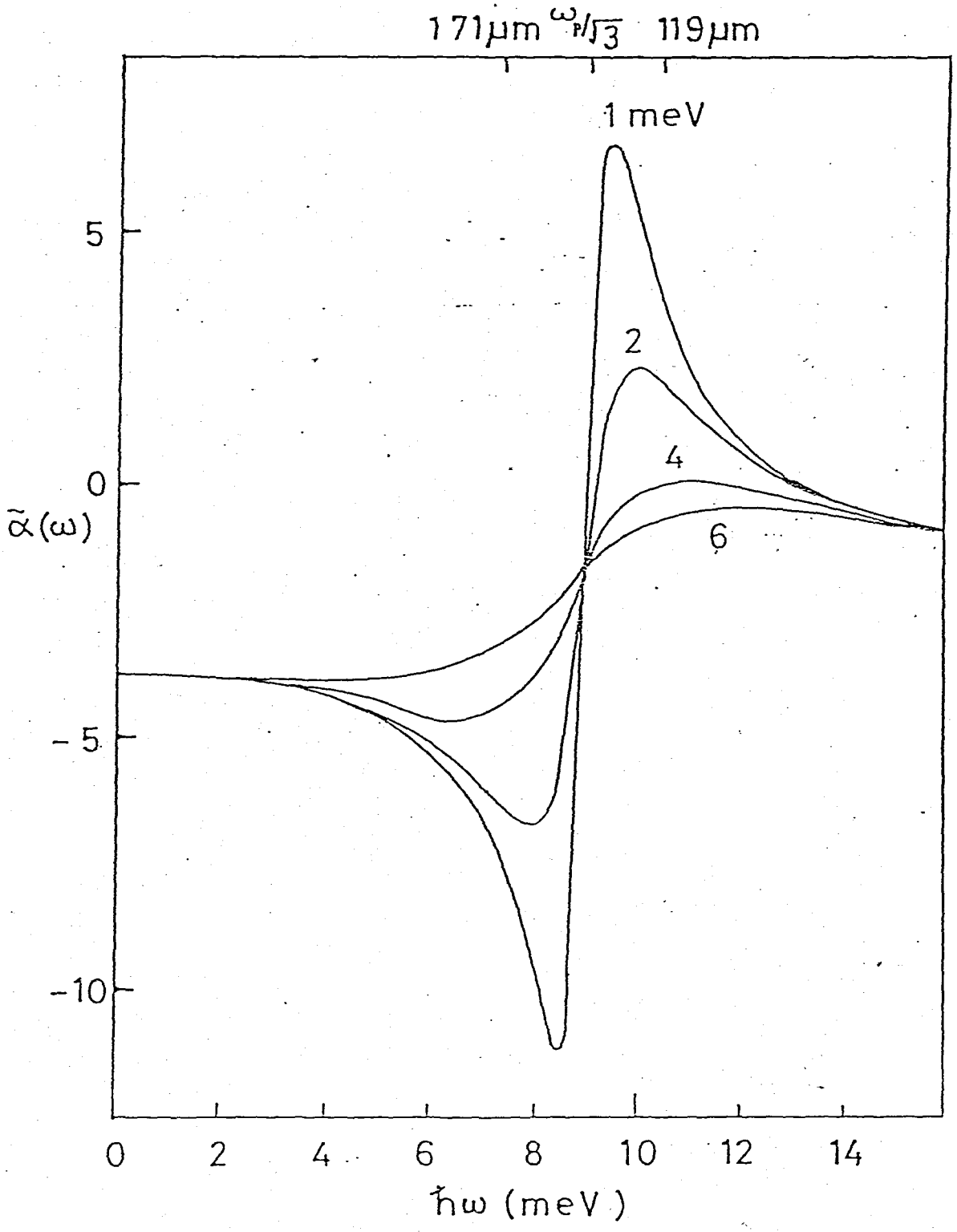
171μm
$\omega_p/\sqrt{3}$
119μm
1 meV
2
4
6
5
0
-5
-10
$\tilde{\alpha}(\omega)$
0
2
4
6
8
10
12
14
$\hbar\omega$ (meV)

Fig.11

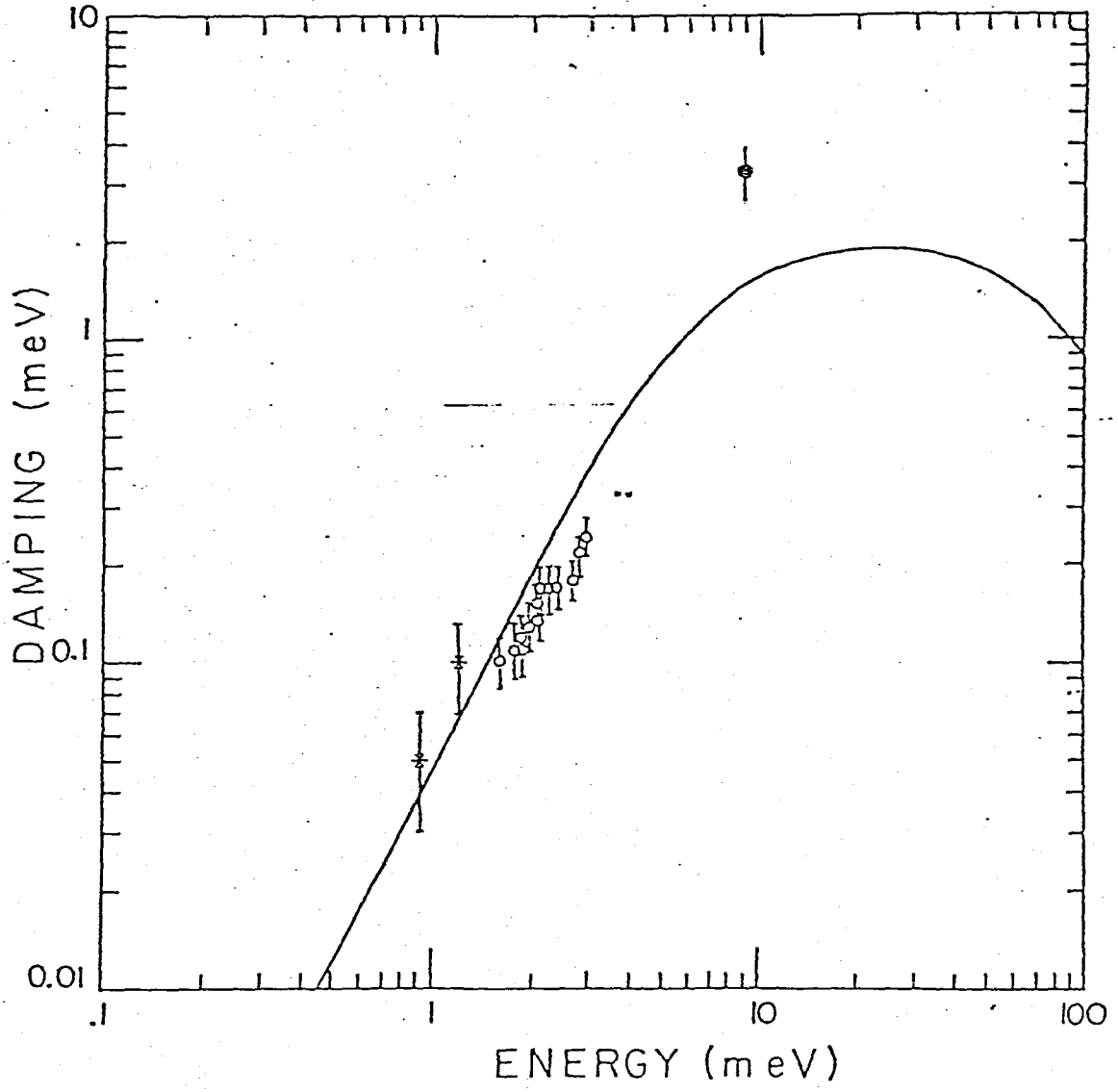

Fig.12

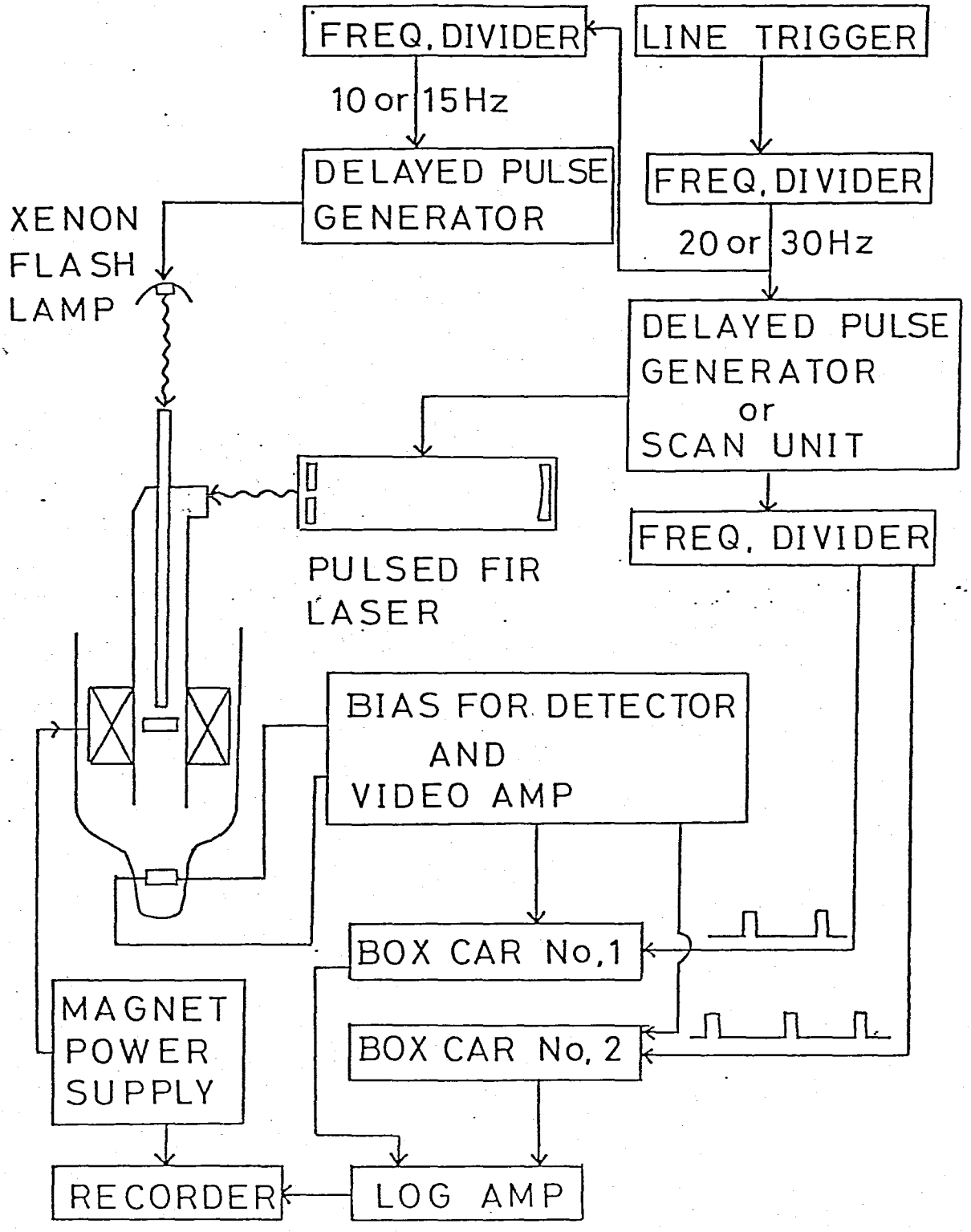
FREQ. DIVIDER
LINE TRIGGER
10 or 15Hz
DELAYED PULSE GENERATOR
FREQ. DIVIDER
XENON FLASH LAMP
20 or 30Hz
DELAYED PULSE GENERATOR or SCAN UNIT
FREQ. DIVIDER
PULSED FIR LASER
BIAS FOR DETECTOR AND VIDEO AMP
BOX CAR No. 1
MAGNET POWER SUPPLY
BOX CAR No. 2
RECORDER
LOG AMP

Fig. 13

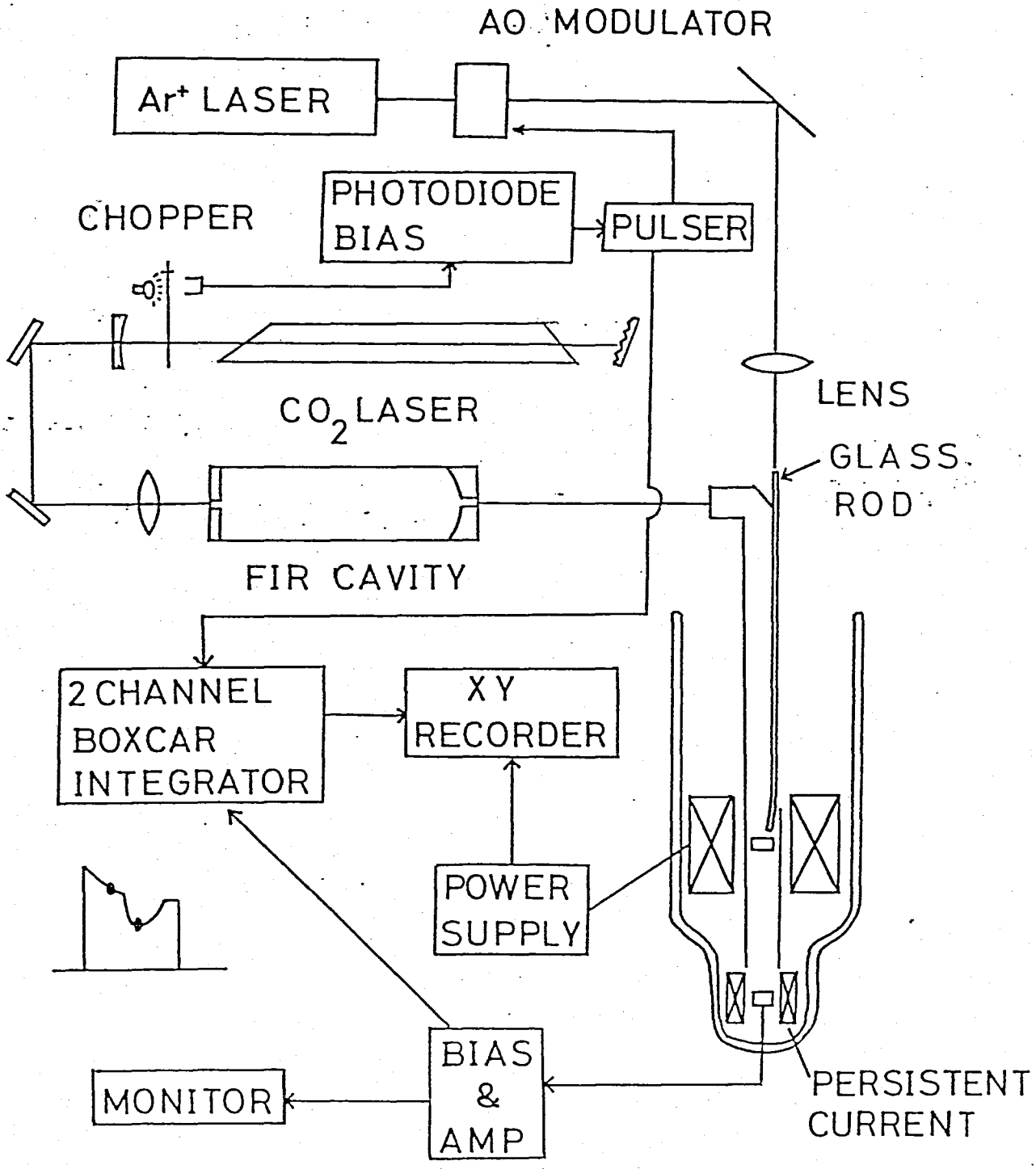
AO MODULATOR
Ar+ LASER
CHOPPER
PHOTODIODE BIAS
PULSER
CO2 LASER
LENS
GLASS ROD
FIR CAVITY
2 CHANNEL BOXCAR INTEGRATOR
XY RECORDER
POWER SUPPLY
BIAS & AMP
MONITOR
PERSISTENT CURRENT

Fig.14

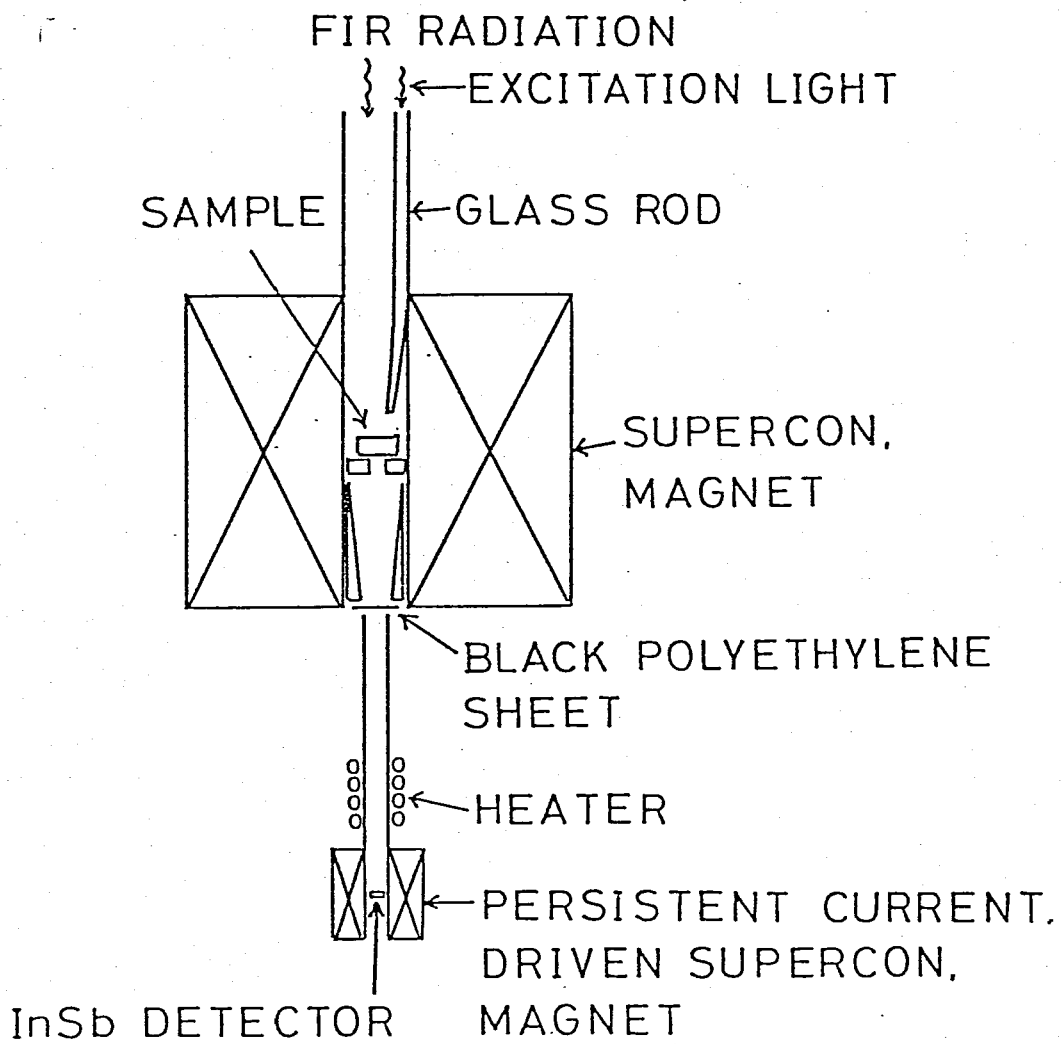
FIR RADIATION
EXCITATION LIGHT
SAMPLE
GLASS ROD
SUPERCON.
MAGNET
BLACK POLYETHYLENE
SHEET
HEATER
PERSISTENT CURRENT.
DRIVEN SUPERCON.
MAGNET
InSb DETECTOR

Fig.15

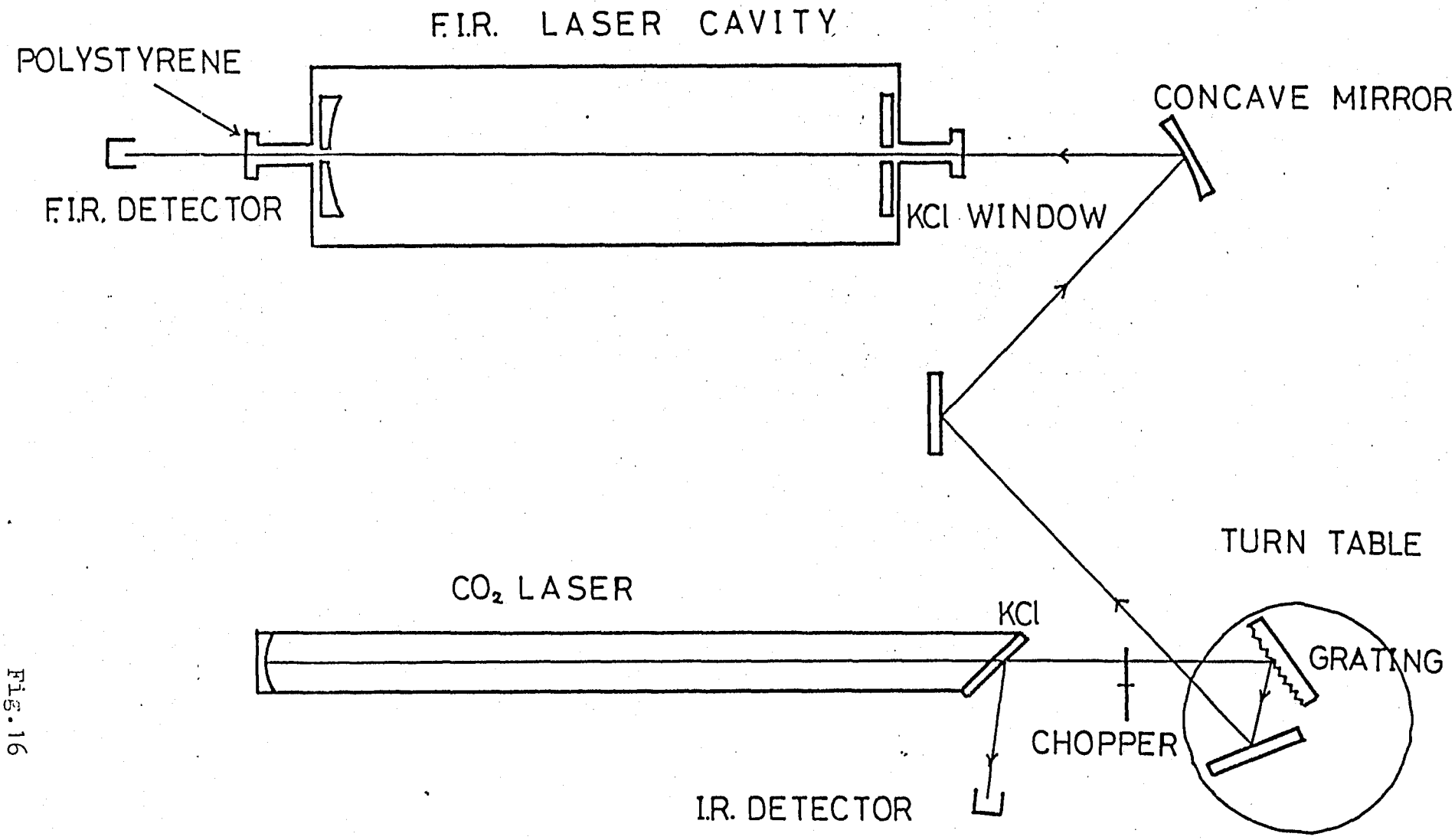
F.I.R. LASER CAVITY
POLYSTYRENE
CONCAVE MIRROR
F.I.R. DETECTOR
KCl WINDOW
TURN TABLE
CO_2 LASER
KCl
GRATING
CHOPPER
I.R. DETECTOR

Fig. 16

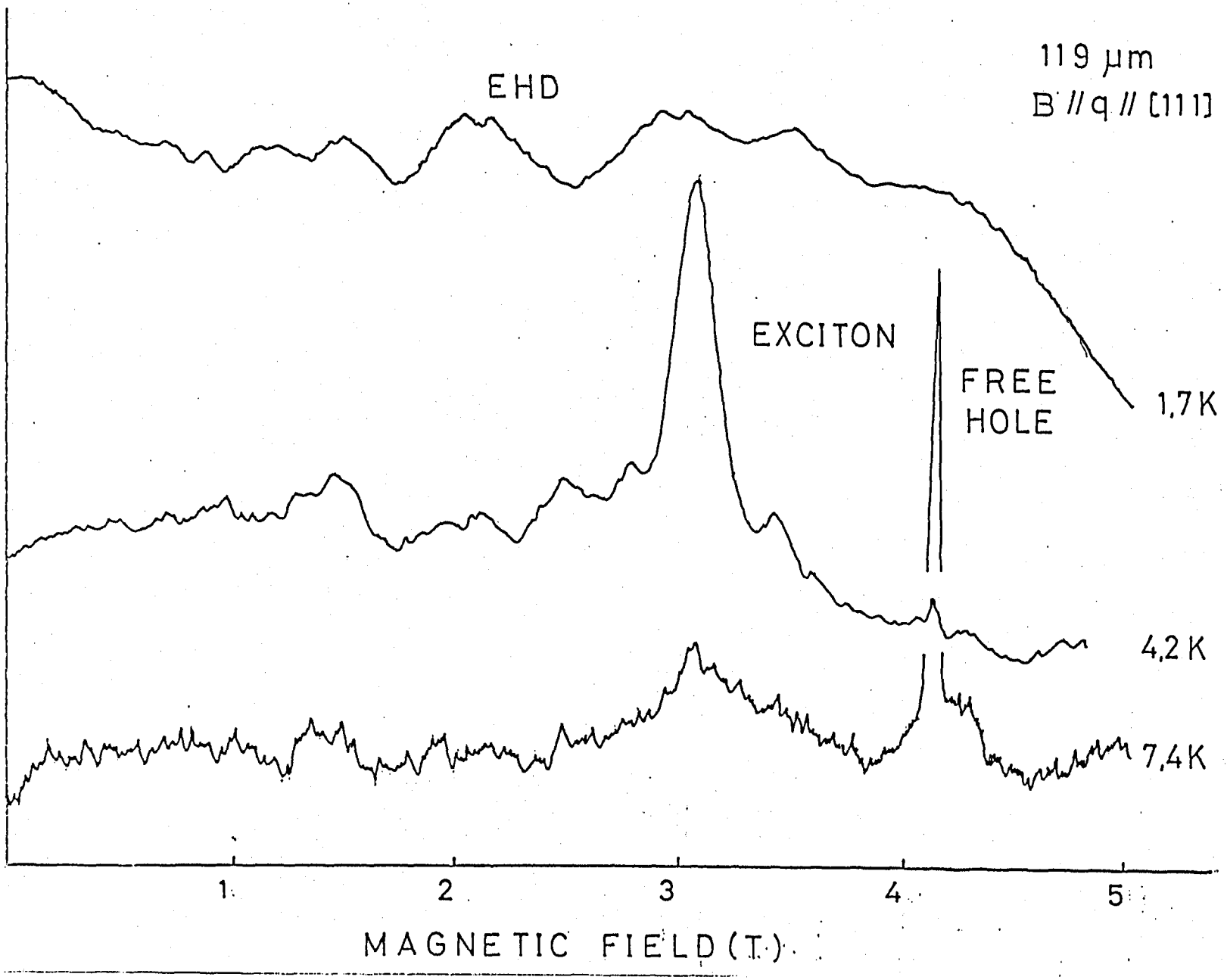
119 µm
B // q // [111]
EHD
EXCITON
FREE
HOLE
1,7 K
4,2 K
7,4 K
ABSORPTION
1
2
3
4
5
MAGNETIC FIELD (T)

Fig.17

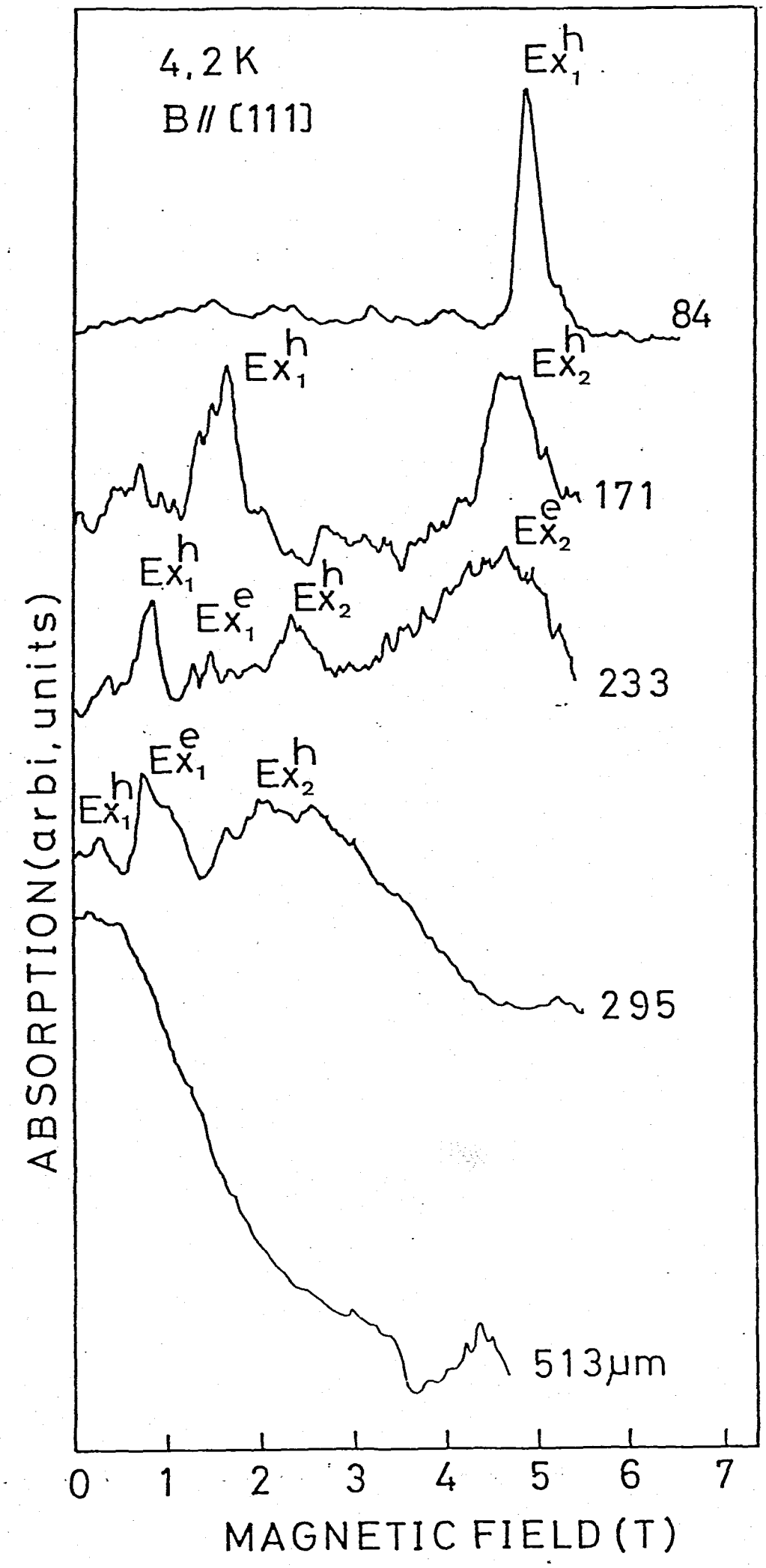
4,2 K
B // [111]
Ex_1^h
84
Ex_1^h
Ex_2^h
171
Ex_2^e
Ex_1^h
Ex_1^e
Ex_2^h
233
Ex_1^e
Ex_1^h
Ex_2^h
295
513μm
ABSORPTION(arbi, units)
0 1 2 3 4 5 6 7
MAGNETIC FIELD (T)

Fig.18

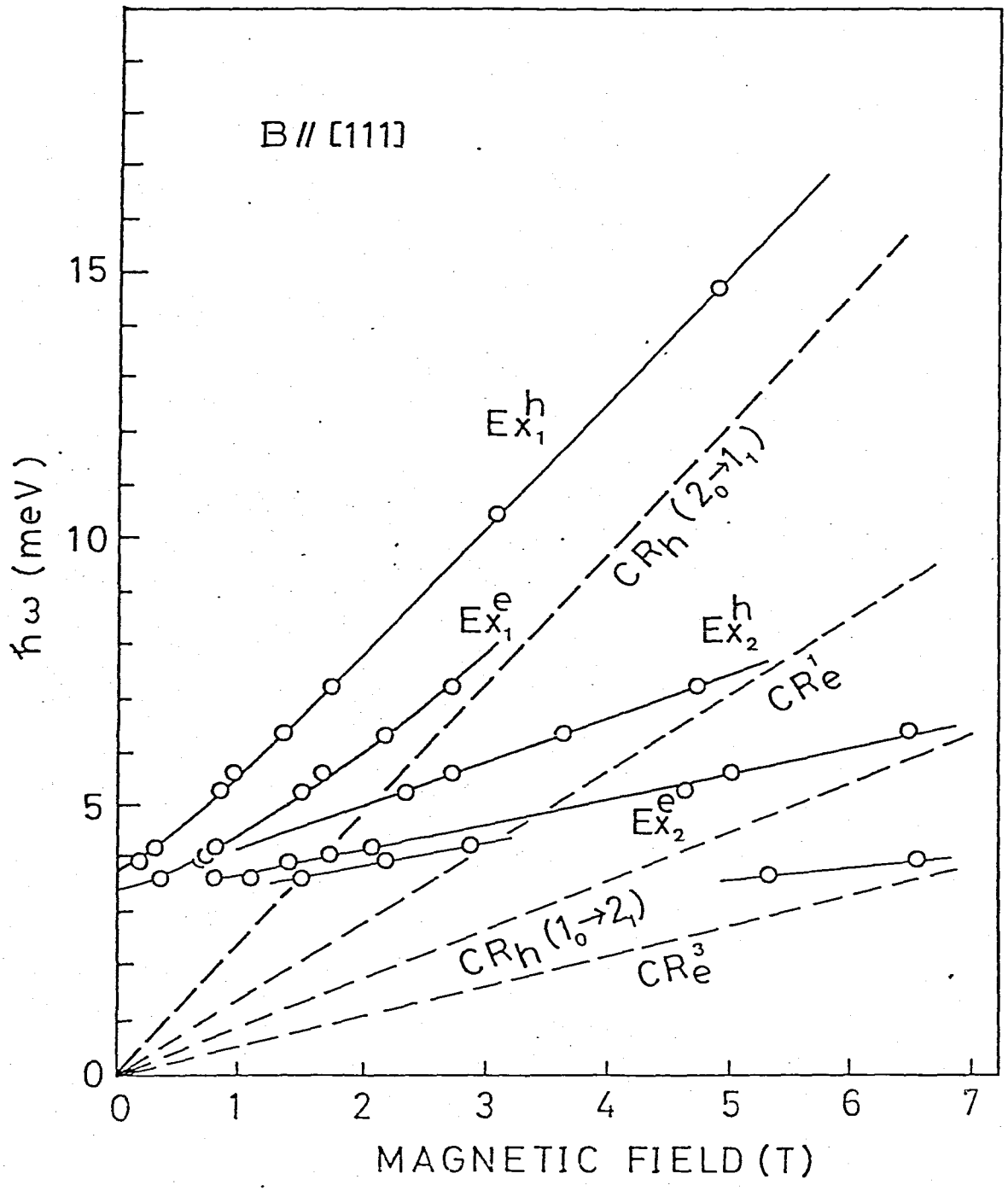
B // [111]
Ex_1^h
Ex_1^e
$CRh(2_0 \to 1_1)$
Ex_2^h
CR_e^1
Ex_2^e
$CRh(1_0 \to 2_1)$
CR_e^3
ħω (meV)
MAGNETIC FIELD (T)
0
5
10
15
0
1
2
3
4
5
6
7

Fig.19

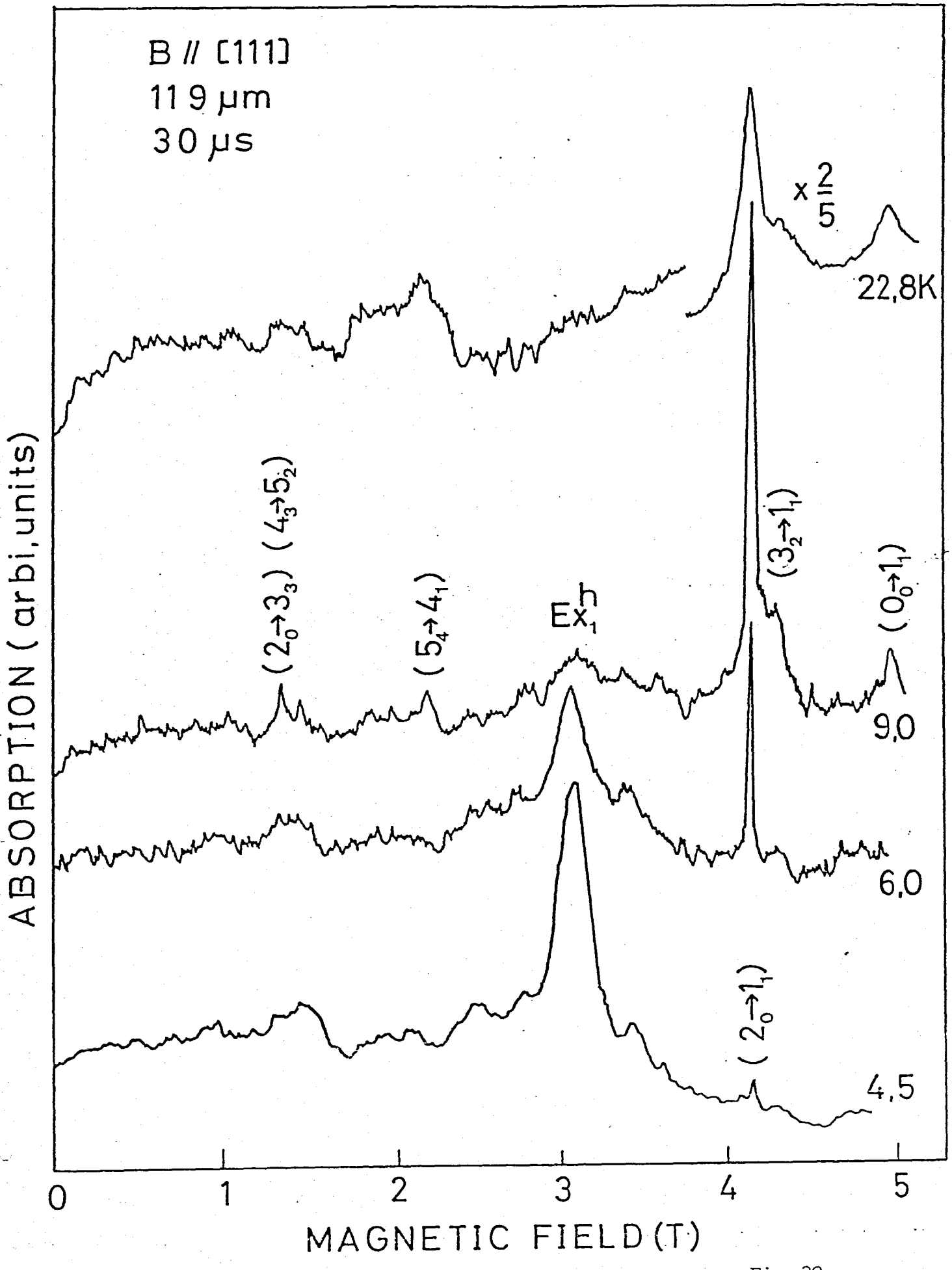
B // [111]
119 μm
30 μs
x 2/5
22,8K
(2₀→3₃) (4₃→5₂)
(5₄→4₁)
Ex^h₁
(3₂→1₁)
(0₀→1₁)
9,0
6,0
(2₀→1₁)
4,5
ABSORPTION (arbi.units)
0
1
2
3
4
5
MAGNETIC FIELD (T)

Fig.20

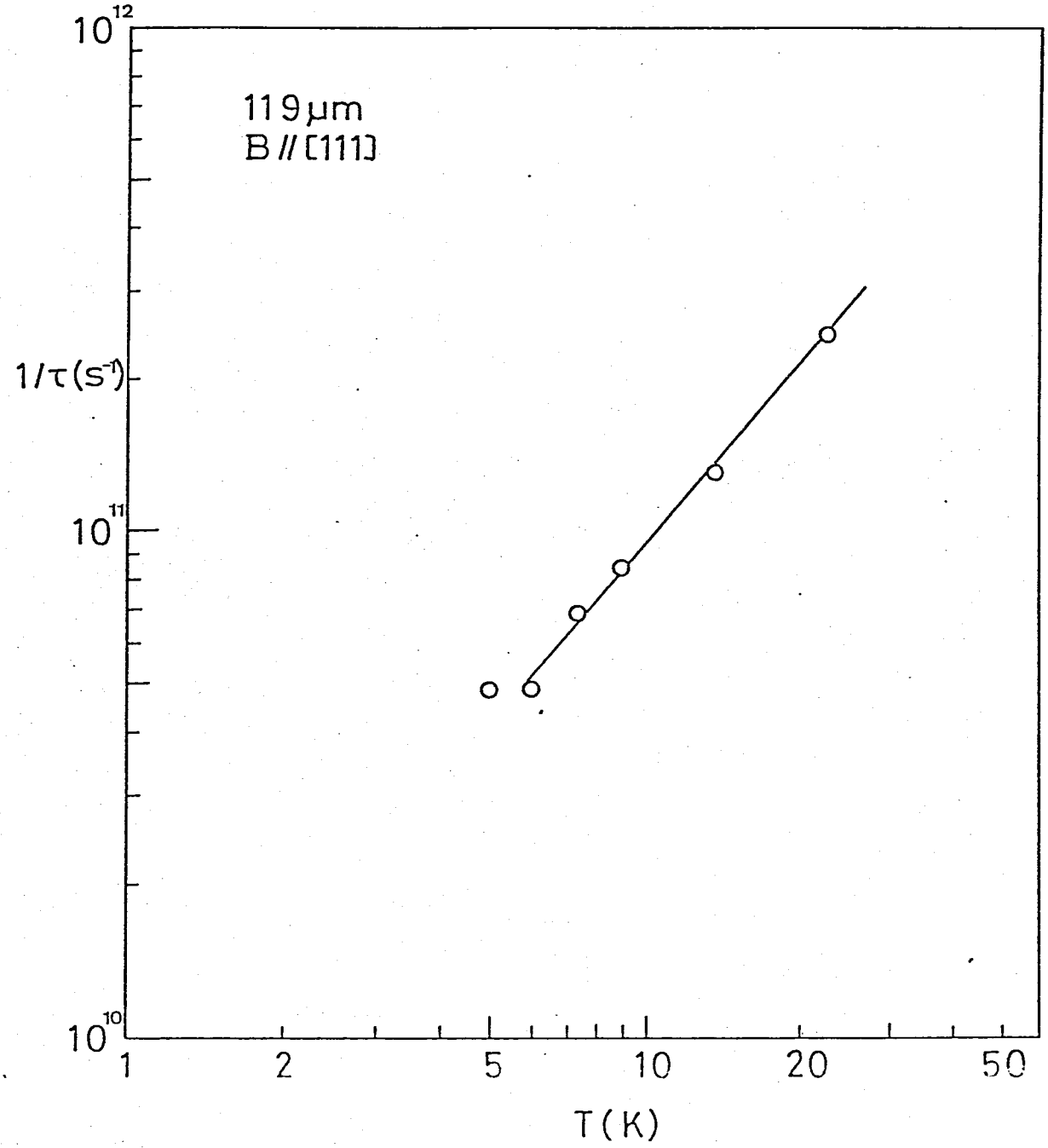

Fig.21

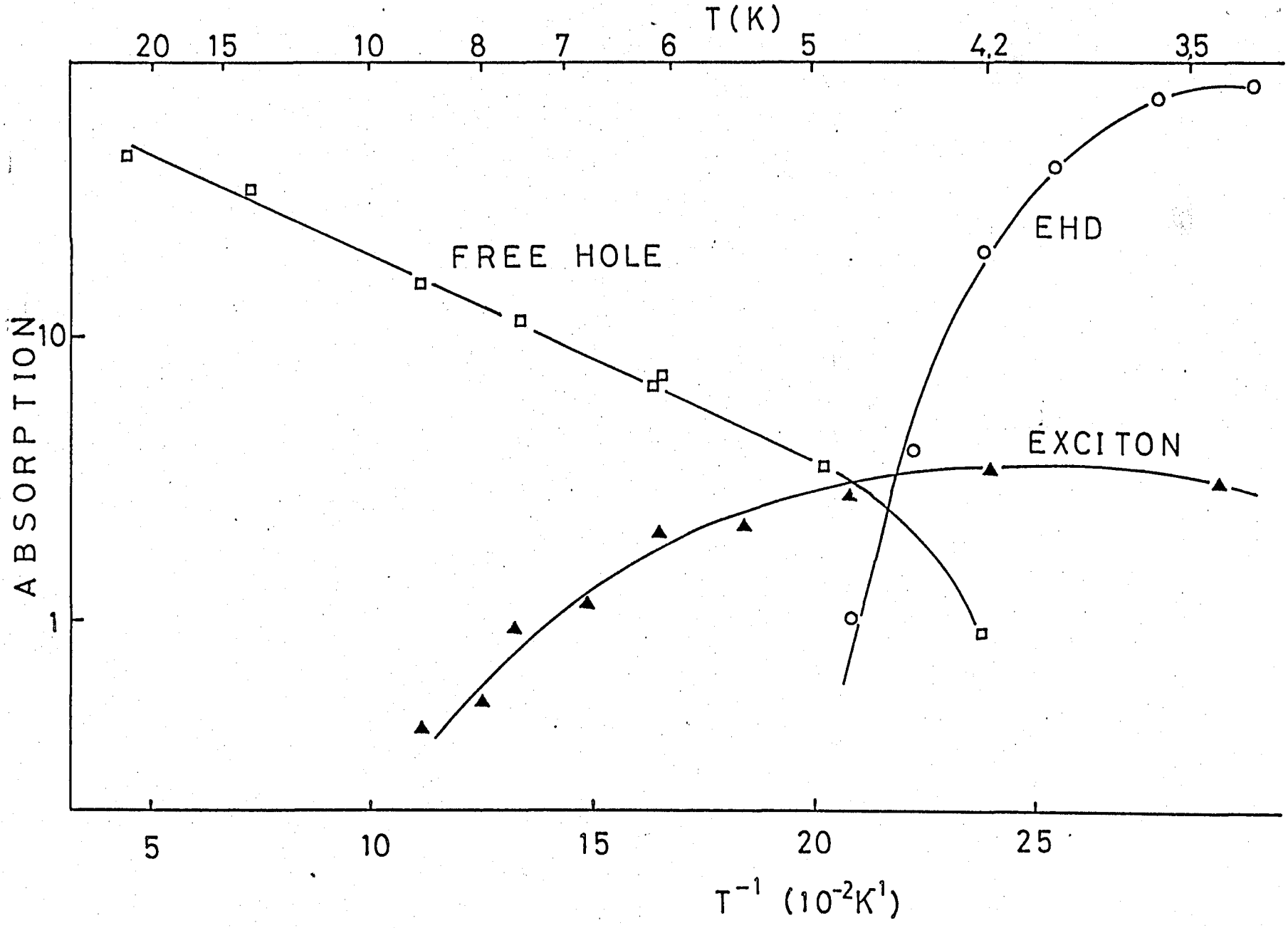
T(K)
20
15
10
8
7
6
5
4,2
3,5
FREE HOLE
EHD
EXCITON
ABSORPTION
10
1
5
10
15
20
25
T⁻¹ (10⁻²K¹)

Fig.22

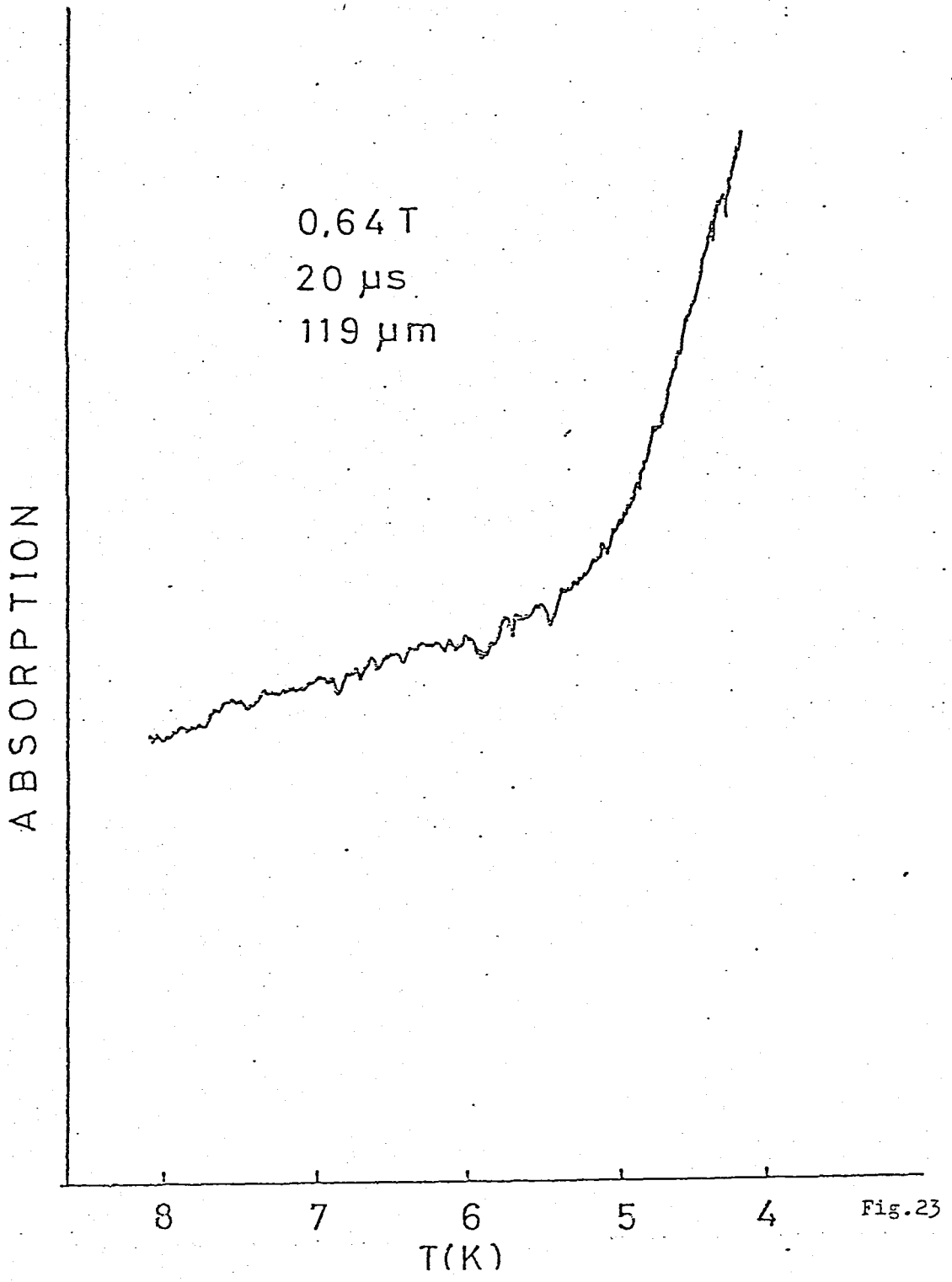

Fig.23

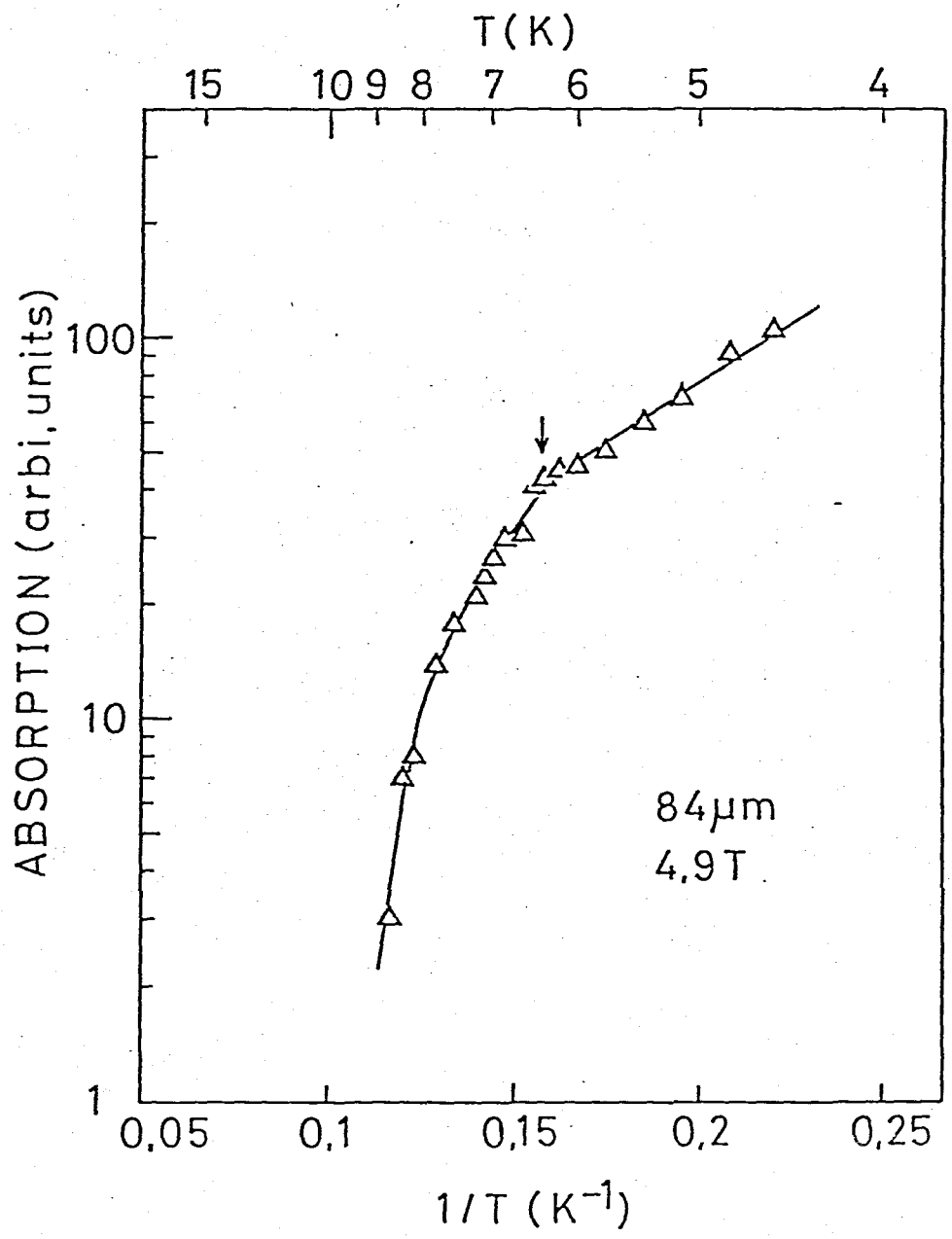
T(K)
15
10
9
8
7
6
5
4
ABSORPTION (arbi. units)
100
10
1
84μm
4,9T
0,05
0,1
0,15
0,2
0,25
1/T (K⁻¹)

Fig.24

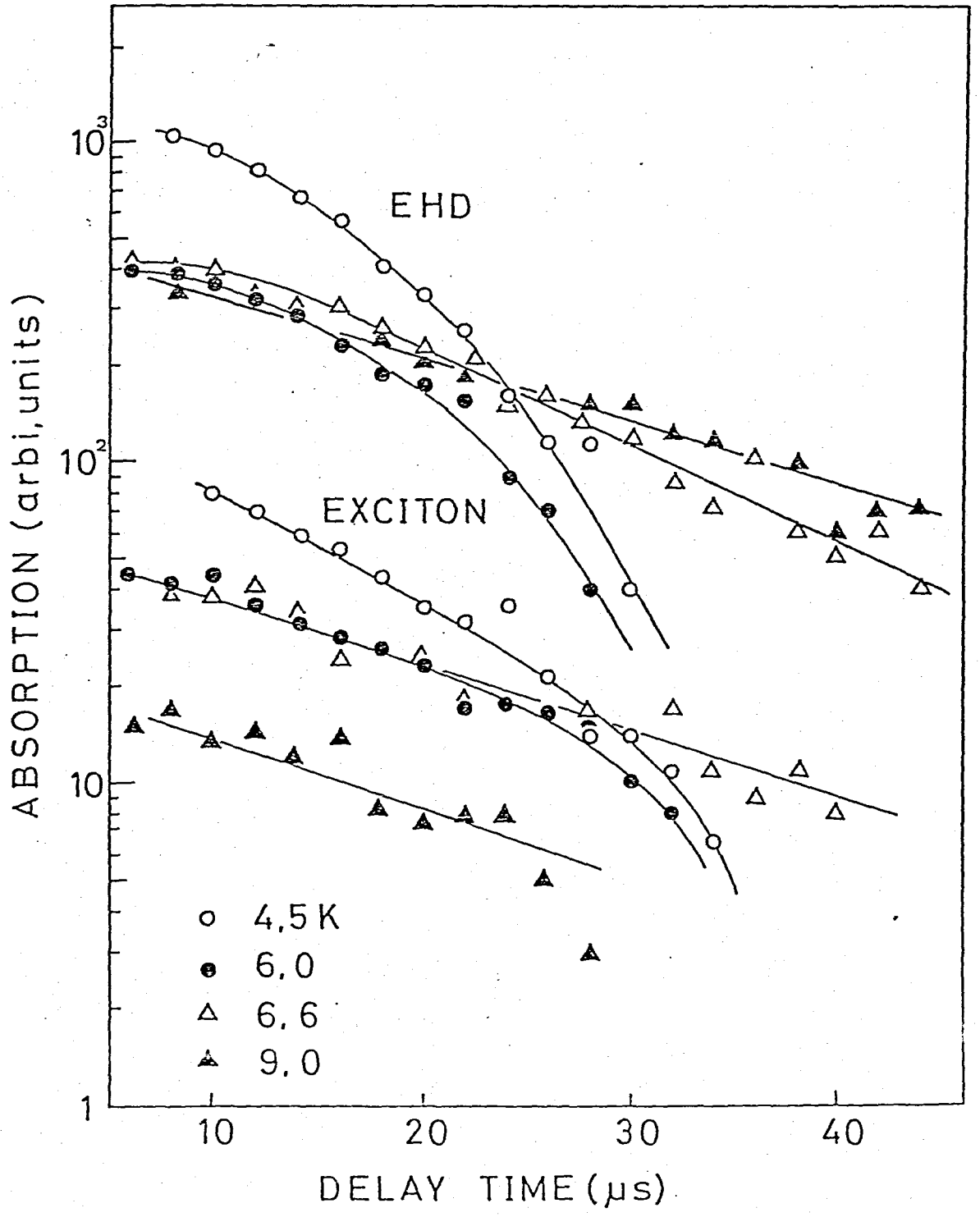
ABSORPTION (arbi,units)
10^3
10^2
10
1
EHD
EXCITON
4,5 K
6,0
6,6
9,0
10
20
30
40
DELAY TIME (μs)

Fig.25

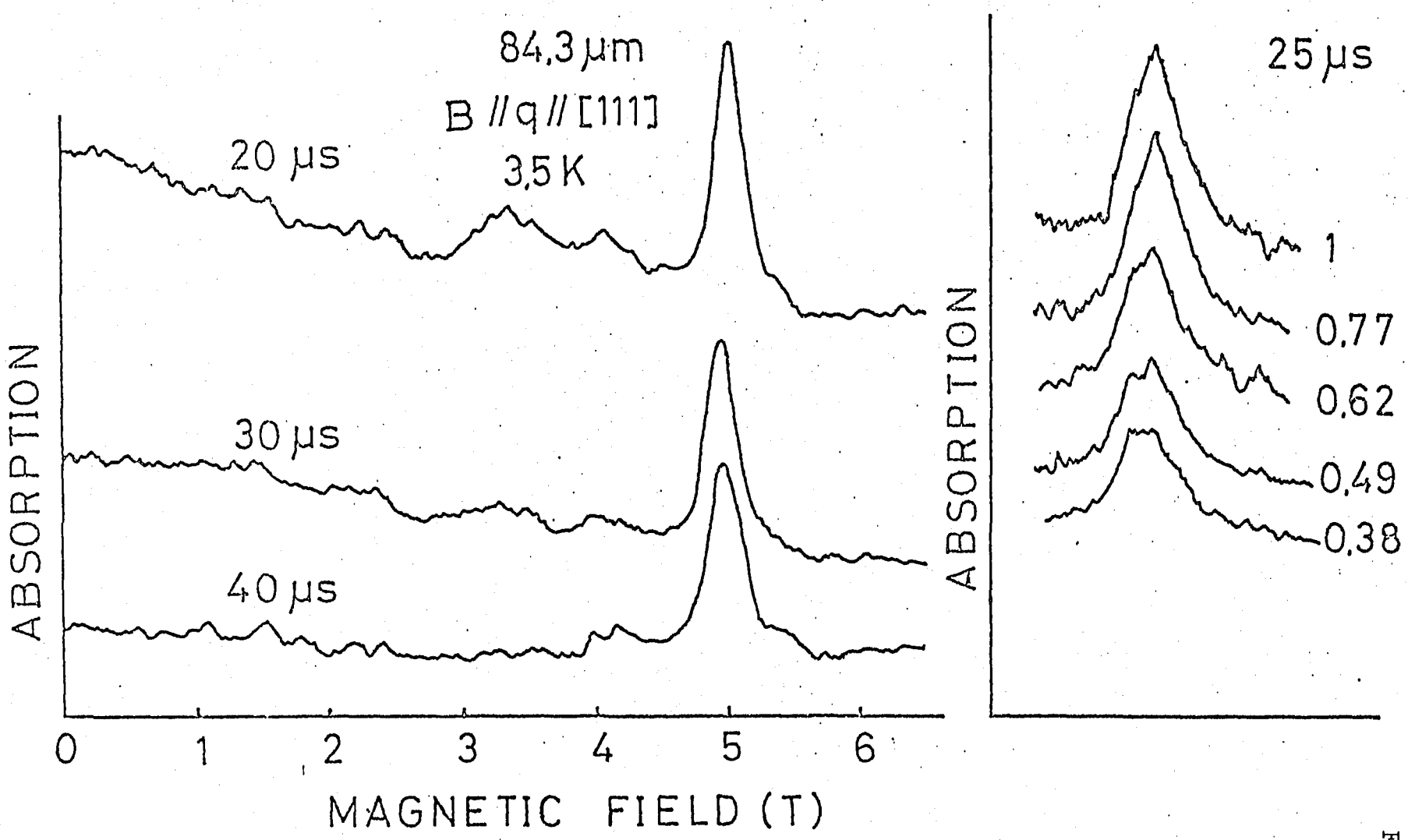
84,3 µm
B // q // [111]
3,5 K
20 µs
30 µs
40 µs
ABSORPTION
0
1
2
3
4
5
6
MAGNETIC FIELD (T)

Fig.27

25 µs
1
0,77
0,62
0,49
0,38
ABSORPTION

Fig.26

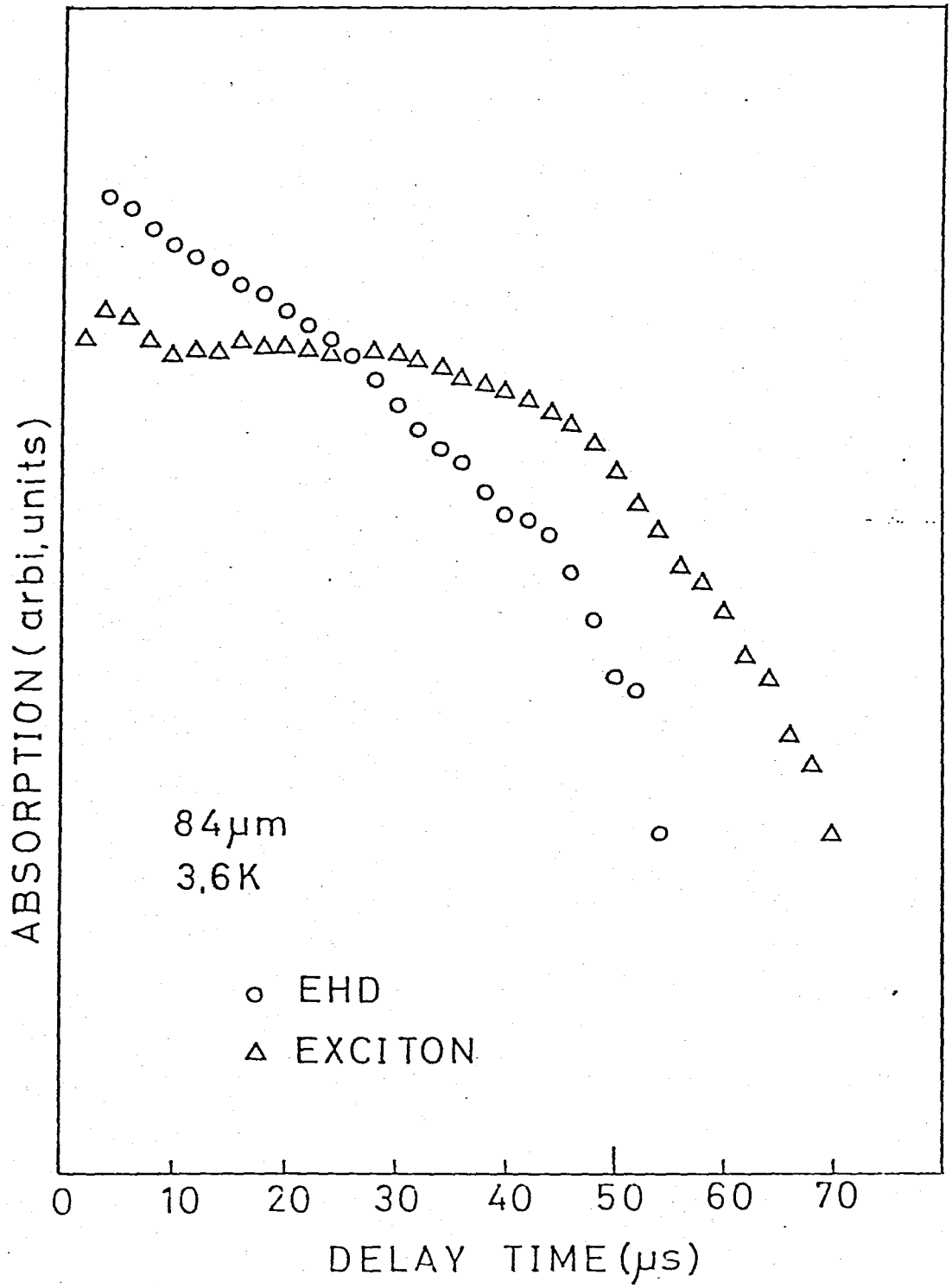
ABSORPTION (arbi, units)
84μm
3.6K
o EHD
Δ EXCITON
0
10
20
30
40
50
60
70
DELAY TIME (μs)

Fig.28

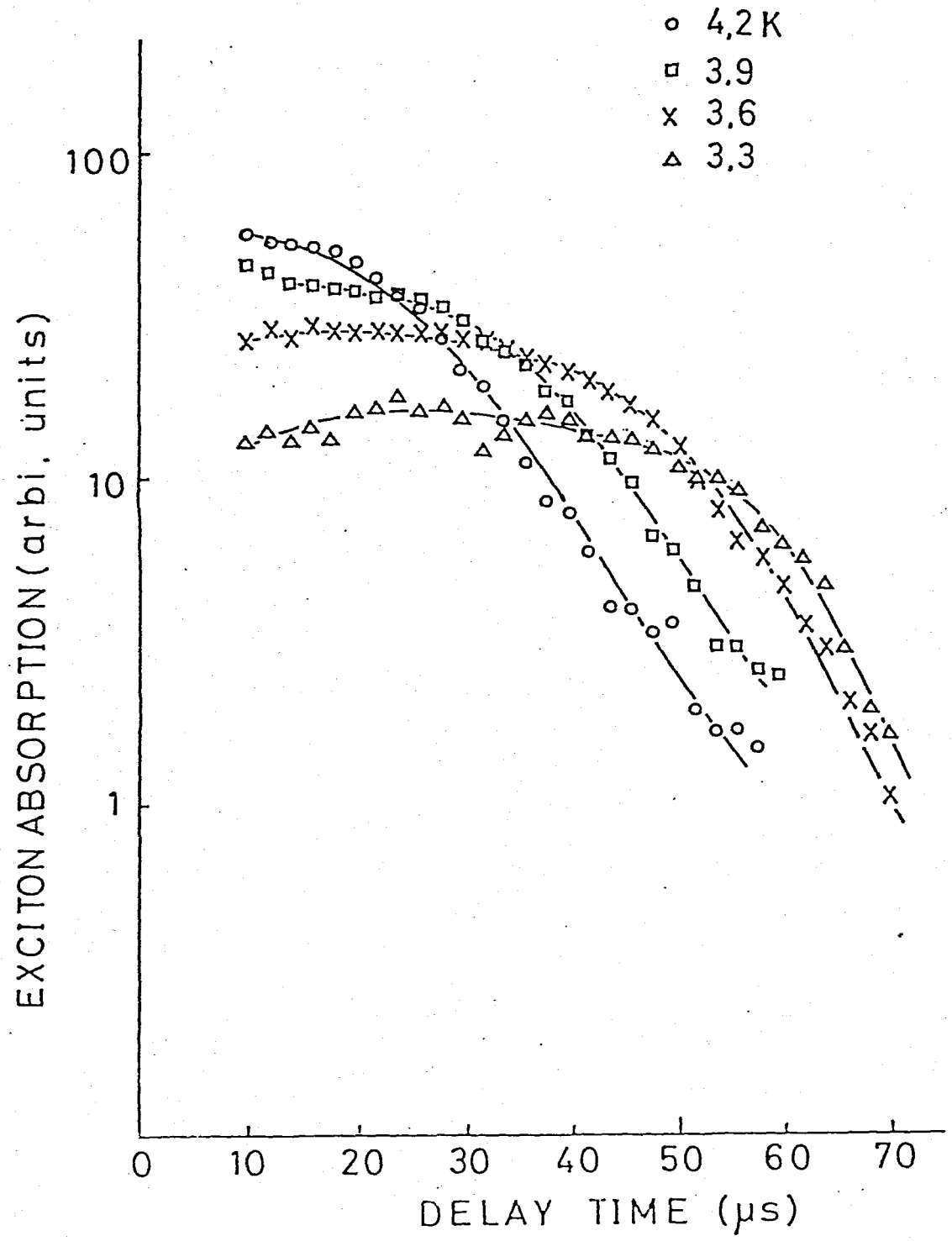
o 4,2 K
□ 3,9
x 3,6
△ 3,3
100
10
1
EXCITON ABSORPTION (arbi. units)
0
10
20
30
40
50
60
70
DELAY TIME (μs)

Fig.29

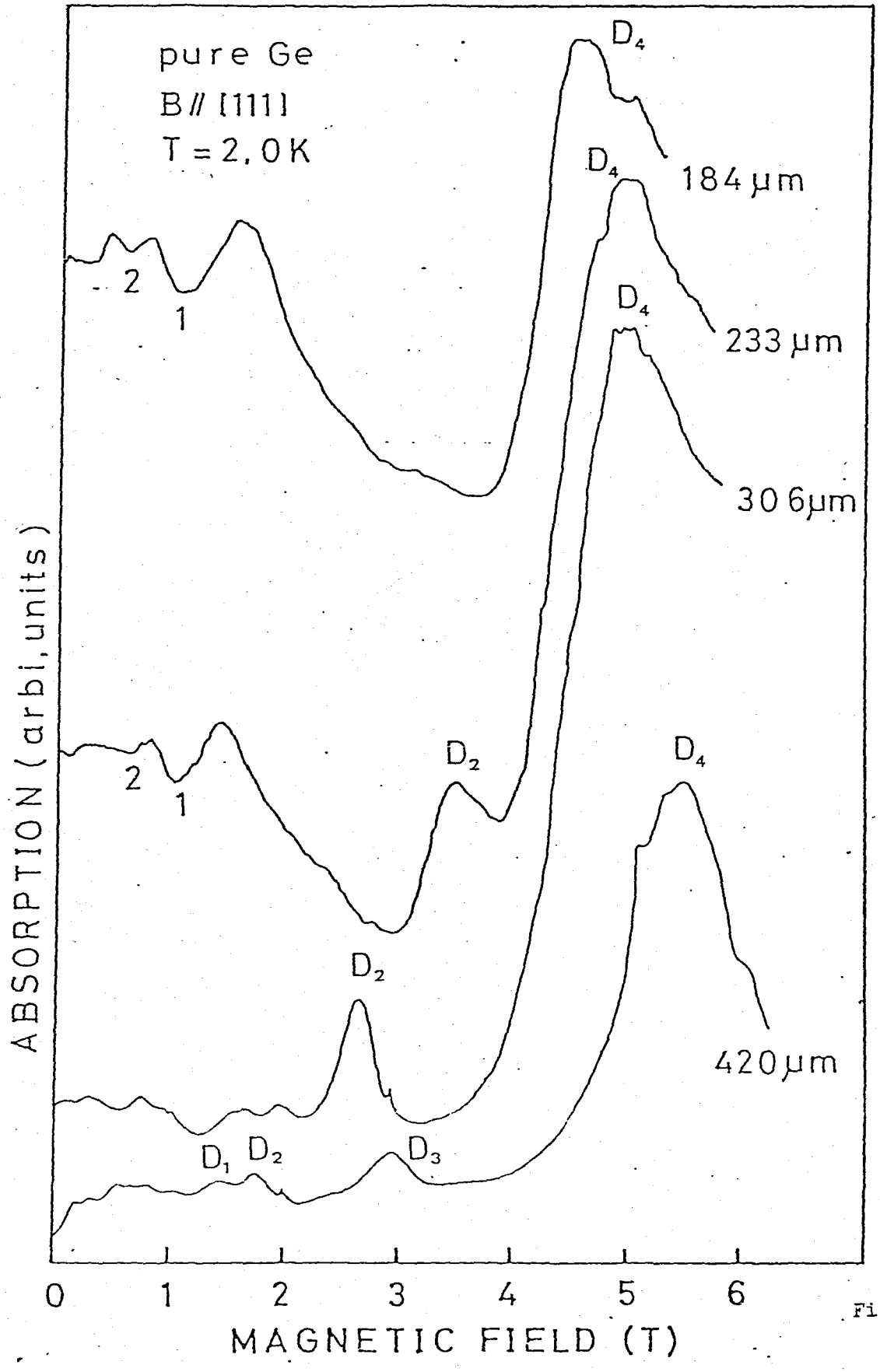
pure Ge
B // [111]
T = 2.0 K
D4
184 μm
D4
233 μm
D4
306μm
2
1
2
1
D2
D4
D2
420μm
D1 D2
D3
ABSORPTION (arbi. units)
0
1
2
3
4
5
6
MAGNETIC FIELD (T)

Fig.30

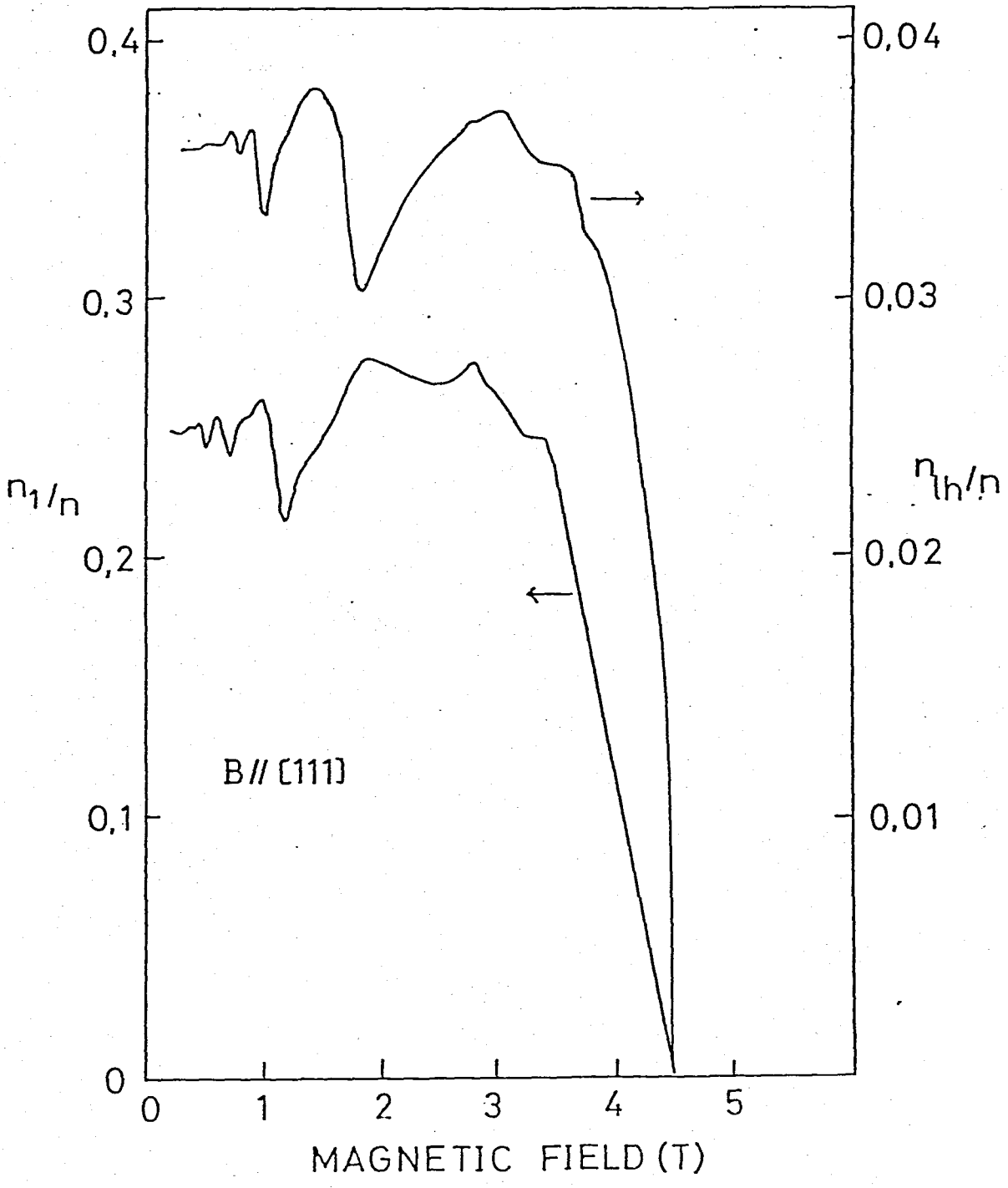
0,4
0,3
0,2
0,1
0
0,04
0,03
0,02
0,01
n_1/n
n_{lh}/n
B // [111]
0
1
2
3
4
5
MAGNETIC FIELD (T)

Fig.31

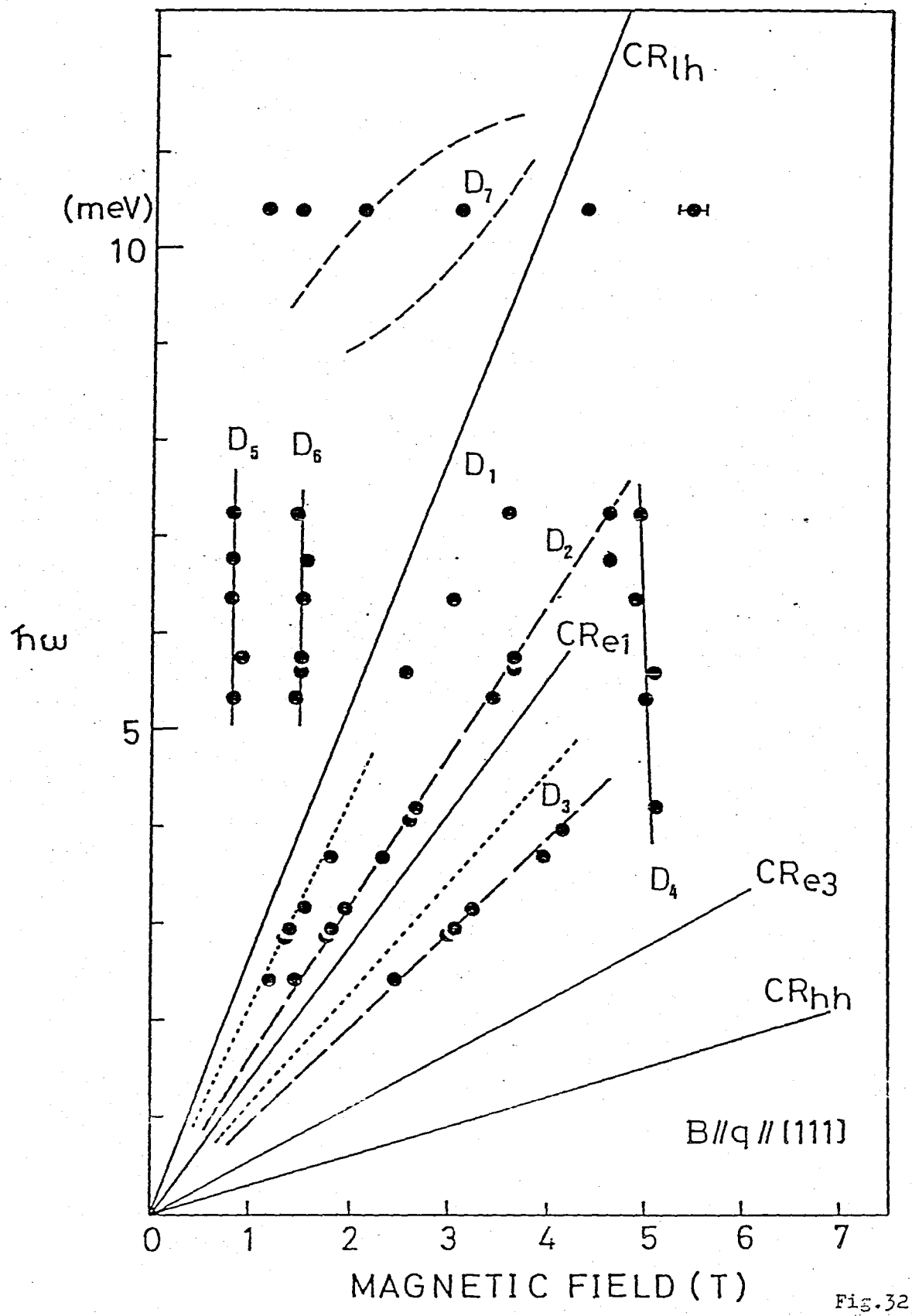
CRlh
D7
(meV)
10
D5
D6
D1
D2
CRe1
ħω
5
D3
D4
CRe3
CRhh
B//q//[111]
0
1
2
3
4
5
6
7
MAGNETIC FIELD (T)

Fig.32

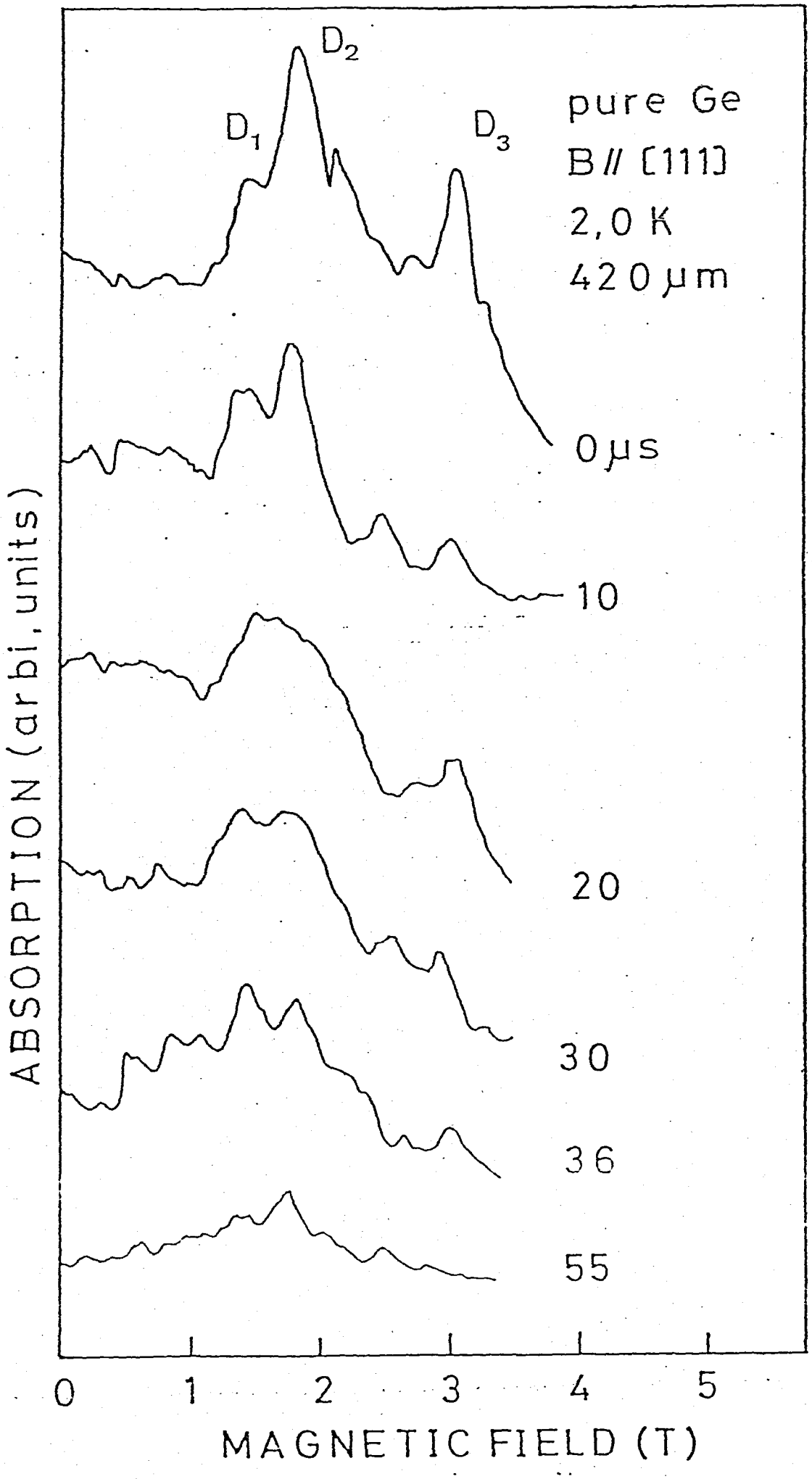
D1
D2
D3
pure Ge
B // [111]
2,0 K
420 µm
0µs
10
20
30
36
55
ABSORPTION (arbi.units)
0
1
2
3
4
5
MAGNETIC FIELD (T)

Fig.33

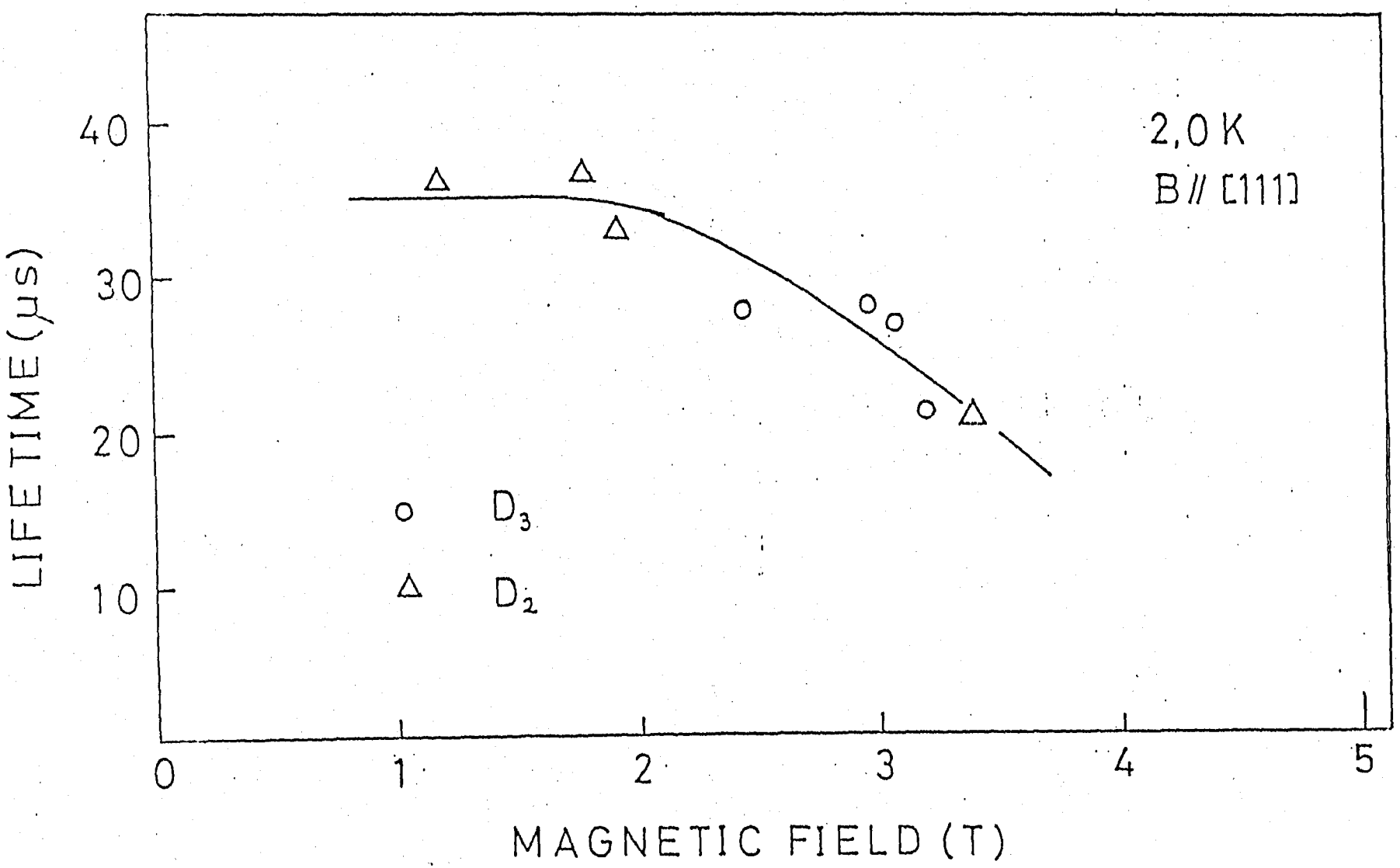

Fig. 34

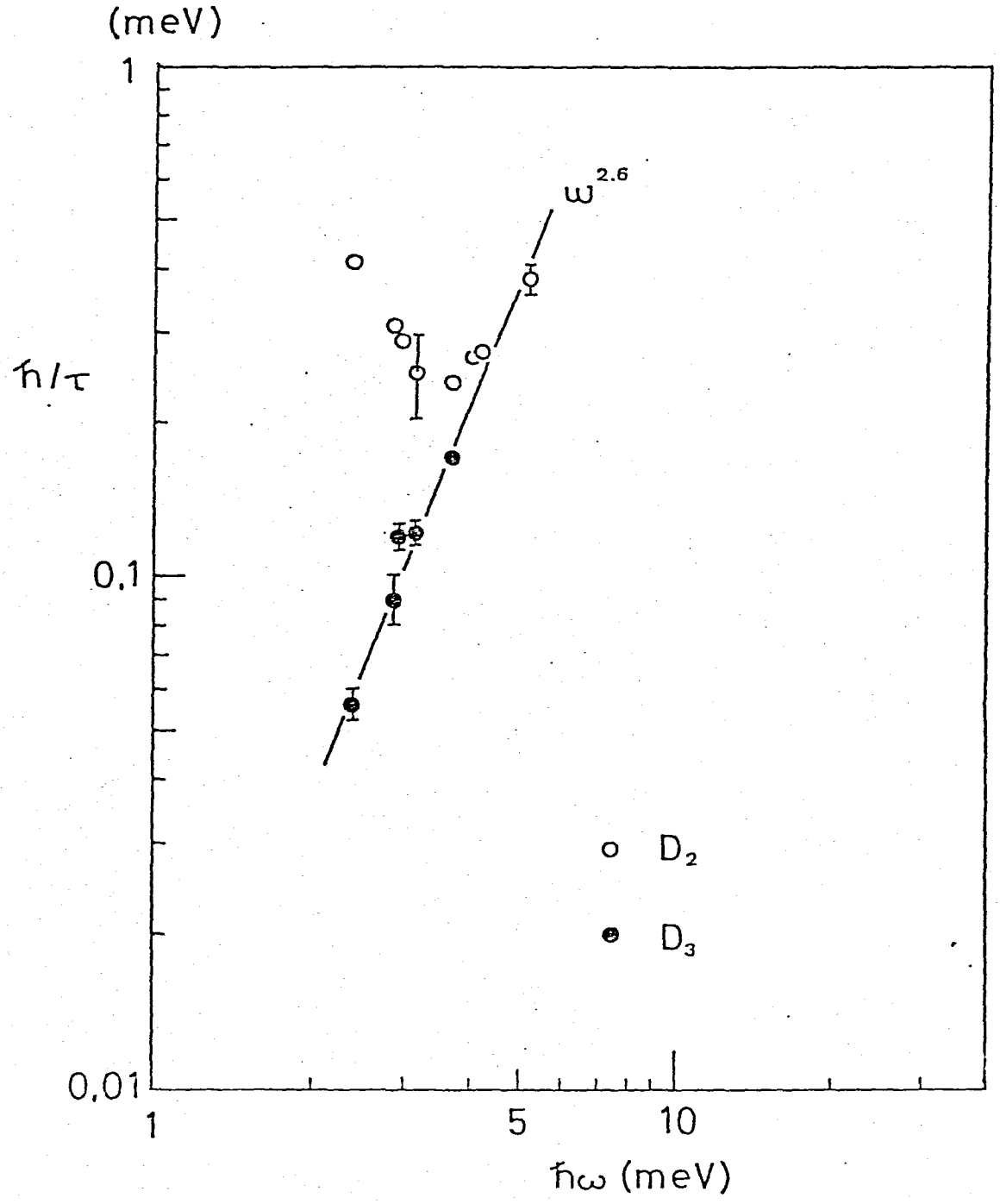

Fig.35

Fig.36

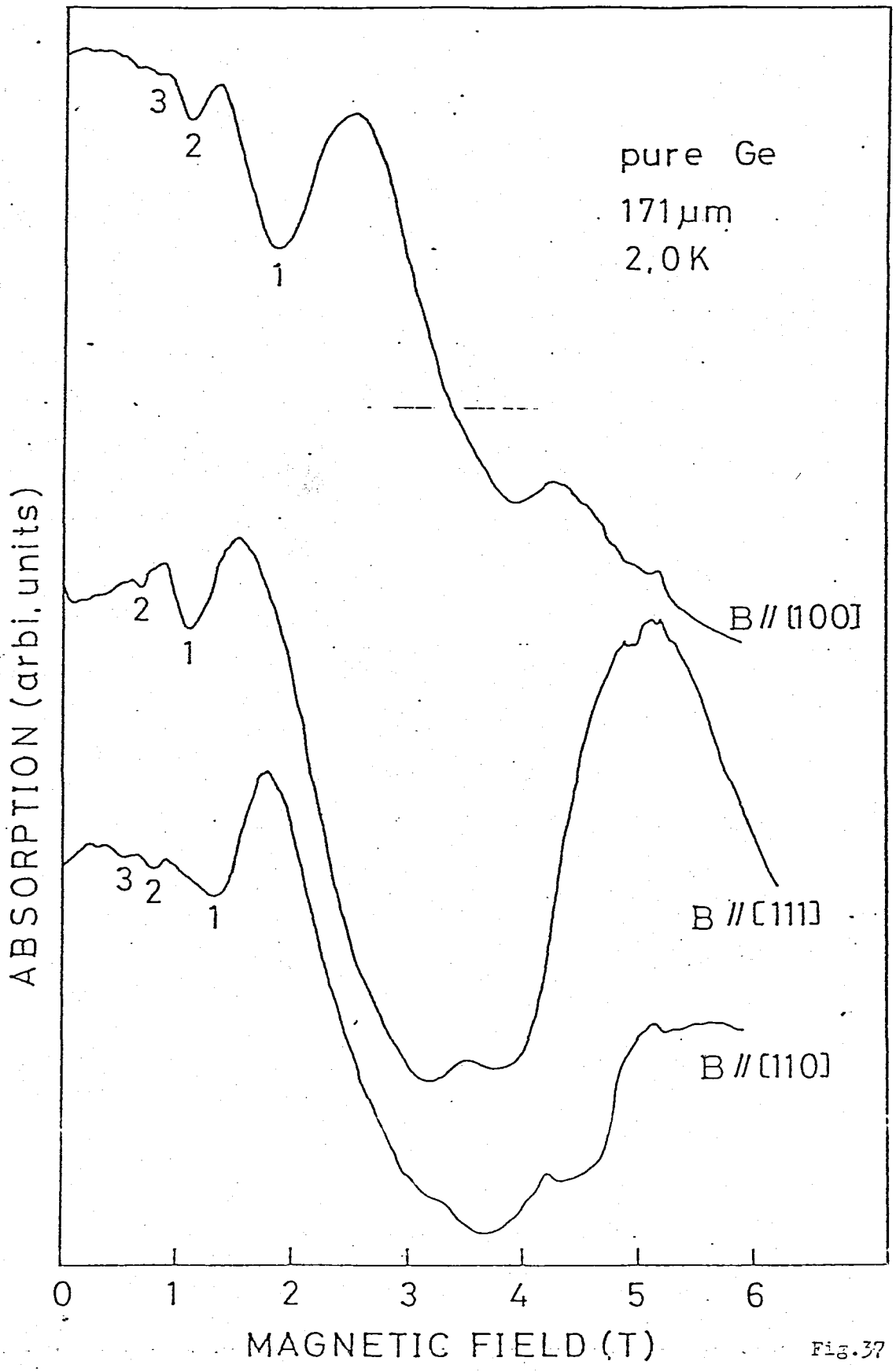
pure Ge
171 μm
2.0 K
B // [100]
B // [111]
B // [110]
3
2
1
ABSORPTION (arbi. units)
0
1
2
3
4
5
6
MAGNETIC FIELD (T)

Fig.37

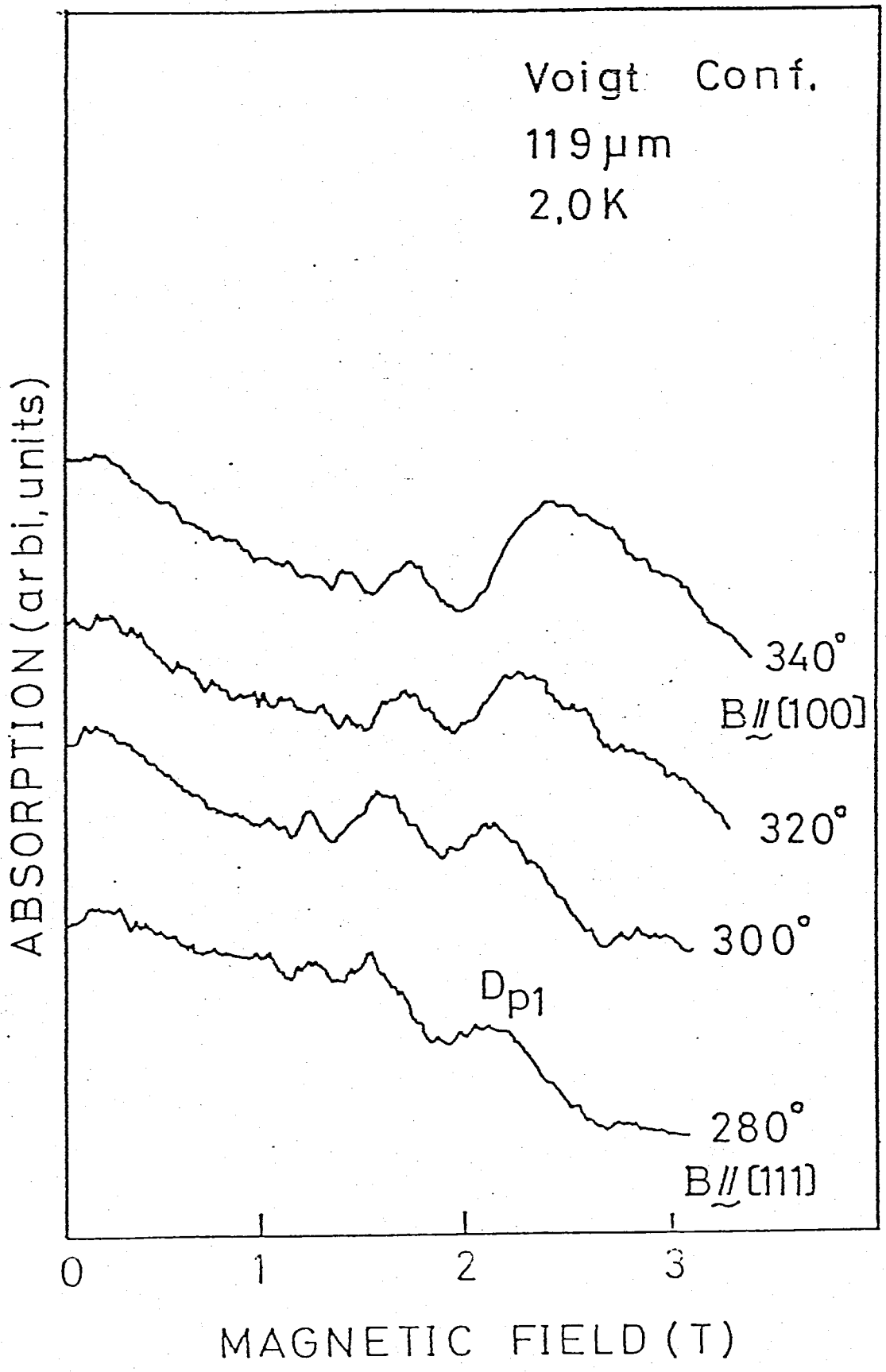
Voigt Conf.
119 µm
2,0 K
340°
B // [100]
320°
300°
D_{P1}
280°
B // [111]
ABSORPTION (arbi, units)
0
1
2
3
MAGNETIC FIELD (T)

Fig.38

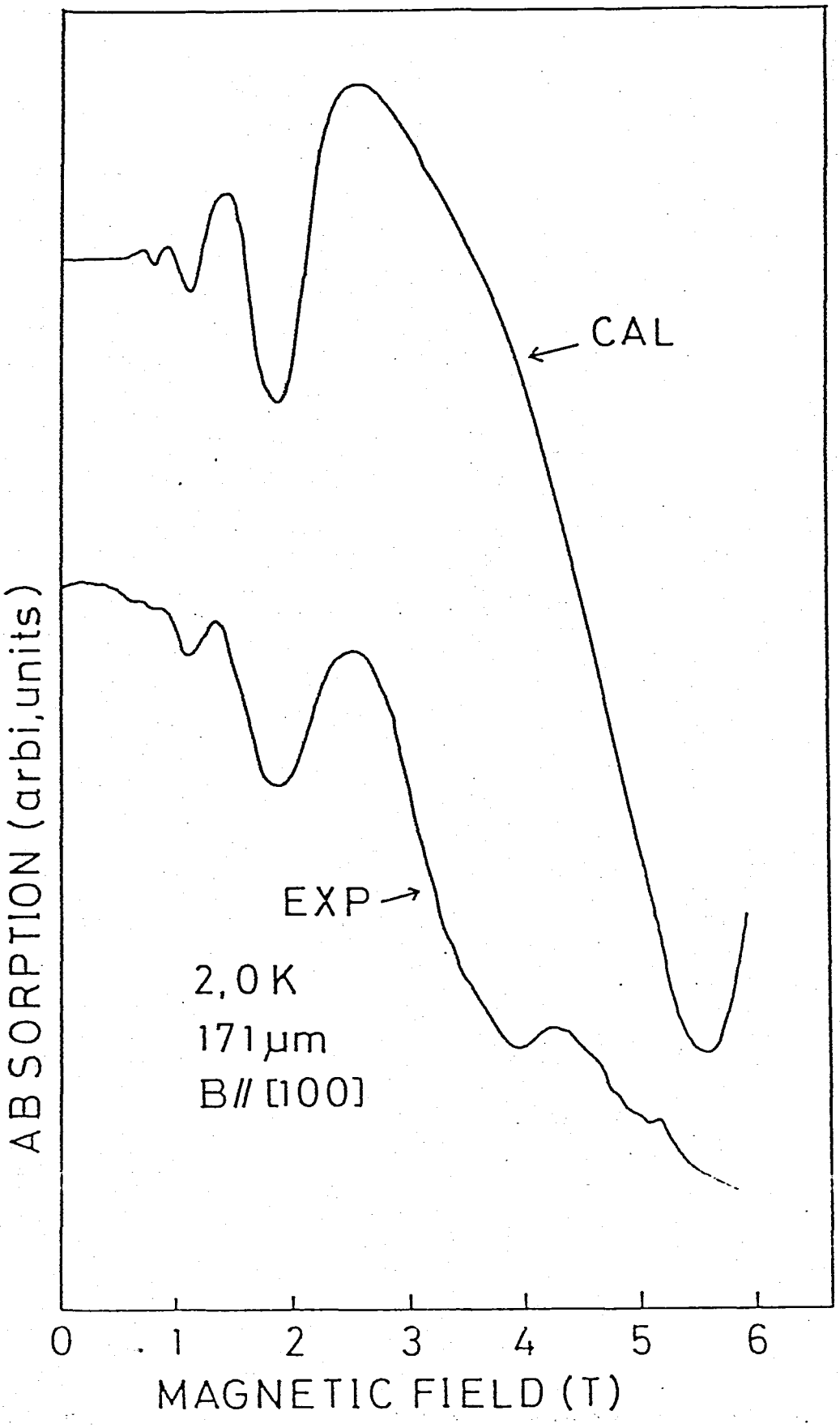
CAL
EXP
2,0 K
171 μm
B// [100]
ABSORPTION (arbi,units)
0
1
2
3
4
5
6
MAGNETIC FIELD (T)

Fig.39

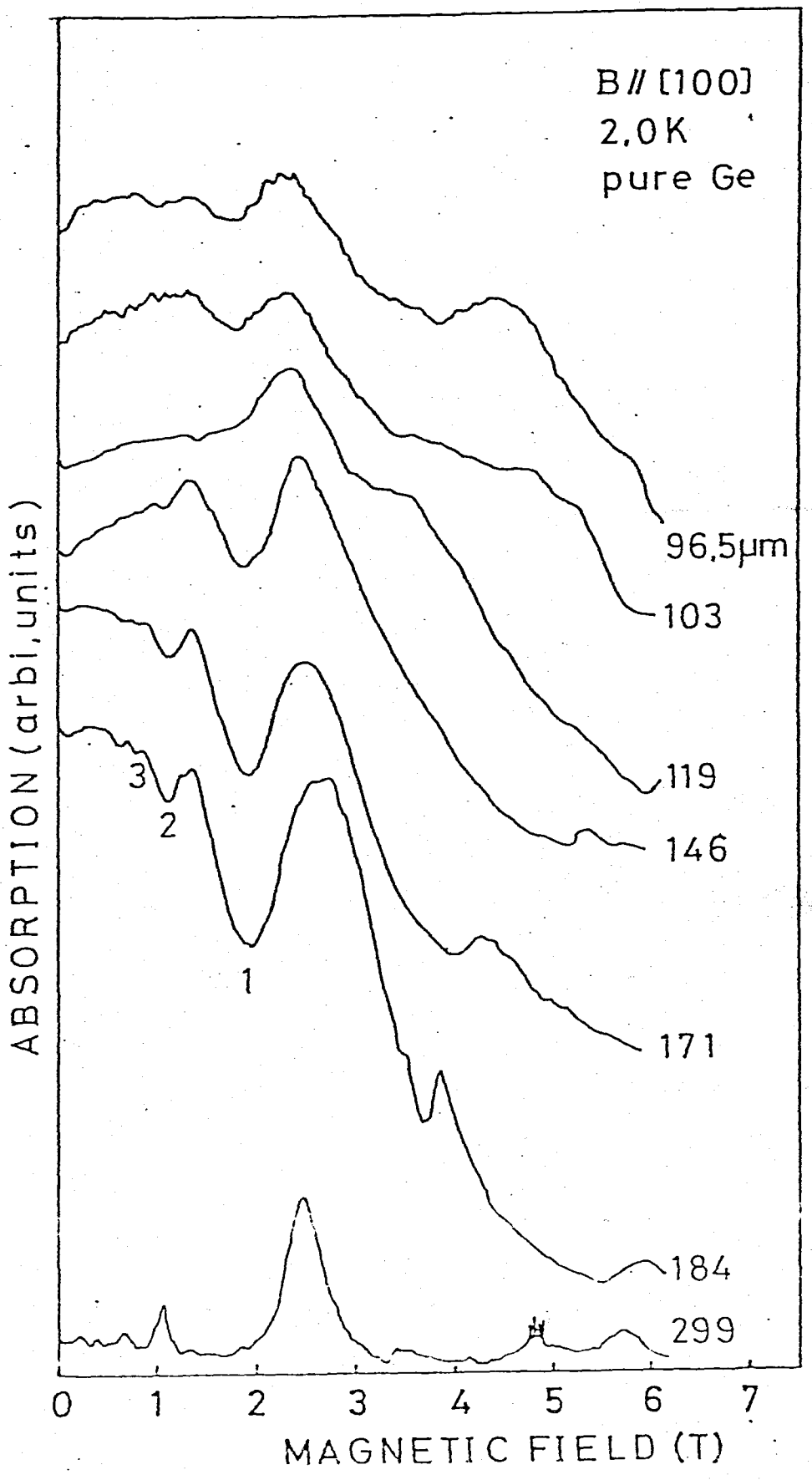
B // [100]
2.0K
pure Ge
96.5μm
103
119
146
171
184
299
1
2
3
ABSORPTION (arbi. units)
0
1
2
3
4
5
6
7
MAGNETIC FIELD (T)

Fig.40

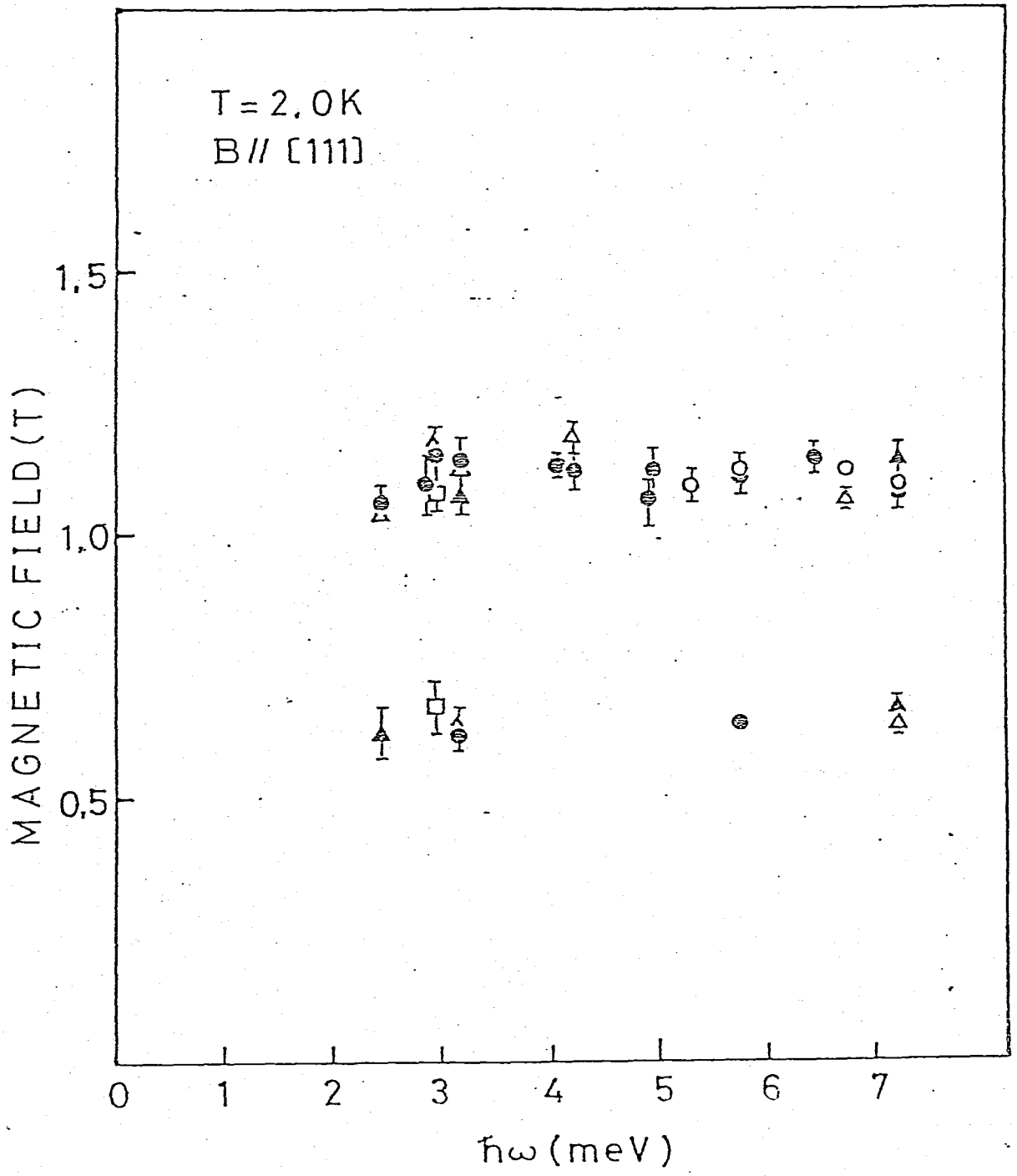

Fig.41

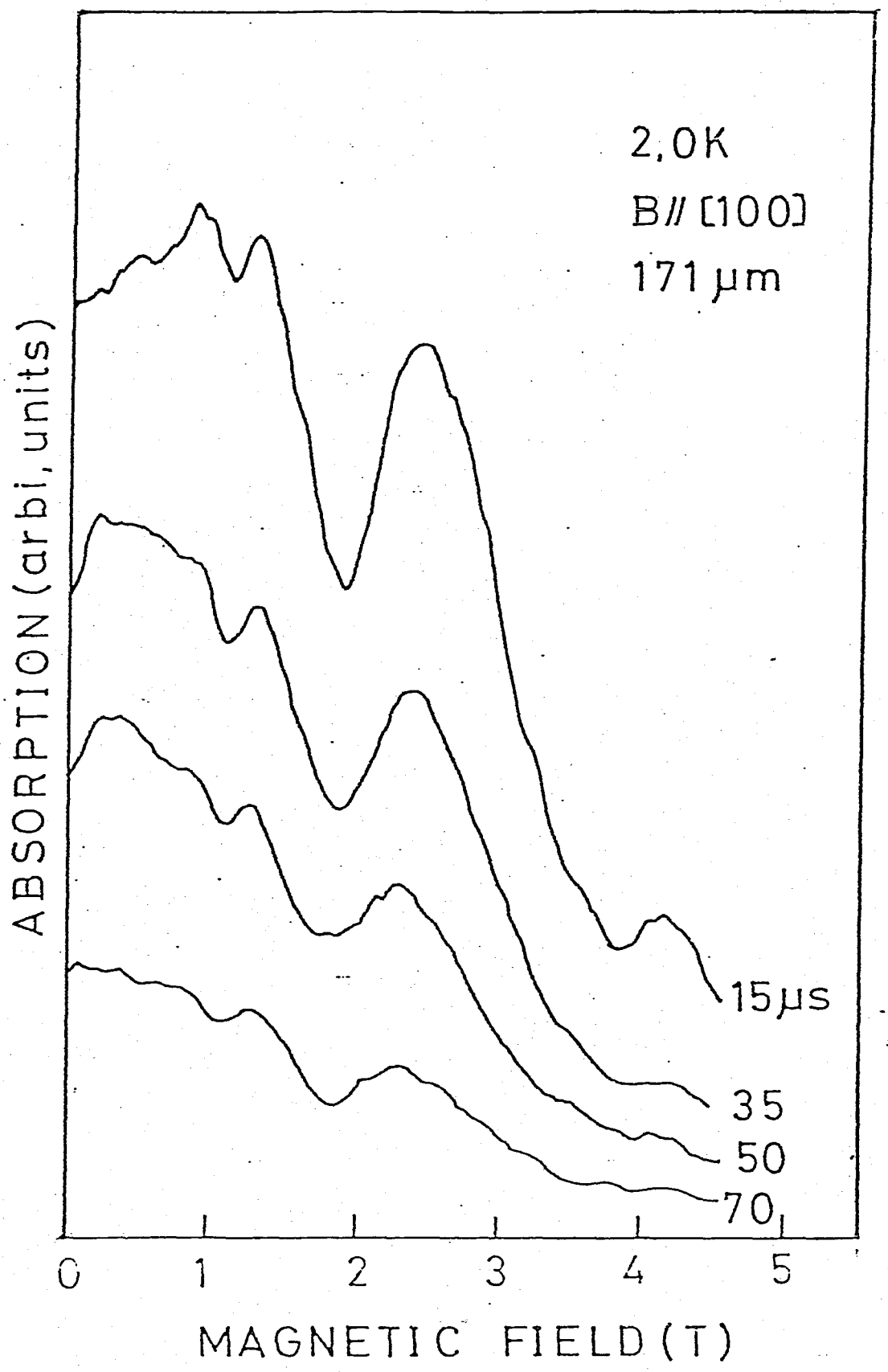
2.0K
B// [100]
171 μm
ABSORPTION (arbi. units)
15μs
35
50
70
0
1
2
3
4
5
MAGNETIC FIELD (T)

Fig.42

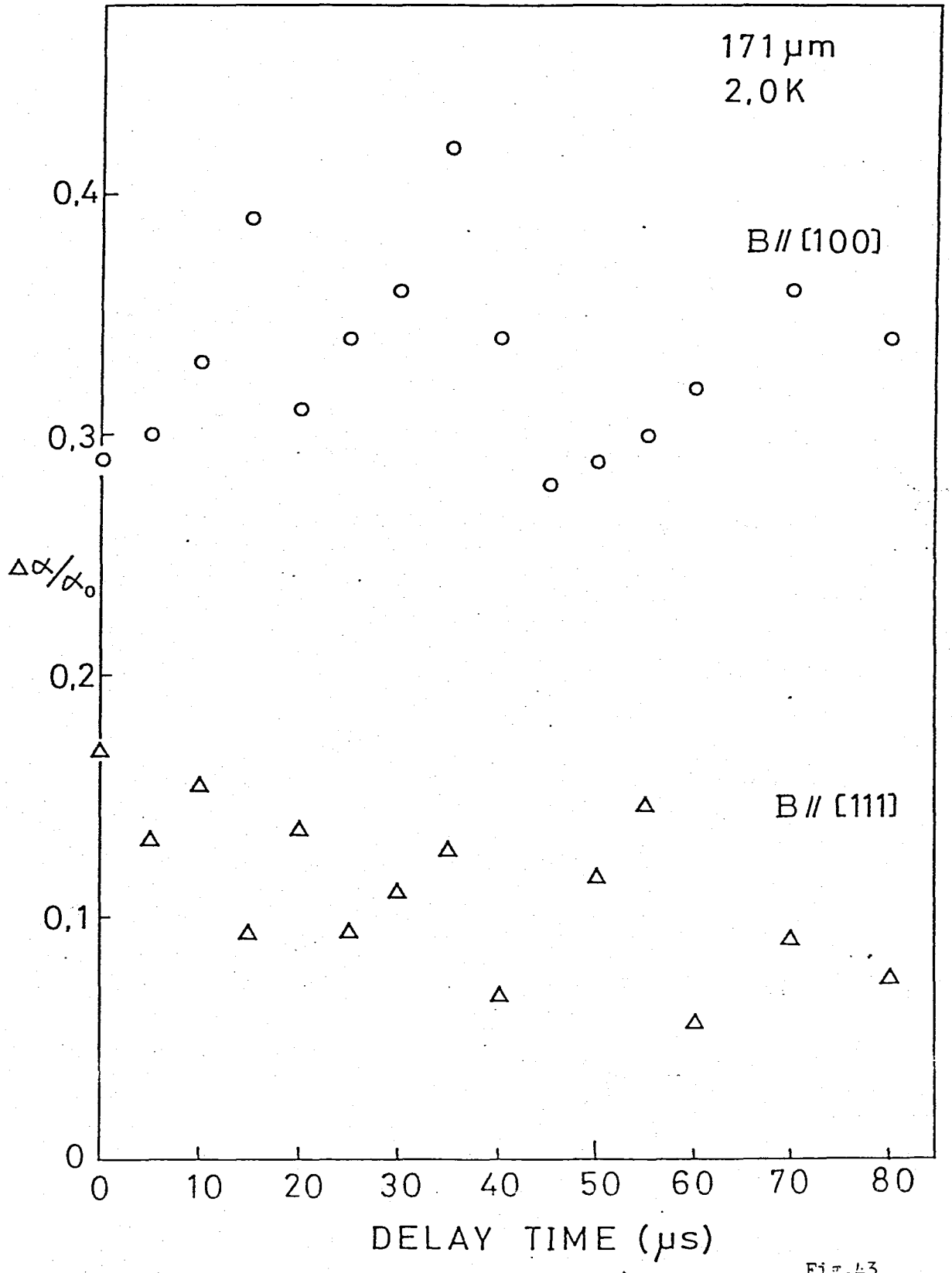
171 µm
2,0 K
B// [100]
B// [111]
0,4
0,3
0,2
0,1
0
Δα/α₀
0
10
20
30
40
50
60
70
80
DELAY TIME (µs)

Fig.43

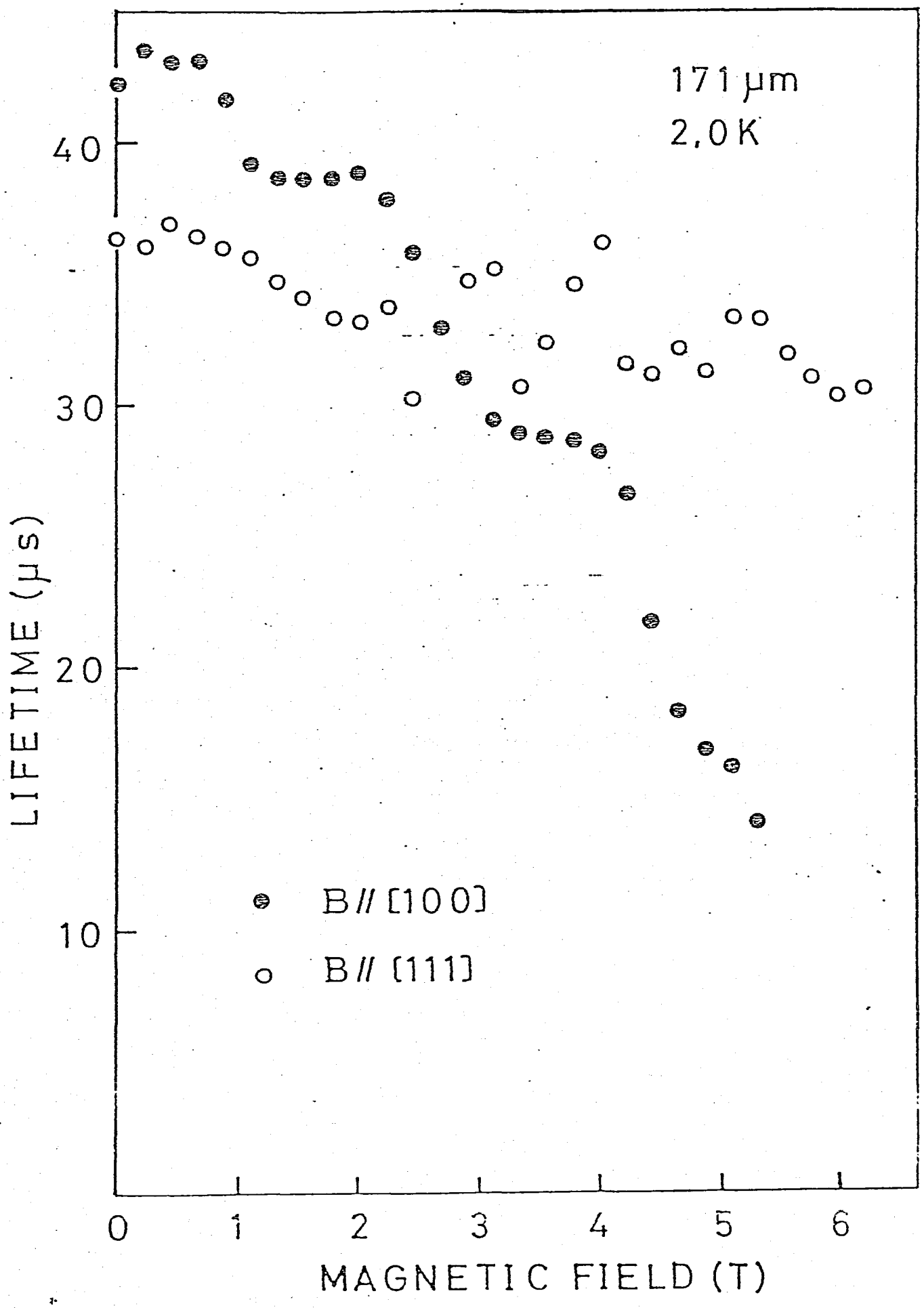
171 μm
2.0 K
40
30
20
10
LIFETIME (μs)
B // [100]
B // [111]
0
1
2
3
4
5
6
MAGNETIC FIELD (T)

Fig.44

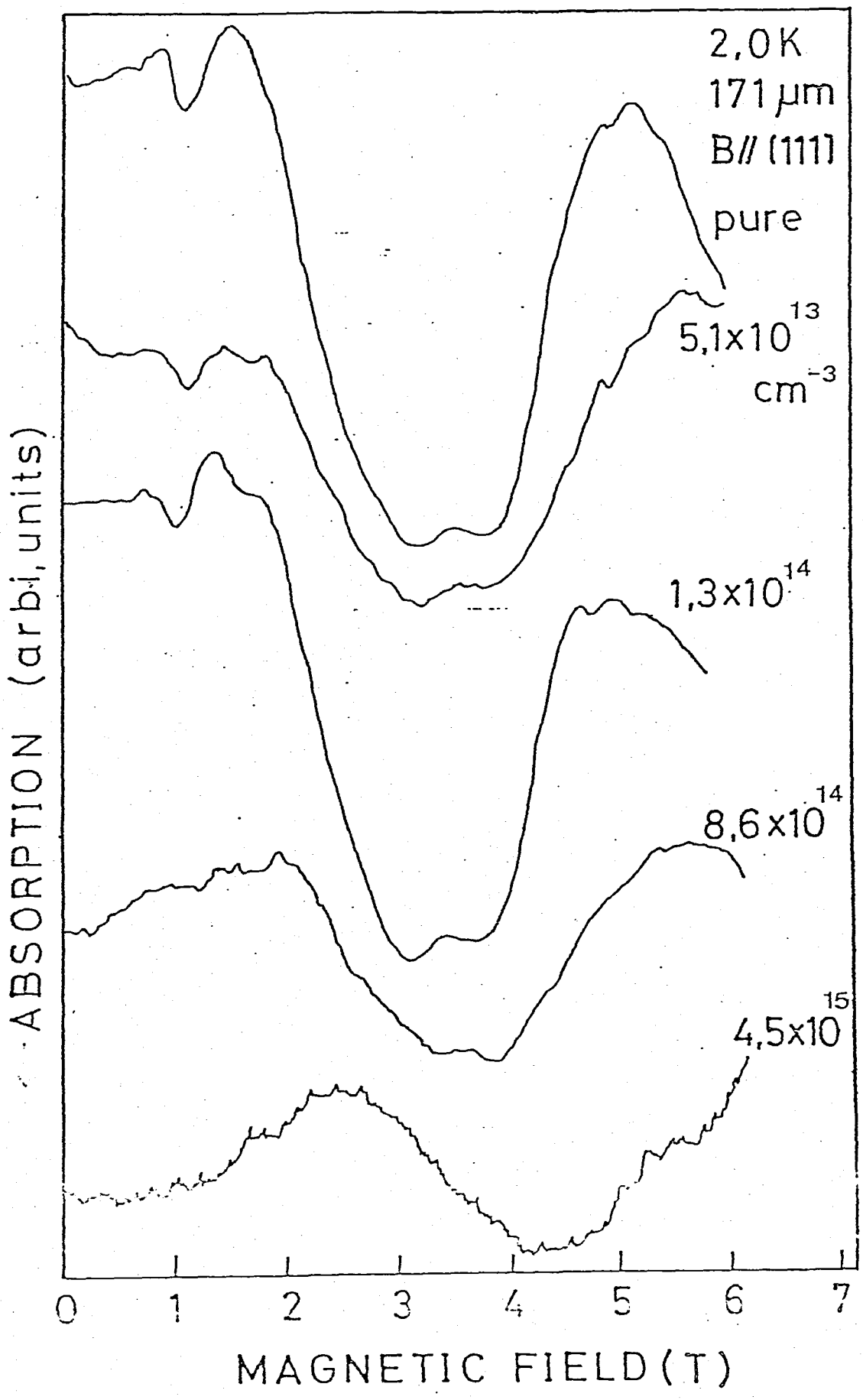
2,0 K
171 µm
B// (111)
pure
5,1x10^13
cm^-3
1,3x10^14
8,6x10^14
4,5x10^15
ABSORPTION (arbi. units)
0
1
2
3
4
5
6
7
MAGNETIC FIELD (T)

Fig.45

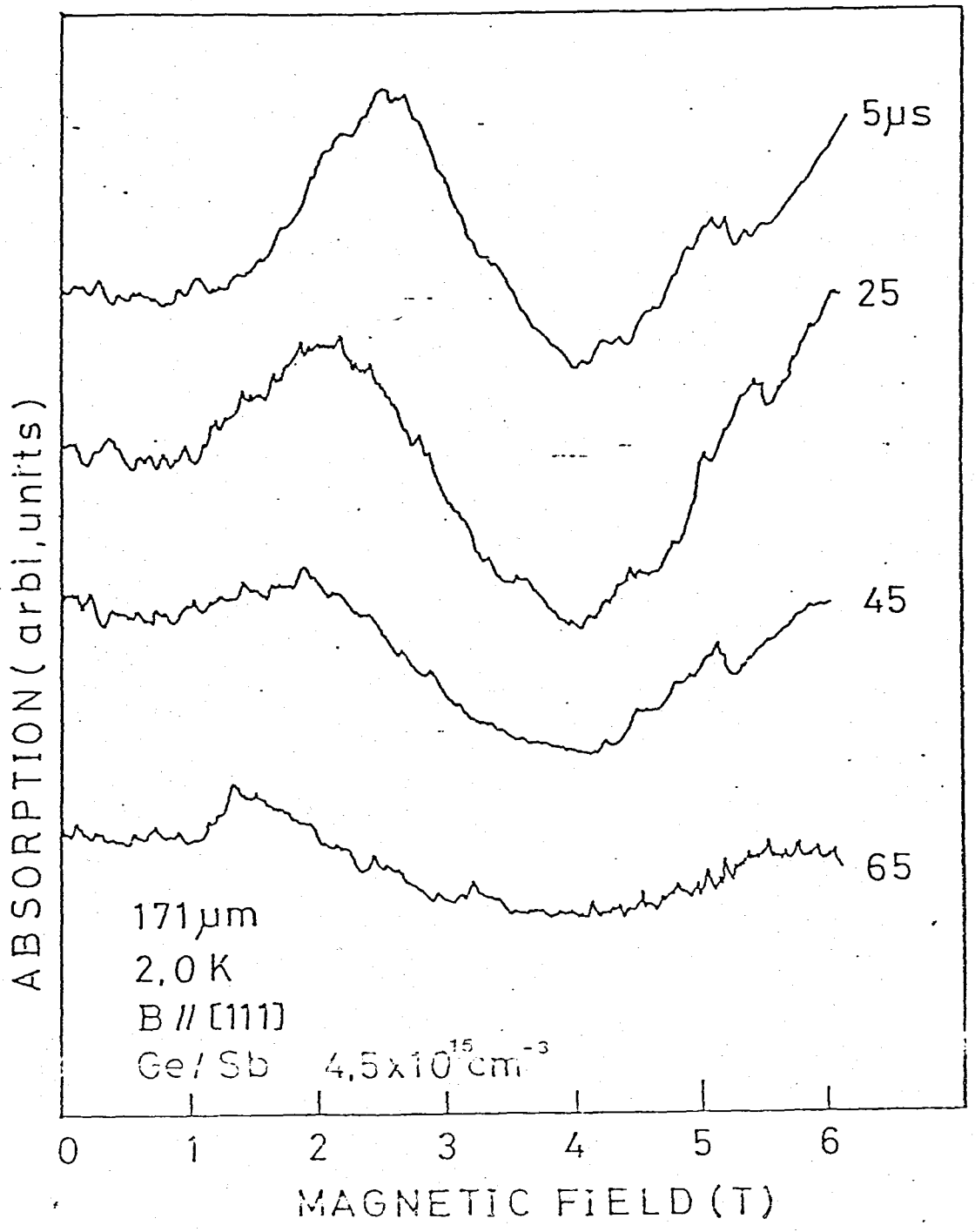
5μs
25
45
65
171μm
2.0 K
B // [111]
Ge / Sb 4.5x10^15 cm^-3
ABSORPTION (arbi. units)
0
1
2
3
4
5
6
MAGNETIC FIELD (T)

Fig.46

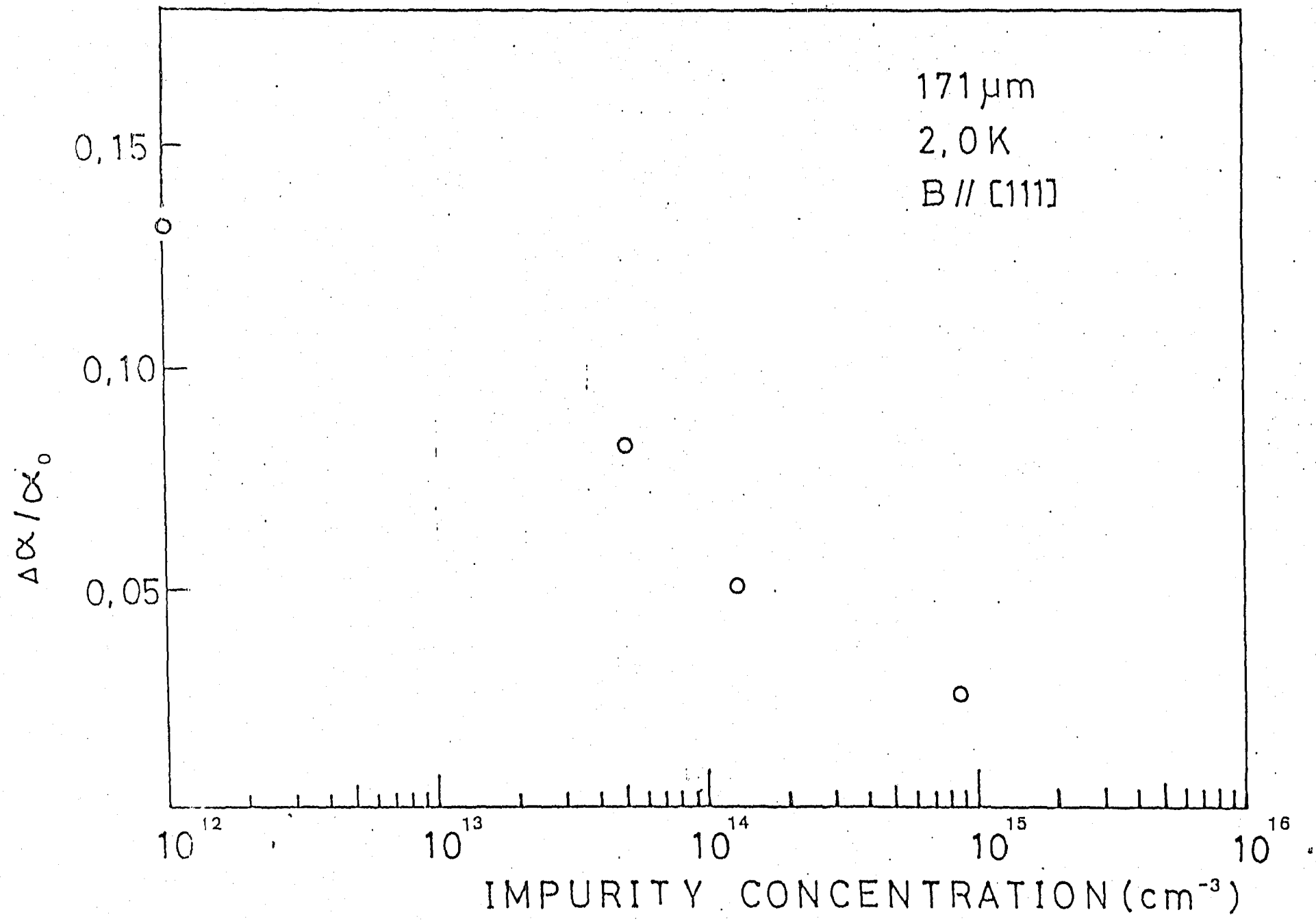
171 μm
2,0 K
B // [111]
0,15
0,10
0,05
Δα / α₀
10^12
10^13
10^14
10^15
10^16
IMPURITY CONCENTRATION (cm^-3)

Fig. 47

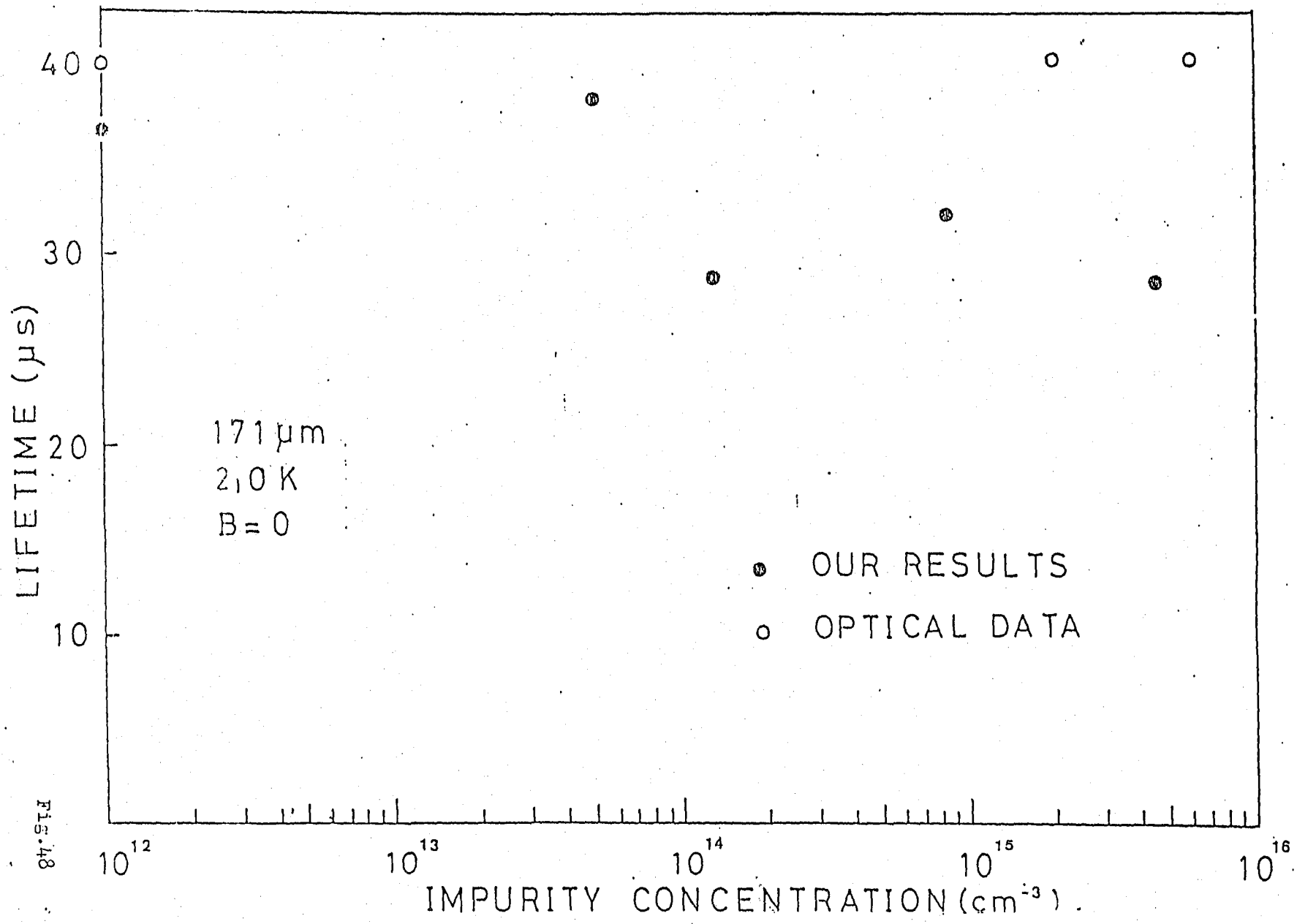
40
30
20
10
LIFETIME (μs)
171 μm
2.0 K
B = 0
OUR RESULTS
OPTICAL DATA
10^{12}
10^{13}
10^{14}
10^{15}
10^{16}
IMPURITY CONCENTRATION (cm^{-3})

Fig. 48

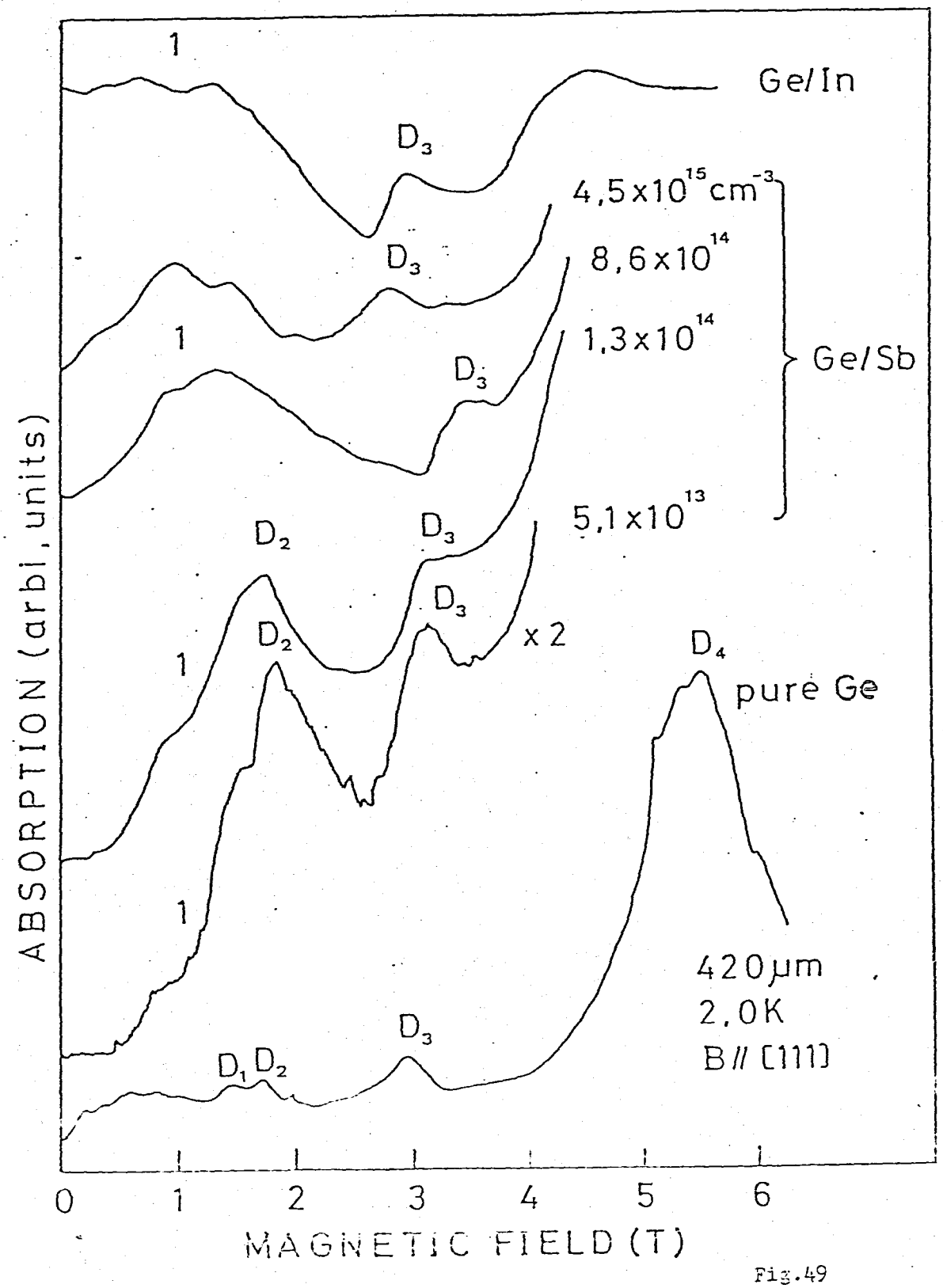
1
Ge/In
D3
4,5x10^15 cm^-3
8,6x10^14
1,3x10^14
Ge/Sb
5,1x10^13
D2
D3
x 2
D4
pure Ge
420µm
2,0K
B // [111]
D1 D2
ABSORPTION (arbi. units)
0
1
2
3
4
5
6
MAGNETIC FIELD (T)

Fig.49

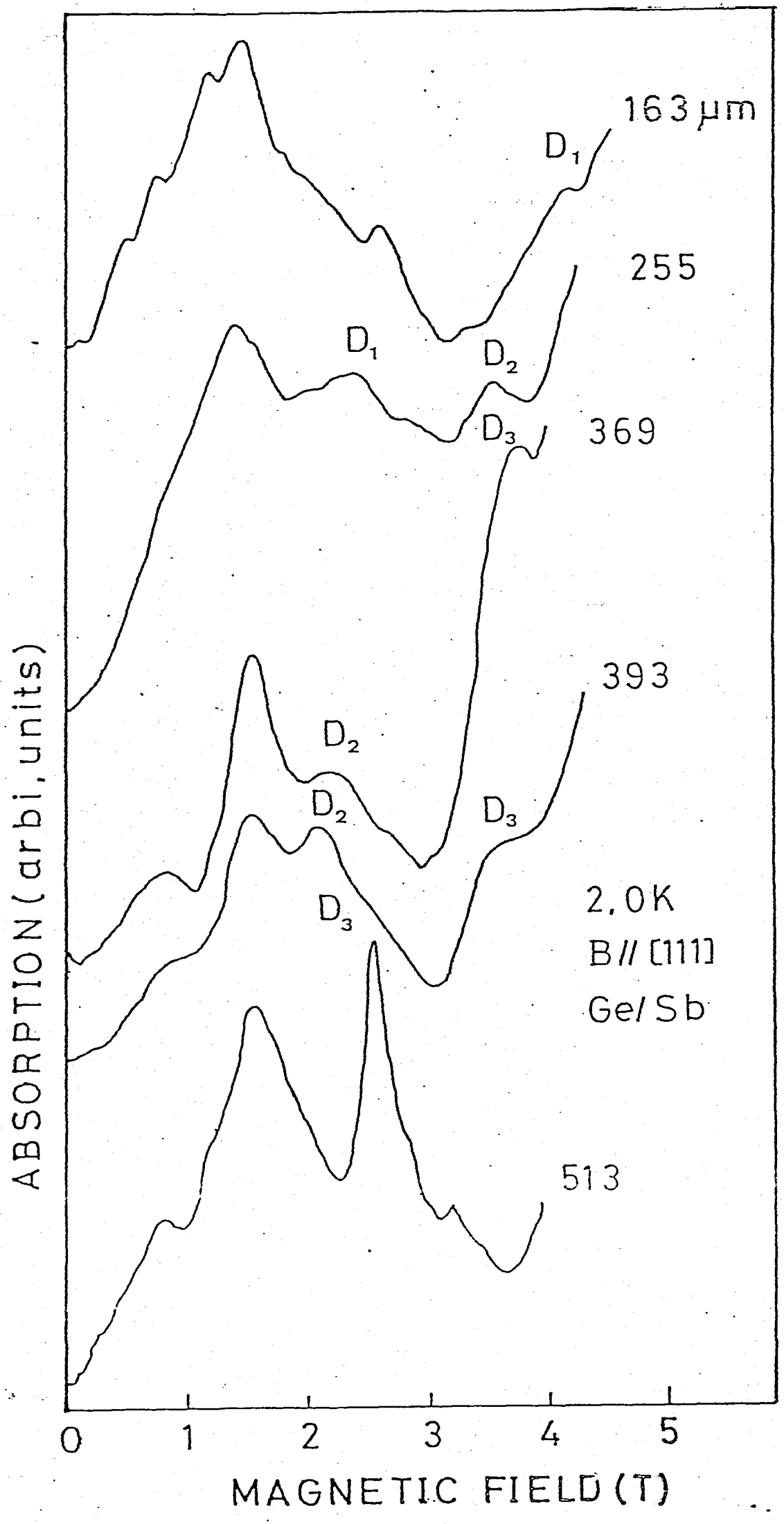
163 μm
D1
255
D1
D2
D3
369
393
D2
D2
D3
D3
2.0K
B // [111]
Ge/Sb
513
ABSORPTION (arbi. units)
0
1
2
3
4
5
MAGNETIC FIELD (T)

Fig.50

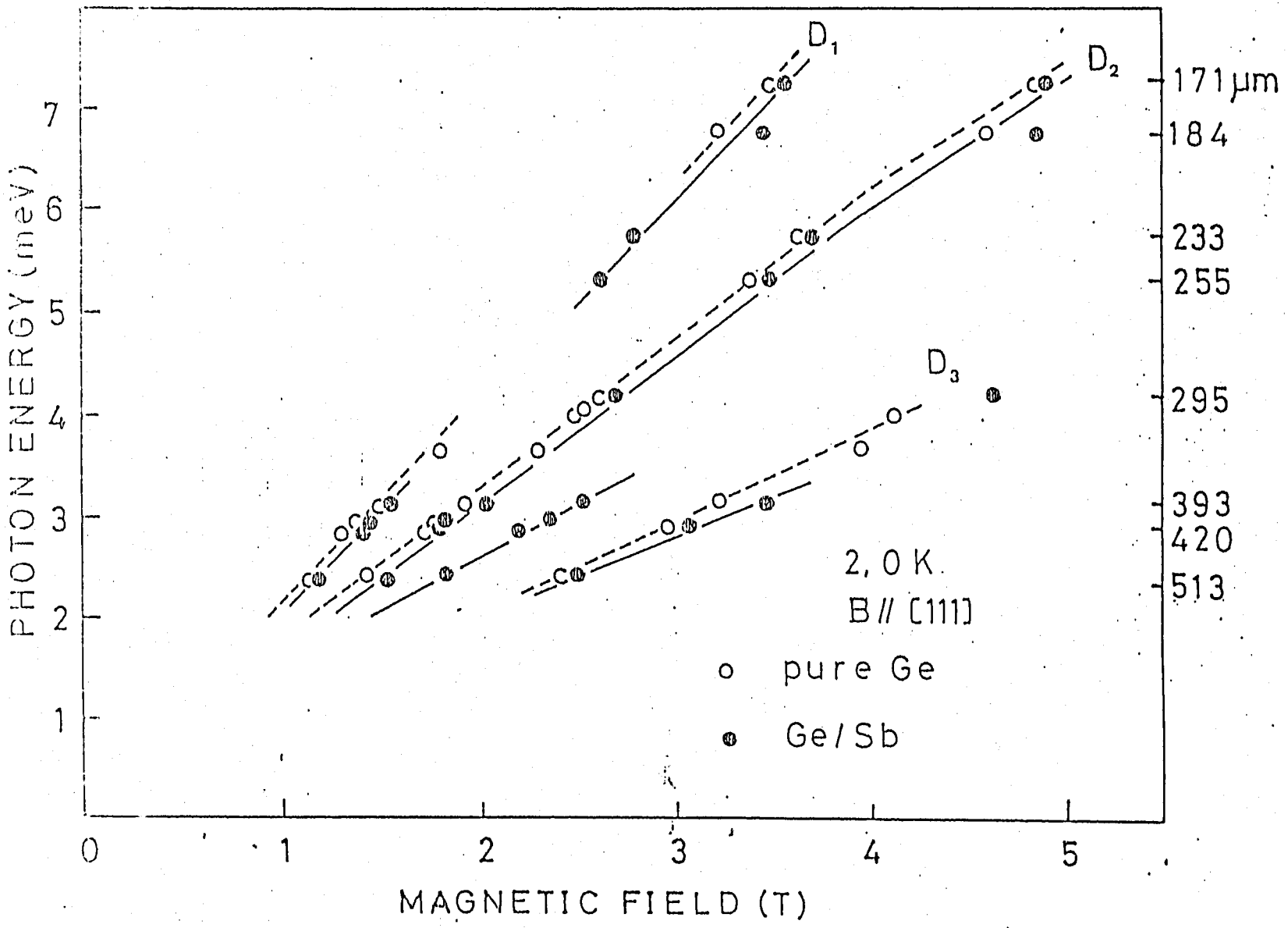
D1
D2
D3
171 μm
184
233
255
295
393
420
513
2.0 K
B // [111]
o pure Ge
Ge/Sb
PHOTON ENERGY (meV)
MAGNETIC FIELD (T)
0
1
2
3
4
5
1
2
3
4
5
6
7

FIG.51

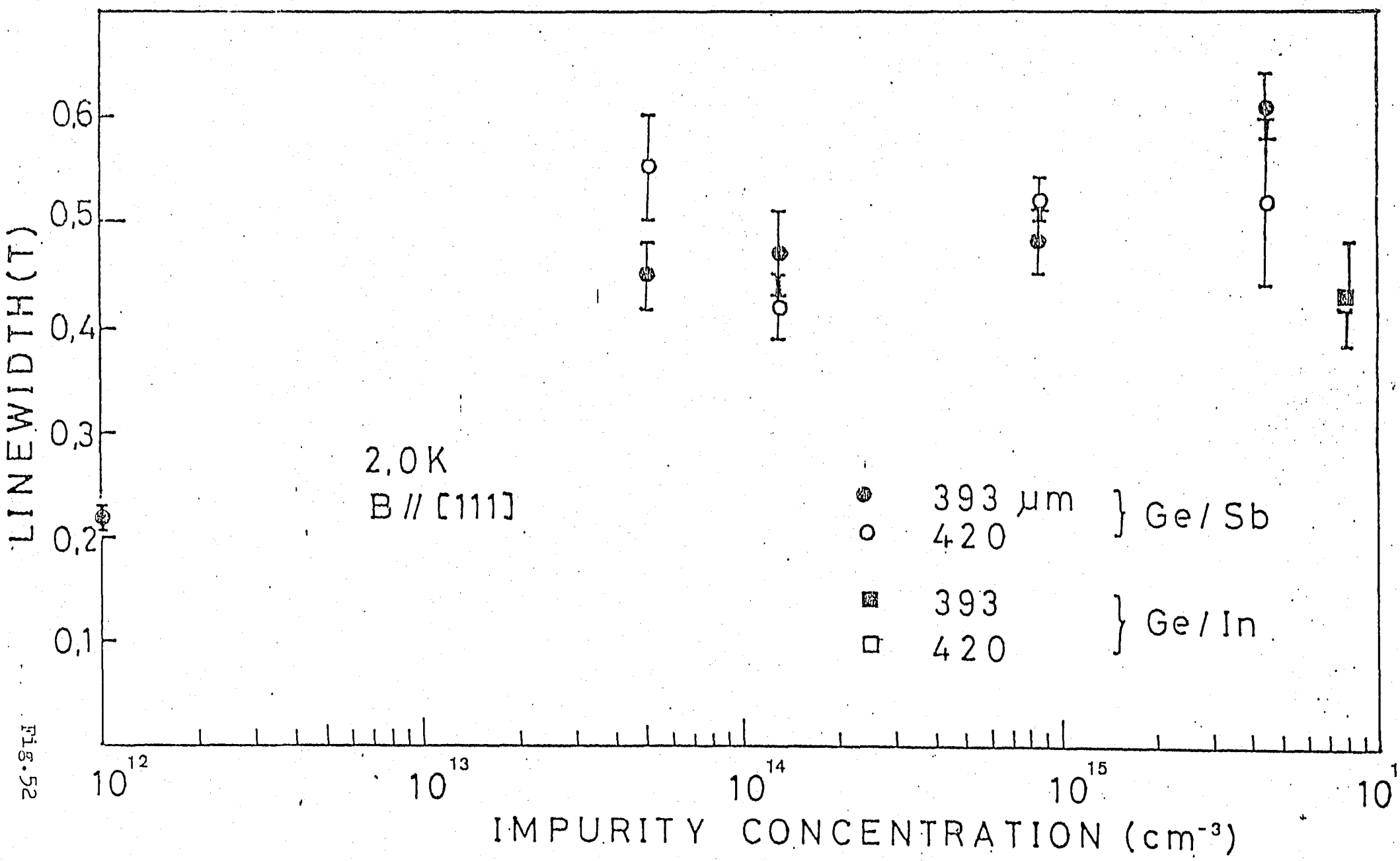
LINEWIDTH (T)
0,6
0,5
0,4
0,3
0,2
0,1
2,0 K
B // [111]
393 μm
420
Ge / Sb
393
420
Ge / In
10^{12}
10^{13}
10^{14}
10^{15}
10^{16}
IMPURITY CONCENTRATION (cm^{-3})

Fig. 52

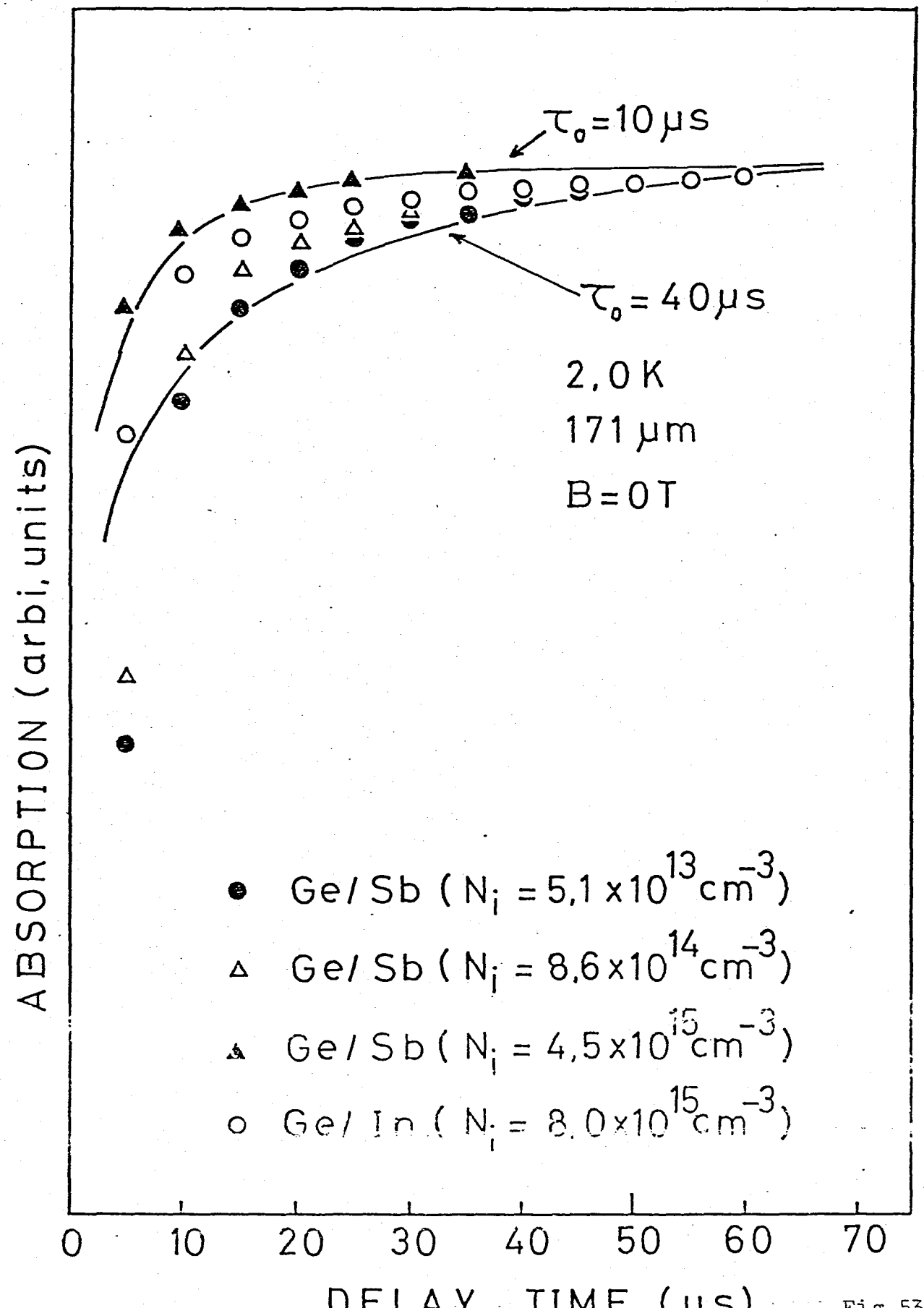
$\tau_0 = 10\,\mu s$
$\tau_0 = 40\,\mu s$
2,0 K
171 μm
B = 0 T
Ge/Sb ($N_i = 5{,}1 \times 10^{13} cm^{-3}$)
Ge/Sb ($N_i = 8{,}6 \times 10^{14} cm^{-3}$)
Ge/Sb ($N_i = 4{,}5 \times 10^{15} cm^{-3}$)
Ge/In ($N_i = 8{,}0 \times 10^{15} cm^{-3}$)
ABSORPTION (arbi. units)
0
10
20
30
40
50
60
70
DELAY TIME (μs)

Fig.53

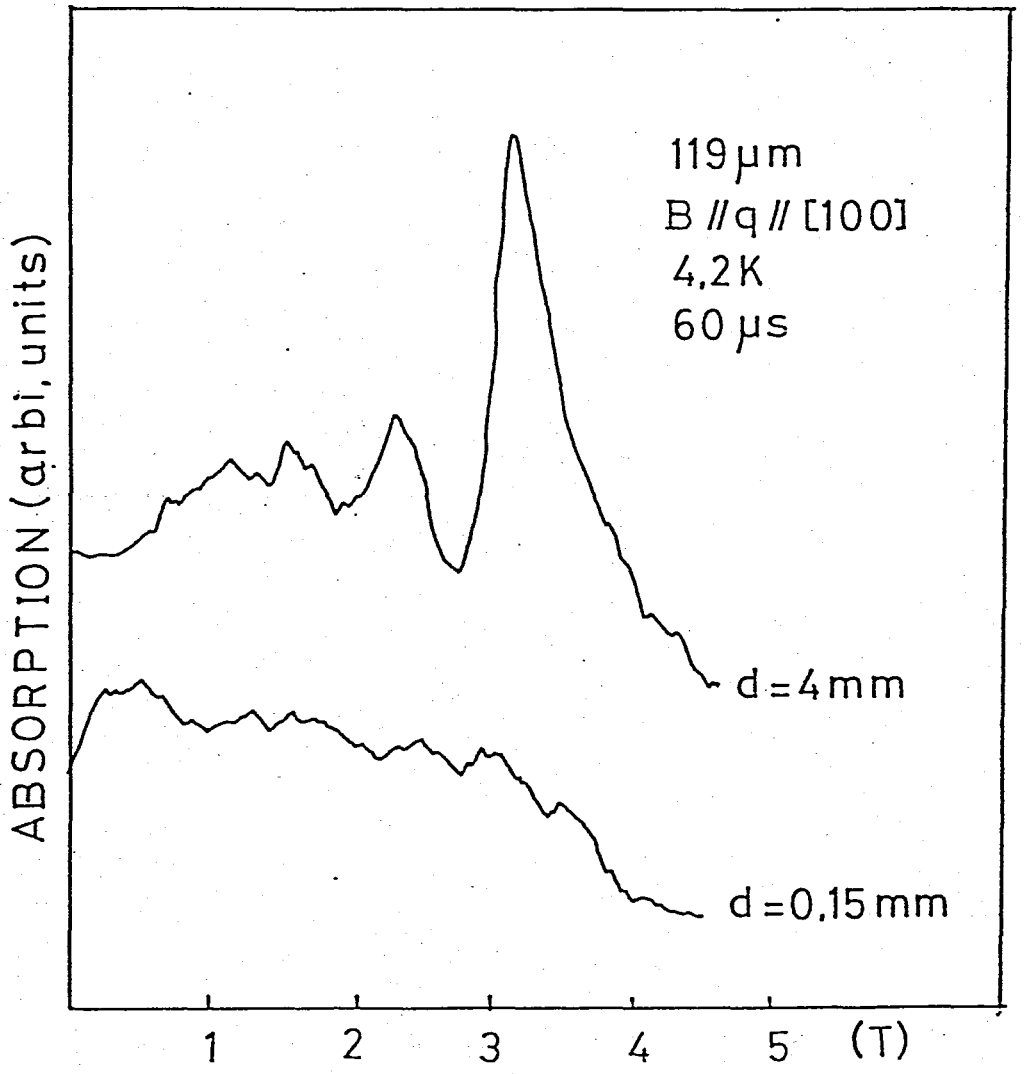
119 µm
B // q // [100]
4,2 K
60 µs
d = 4 mm
d = 0,15 mm
ABSORPTION (arbi. units)
1
2
3
4
5
(T)

Fig.54

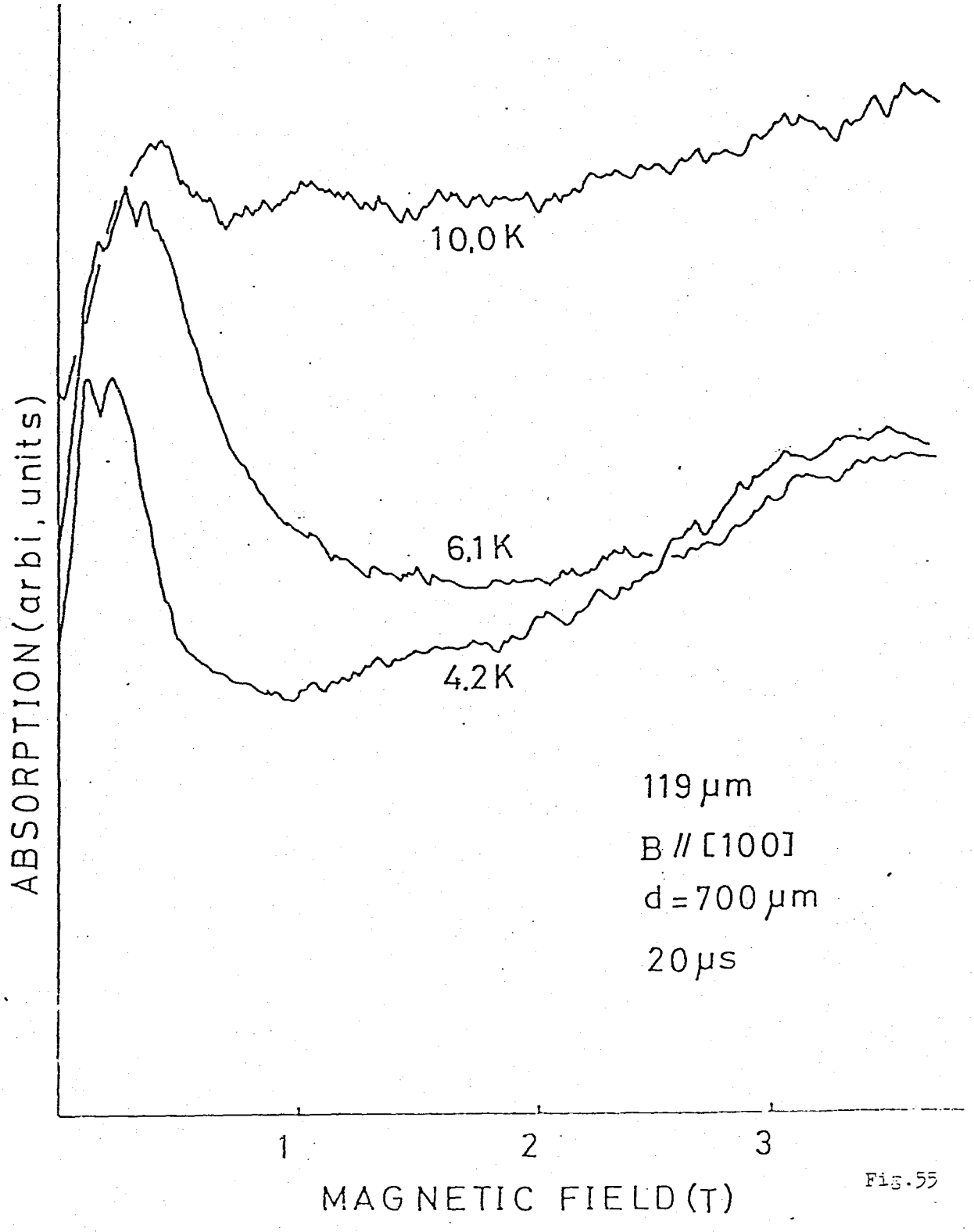
10.0 K
6.1 K
4.2 K
119 μm
B // [100]
d = 700 μm
20 μs
ABSORPTION (arbi. units)
1
2
3
MAGNETIC FIELD (T)

Fig.55

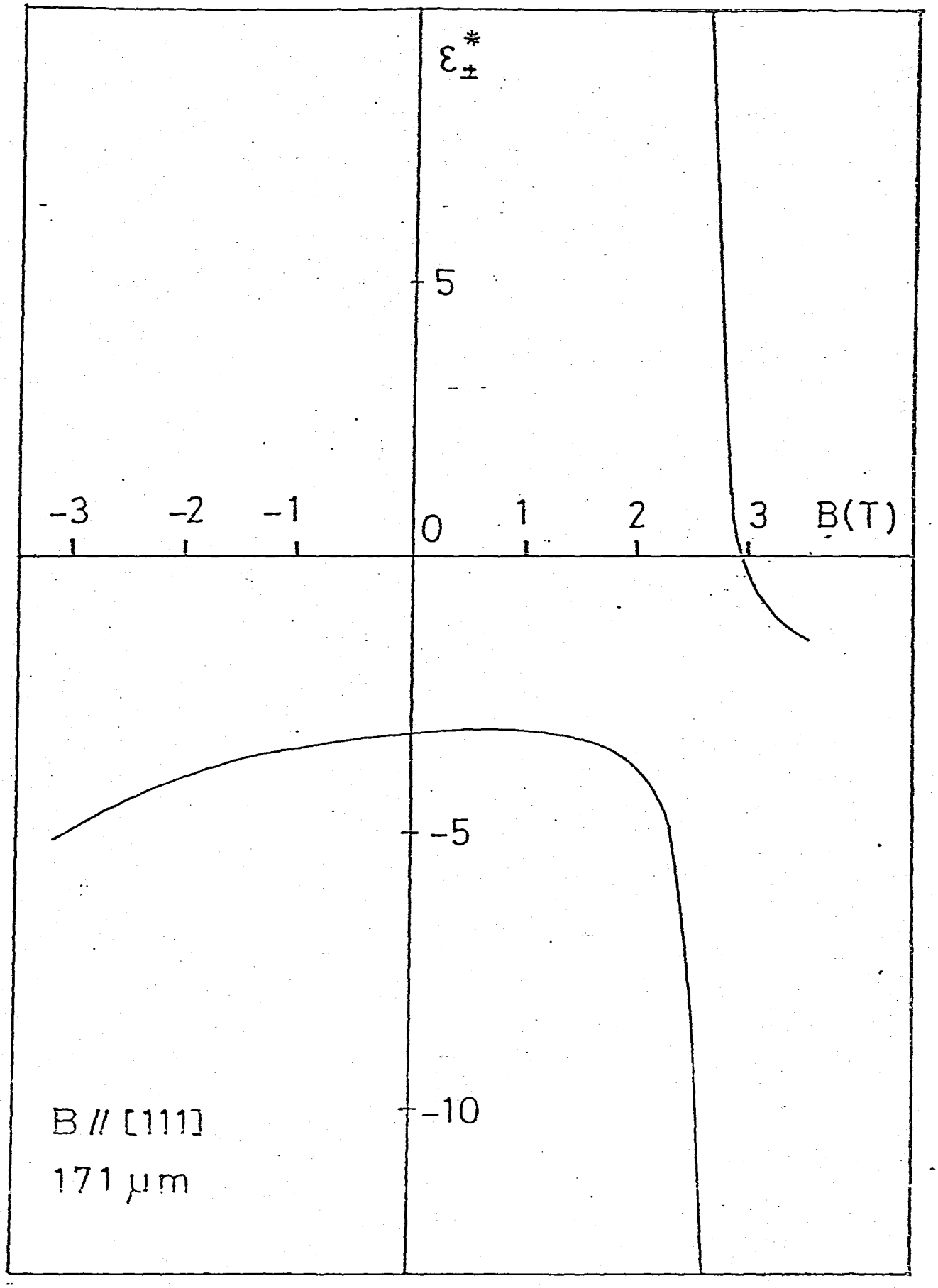

Fig.56